Electrically Active Ceramics for Bone Graft Substitution

Baxter, Frances

Award date:
2008

Awarding institution:
University of Bath

ELECTRICALLY ACTIVE CERAMICS FOR BONE GRAFT SUBSTITUTION

Frances Rachel Baxter

A thesis submitted for the degree of Doctor of Philosophy

University of Bath

Department of Mechanical Engineering

December 2008

Abstract

Hydroxyapatite (HA) bioceramics are commercially available as bone graft substitute materials. The aim of the current research was to characterise the electrical properties of hydroxyapatite-barium titanate (HABT) composites and to assess *in vitro* biological responses to the composites in order to investigate their potential use as bone graft substitutes.

A range of HABT ceramics of different compositions was manufactured and their electrical properties were measured. The microstructure and piezoelectric properties of the ceramics were both dependent on the proportion of barium titanate (BT) present. Composites containing more than 70% BT displayed piezoelectric charge coefficients (d_{33}) of up to 86.3±7.9pCN^{-1} (95% BT). The ferroelectric nature of the 90 and 95% BT materials was confirmed by assessment of their ferroelectric hysteresis loops. The highest piezoelectric voltage coefficient (g_{33}) recorded was 14x10^{-3}Vm^{-1}Pa^{-1} (90% BT). Following the assessment of the electrical properties, the HABT ceramic containing 90% BT was selected for the assessment of biological responses to the composites.

The proliferation, viability, activity and morphology of human osteoblast-like cells cultured on HABT were comparable to those cultured on hydroxyapatite (HA) up to 7 days after seeding. The remnant polarisation of poled HABT induced an increase in cell attachment. This influence was independent of the nature (positive or negative) of the polarisation. Poling was not found to influence cell morphology, activity or differentiation in the first 7 days of incubation. At 14 days after seeding, results were inconsistent, indicating some variations in cell population and differentiation depending on the composition and poling of the ceramics respectively.

This study has substantially defined the electrical properties of a range of HABT ceramics. It indicates their *in vitro* biocompatibility and thus their potential for use as bone graft substitutes. These results provide a benchmark against which future work investigating the influence of mechanical loading and longer term studies may be measured.

For my Dad

Acknowledgements

I would like to thank Dr Irene Turner, Dr Christopher Bowen and Professor Julian Chaudhuri for their supervision, support and guidance throughout the course of this project.

I will be eternally grateful to Dr Richard Forsey, who has generously shared his expertise in cell culture and analysis over the last three years. Many thanks also to Dr Andrew Dent for patiently answering many questions about electroceramics. It has been a pleasure working with you both.

Thanks to Dr Amanda Mackenzie and Samantha Moore for their help with the macrophage study and to Ursula Potter and Anne O'Reilly in the Centre for Electron Optical Studies.

I gratefully acknowledge the funding of this work by the EPSRC and the support of the Royal Academy of Engineering through the Research Student Development Fellowship.

Thanks to my parents and to Mary, for all of their love and support. Keri, Auguste and Sarah are brilliant and wonderful friends and deserve more thanks than I can possibly express here.

Contents

List of figures

List of tables

List of abbreviations

ALP	Alkaline phosphatase
APT	Adenosine triphosphate
BMP	Bone morphogenetic protein
BT	Barium titanate
CaP	Calcium phosphate
DMSO	Dimethyl sulfoxide
DNA	Deoxyribonucleic acid
ECM	Extra-cellular matrix
EDTA	ethylenediaminetetraacetic acid
FCS	Foetal calf serum
FGF	Fibroblast growth factors
GAG	Glycosaminoglycan
HA	Hydroxyapatite
HABT	Hydroxyapatite – barium titanate composite
IGF	Insulin-like growth factor
IL1	Interleukin-1
LDH	Lactate dehydrogenase
LPS	Lipopolysaccharide
M-CSF	Macrophage colony stimulating factor
MTT	Dimethylthiazol-2-yl)-2,5-diphenyltetrazolium bromide
OD	Optical density
PBS	Phosphate buffered saline
PG	Proteoglycan
PTFE	Polytetrafluoroethylene
PTH	Parathyroid hormone
P(VDF-TrFE)	poly(vinylidene-trifluoroethylene)
PZT	Lead zirconium titanate

RANKL	Receptor activator for nuclear factor κ B ligand
RER	Rough endoplasmic reticulum
RNA	Ribonucleic acid
SBF	Simulated body fluid
SEM	Scanning electron microscopy
SGP	Stress generated potentials
TCP	Tricalcium phosphate
THR	Total hip replacement
TKR	Total knee replacement
TNF	Tumour necrosis factor
UHMWPE	Ultra-high molecular weight polyethylene
XRD	X-ray diffraction

List of symbols and units

Applied stress	T	Nm^{-2}
Charge	Q	C
Current	I	a
Density	ϱ	kgm^{-3}
Electrical displacement	D	Cm^{-2}
Electrical field	E	Vm^{-1}
Permittivity	ε	Fm^{-1}
Piezoelectric charge coefficient	d	CN^{-1} or mV^{-1}
Piezoelectric voltage coefficient	g	mVN^{-1}
Polarisation	P	Cm^{-2}
Strain	S	
Surface area	A	m^2
Time	t	h
Volume fraction	υ	

Glossary

Adsorption	The adhesion of a substance to the surface of a solid or liquid
Apoptosis	Programmed cell death
Bioactivity	The induction of a biological response by a material or drug
Biocompatibility	The ability of a material to perform with an appropriate host response in a specific situation
Confluence	The entirety of the cell culture surface covered with cells
Cytokines	Signalling proteins
Cytotoxic	Causing damage to cell structure or function
Dielectric	A material which does not conduct electrical current
Dipole	A system composed of two charges of opposite sign separated by a distance
Endotoxin	A toxic compound found inside pathogens such as bacteria
Ferroelectricity	A physical property of a material whereby it exhibits a spontaneous electric dipole moment
Filopodia	Long, thin protrusions at the periphery of cells
Genotype	The genetic identity of an organism
Glycosaminoglycan	Long polysaccharide molecules, an important component of connective tissues
Haemopoietic stem cells	Stem cells that give rise to blood cells
Innervated	Supplied with nerves
Lamellipodium	Sheet-like projection at the edge of a cell
Macrophage	A phagocytic cell that helps to protect the body against infections and harmful substances
Mechanotransduction	The mechanisms by which cells convert mechanical stimulus into chemical activity

Mesenchymal stem cells	Multipotent cells that can differentiate into a range of cells including osteoblasts, chondrocytes and adipocytes,
Mitochondria	The organelles within a cell responsible for energy production
Osteoconduction	The ability to guide bone formation on the surface of a material or scaffold in a bony environment
Osteogenesis	The laying down of new bone
Osteoinduction	The induction of bone formation
Osteolysis	The active resorption or dissolution of bone tissue as part of an ongoing disease process
Osteosarcoma	Cancer of the bone
Permittivity	A physical quantity that describes how an electric field affects and is affected by a dielectric medium
Phagocytose	The process by which mechanical loading is converted into biochemical signal
Phenotype	The physical expression of an organism's genotype
Pluripotent	The ability of a cell to differentiate into many different cell types
Proteoglycans	A molecule that contains proteins and glycosaminoglycans, a component of extracellular matrix
RANKL	Cell surface molecule involved in the activation of osteoclasts
Resorption	The process of breaking down or assimilating something
Serum	The fluid, non-cellular portion of blood
Vascularisation	The development of blood vessels

1 Introduction

Bone grafts are used to replace bone tissue lost through injury or disease or following orthopaedic surgery [1]. The current "gold standard" graft material is autograft (bone tissue harvested from the patient themselves) though the use of allograft (transplantation of donor tissue) is also common. However, there are inherent problems associated with the use of both autograft and allograft. This situation has led to interest in the development of synthetic bone graft materials. Hydroxyapatite (HA) materials make up a large proportion of the bone graft substitutes currently available [2].

Recent research has shown modifications in osteoinduction and bone cell responses on the surfaces of charged materials [3]. The mechanism by which this occurs remains unclear at present. It is also known that bone displays piezoelectric properties and it has been suggested that the stress generated potentials induced in bone are responsible for triggering the remodelling cycle [4, 5].

It has been proposed previously that it may be possible to take advantage of bone's response to electromechanical stimuli to produce a high-performing HA based bone graft substitute material [6]. The aim of this research is to investigate the possible use of HA-piezoelectric composite ceramics as bone graft substitutes. Specifically, this study seeks to provide details of the sintered composition, microstructure and piezoelectric properties of such a material. Further, *in vitro* biological responses to the composite will be tested in order to establish the usefulness of testing this material under mechanical loading and the feasibility of pursuing it as a bone graft substitute.

The structure of the thesis will now be discussed.

Thesis outline

Chapter 2 comprises a summary of background information and a review of relevant literature. The structure, composition, mechanical properties and biology of bone are considered alongside current practice in bone grafting and bone graft substitutes. Existing work on the use of charged and electrically active materials in bone grafting is then discussed. Based on this literature review, a suitable hydroxyapatite (HA) - piezoelectric composite (hydroxyapatite – barium titanate, HABT) is selected for further investigation. Chapter 3 describes the materials and methods used for the current investigation. Techniques for the analysis of both the characteristics of the electrically active composites and the biological response to the various materials are presented.

The electrical characteristics of hydroxyapatite-barium titanate (HABT) composites are investigated in Chapter 4. The influence of the addition of the non-ferroelectric ceramic (HA) to the barium titanate (BT) on its piezoelectric properties is examined. Specifically, the piezoelectric coefficients, composition, microstructure of the materials are examined. An appropriate HABT composite for the *in vitro* testing of biological responses is selected.

Chapter 5 examines the response of osteoblast-like cells to the selected HABT ceramic in short- and long-term culture respectively. The effect of adding BT on the biocompatibility of the material is assessed along with the influence of poling the composite on biological responses. Cell culture methods are also verified in order to ensure the reliability of results. These results are discussed in the context of the material characterisation and published literature and conclusions on the suitability of HABT composites for use as bone graft are made. The results of a preliminary investigation into inflammatory responses to HABT composites are then presented. The conclusions of the thesis are summarised, along with suggestions for future work, in Chapter 6.

2 Literature review

This review covers relevant aspects of bone biology, bone grafting and artificial bone graft materials before focussing on the use of electrically active materials as bone graft substitutes. Finally, relevant techniques in biomaterials testing, including cell culture and assays for the evaluation of cell attachment, proliferation and differentiation, are considered.

2.1 Bone

Bone is a connective tissue facilitating muscle actuation and body movement, providing structural support and protecting internal organs [7]. In order to create an appropriate bone replacement material, it is necessary to understand the nature of bone itself. This section reviews the structure and remodelling behaviour of bone, focusing on aspects which are particularly relevant to the response of bone to graft materials.

2.1.1 Structure and composition

Structure

In adults, bones comprise a core of cancellous bone surrounded by an outer shell of cortical bone. Cortical (compact) bone is dense (1850 kgm^{-3} [8]) and contains only microscopic channels. Cancellous (spongy) bone is far less dense (1080 kgm^{-3} [8]), having an open porous structure made up of trabeculae as shown in Figure 2.1.

At the microscopic level, bone can exist in more than one form. Woven bone is made up of interwoven collagen fibres. It is formed during the healing of fractures in adults and is present in cancellous bone up to the age of about three years, at which time it is replaced with lamellar bone [9]. Lamellar bone is made up of layers called lamellae. In cortical bone, these lamellae are arranged in concentric rings surrounding a vascular channel. This structure is known as an osteon or Haversian system. Interstitial

lamellae fill the gaps between osteons, and circumferential lamellae form around all or part of the circumference of the bone shaft. Cancellous bone is made up of hemiosteons shaped like shallow crescents. Bone cells are found in small cavities (lacunae) between lamellae. Lacunae are connected to each other and to the Haversian canal by canaliculi. These small channels allow nutrients from the Haversian canal to reach bone cells and waste products to be removed.

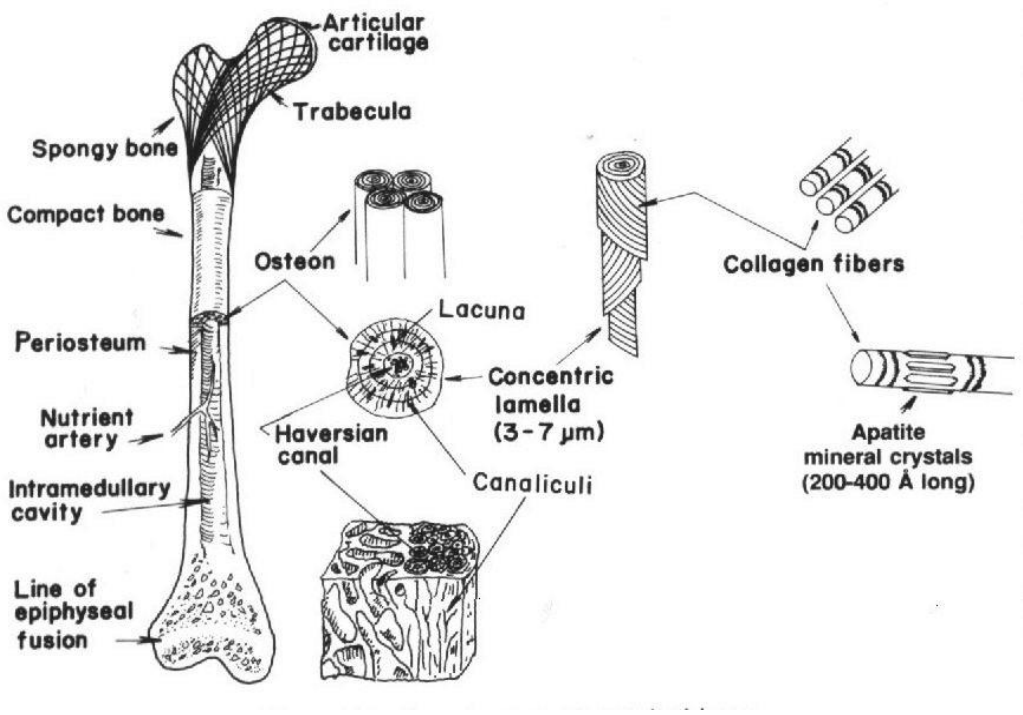

Figure 2.1 Levels of structural organisation in a typical bone [10]

Bones have an excellent blood supply, ensuring a good flow of nutrients necessary for growth and remodelling. The nerve supply to bone is not well understood, though it is known that the Haversian canals, periosteum and medullary vessels are innervated [9]. The surface of long bones is covered by the periosteum, a dense fibrous membrane, or by articular cartilage (in the joints).

Composition

Bone is essentially a composite material comprising two types of material, organic and inorganic. The organic component is made up of bone cells surrounded by a collagen extra-cellular matrix (ECM). Around the collagen fibres is a gelatinous substance consisting mainly of proteins including polysaccharides and glycosaminoglycans (GAGs) in the form of complex macro-molecules called proteoglycans (PGs). Embedded in the ECM is the inorganic component, which is largely made up of calcium phosphate in the form of hydroxyapatite ($Ca_{10}(PO_4)_6(OH)_2$). The calcium phosphate in bone is non-stoichiometric and contains ions other than its base components, such as carbonates, sodium and silicon ions. Bone also contains a large quantity of water (5 to 8% of the organic matrix by weight) [7].

2.1.2 Properties of bone

From a materials perspective, bone acts as a biphasic composite, with the mineral as one phase and the organic material as the other. The properties of bone vary greatly depending on factors such as the humidity, mode of applied load (compressive or tensile), rate of loading, degree of mineralisation, porosity, structural anisotropy and histology [10, 11]. Table 2.1 gives some mechanical properties of compact bone. These figures clearly demonstrate the anisotropy of the material, its relatively low Young's Modulus and the strain rate dependence of its fracture properties. It is important to consider these properties when designing a bone replacement material.

Table 2.1 Mechanical properties of human compact bone [12]

	Test direction related to bone axis	
	Parallel	**Normal**
Tensile strength (MPa)	124-174	49
Compressive strength (MPa)	170-193	133
Bending strength (MPa)	160	Not stated
Shear strength (MPa)	54	Not stated
Young's modulus (GPa)	17.0-18.9	11.5
Work of fracture (J/m^2)	6000 (low strain rate)	Not stated
	98 (high strain rate)	Not stated
Ultimate tensile strain	0.014-0.031	0.007
Ultimate compressive strain	0.0185-0.026	0.028
Yield tensile strain	0.007	0.004
Yield compressive strain	0.010	0.011

The basic structure and properties of bone have been described. The following section introduces the types of cells present in bone.

2.1.3 Cells

The four principal types of cells in bone are osteoclasts, osteoblasts, osteocytes and bone-lining cells [9]. These cells and their locations during a remodelling cycle are shown in Figure 2.2 which illustrates areas of bone resorption and formation in close proximity. Further details of the bone remodelling cycle are given in the following sections.

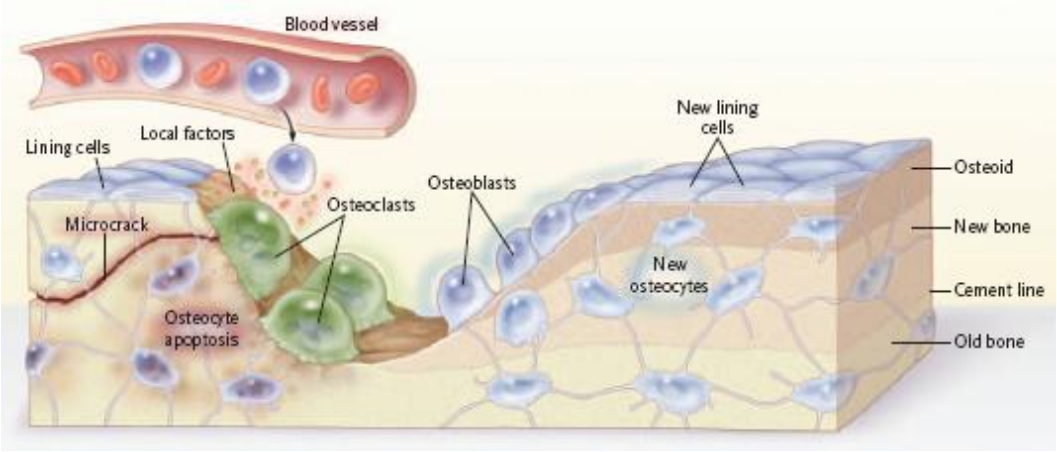

Figure 2.2 Bone cells during the remodelling cycle [13]. Note that osteoblasts measure 20-30μm [14].

Osteoclasts

Osteoclasts are multinucleated cells responsible for bone remodelling [9]. Resorption of mineralized tissues is obligatory for normal skeletal maturation [15]. The diameter of osteoblasts ranges from 20 to 100μm and they have a life span of up to seven weeks [16]. The area of the cell in contact with the bone has a ruffled border surrounded by a "clear zone". The cell adheres to the bone at this clear zone, allowing the formation of the microenvironment required for bone absorption [16]. When active, osteoclasts sit directly on the bone surface [17], and are usually found in cavities known as Howship's lacunae. To absorb bone, they secrete acids and hydrolases including H^+ ions, which dissolve the bone mineral. After resorption stops at a particular site, osteoclasts migrate into adjacent bone marrow and undergo apoptosis [16].

Osteoclasts originate from haemopoietic stem cells derived from bone marrow. The regulation of osteoclast differentiation and function is complex, and is closely linked to the function of macrophages, as shown in Figure 2.4.

Osteoblasts

Osteoblasts are fully differentiated mononucleated cells responsible for the formation of bone matrix. When inactive, osteoblasts become flattened and are referred to as bone-lining cells [18]. Active osteoblasts, however, have a cuboidal shape [19]. They have a relatively large nucleus, a pronounced Golgi area (responsible for storage and packing of materials to be exported from the cell), and a well-developed rough endoplasmic reticulum (RER) for the synthesis and export of ECM proteins. Osteoblasts contain a large amount of ribonucleic acid (RNA) [20]. Active human osteoblasts have a maximum dimension of 20-30μm [14].

Osteoblasts originate from mesenchymal stem cells, which are found near bone surfaces and in bone marrow. The differentiation of these pluripotent stem cells into osteoblasts is controlled by the tissue-specific transcription factor Runx2/Osterix [21]. Differentiation and proliferation of osteoblasts is regulated by various growth factors including bone morphogenetic proteins (BMPs) [22], fibroblast growth factors (FGFs) and the Indian Hedgehog Homologue (IHH) gene [23]. The bone-forming functions of these cells are influenced by levels of vitamin D [24], parathyroid hormone (PTH, a regulator of calcium homeostasis) [25] and insulin-like growth factors (IGFs) [26].

The protein expression of an osteoblast varies throughout its life as described in Table 2.2. It is therefore possible to accurately identify the stage to which an osteoblast has matured by the measurement of these proteins.

Table 2.2 Osteoblast protein expression (Adapted from [19])

Developmental stage	Proteins expressed
Preosteoblast	TGF-β osteopontin
Proliferating osteoblast	Histones, collagen type I
Maturing osteoblast/early differentiation	Alkaline phosphatase
Differentiating osteoblast	Osteopontin, bone sialo protein
Mineralisation	Osteocalcin

The functional lifespan of an osteoblast ranges from 3-18 months with an average life of 5-6 months [27]. Approximately 50-70% of osteoblasts die through apoptosis (Jilka *et al* cited by [19]), with the remainder becoming osteocytes or bone-lining cells. Active osteoblasts lay down bone matrix on the surface of trabeculae or Haversian systems via the synthesis of osteoid, which contains type I collagen and non-collagenous proteins (see the right hand side of Figure 2.2). Osteoid is subsequently mineralised to form the bone extracellular matrix (ECM). In addition to laying down osteoid, osteoblasts are thought to be implicated in the regulation of osteoclast activity [9].

Osteocytes

Osteocytes are the most numerous cells in mature bone. They are formed by the incorporation of an osteoblast into the bone matrix. During the transformation from osteoblast to mature osteocyte a cell loses 70% of its volume, though their length may increase to 20-60μm [16]. These cells are long-lived, but not immortal [28].

Osteocytes have a small amount of cytoplasm surrounding the nucleus and long cytoplasm extensions which spread out through the canaliculi of the bone to link the cells to other osteocytes. These cells are responsible for bone maintenance, having the ability to synthesise and resorb matrix locally [29]. They are thought to stabilise the

bone mineral by maintaining the ionic concentration that controls the exchange of calcium ions. They detect local damage to the bone and respond to strain [30].

Bone-lining cells

Bone-lining cells cover surfaces that are undergoing neither bone formation nor resorption [17]. It is possible for them to be reactivated into osteoblasts (Chow *et al*, 1998, cited by [19]). Bone-lining cells also have a role in the activation of bone remodelling via the production of signals for the activation of osteoclasts [31]. Before bone resorption begins, these cells digest the endosteal membrane and retract to expose the bone mineral [16].

2.1.4 Bone growth

Osteogenesis

During the growth of the skeleton, the majority of bone is formed by endochondral growth. This is the process by which cartilage matures, calcifies and is invaded with blood vessels [17]. The other mechanism by which bone grows is known as intramembranous ossification. In this process, bone forms without the intermediate formation of cartilage [9]: instead, connective tissue forms at the bone growth site. Some cells within the connective tissue differentiate into osteoblasts and lay down osteoid to form new bone [32].

Remodelling

In adults, continuous bone remodelling is necessary to maintain biomechanically and metabolically functioning tissue; it begins with the replacement of primary bone during infancy and continues throughout life [9]. This continuous remodelling allows bone to adapt its shape and architecture to form an efficient load-bearing structure [33]. Remodelling consists of a cycle of bone resorption and formation [34] as shown in

Figure 2.3. The cycle may be triggered by dynamic mechanical loading [33] or by hormonal responses to changes in calcium or phosphorus levels [35].

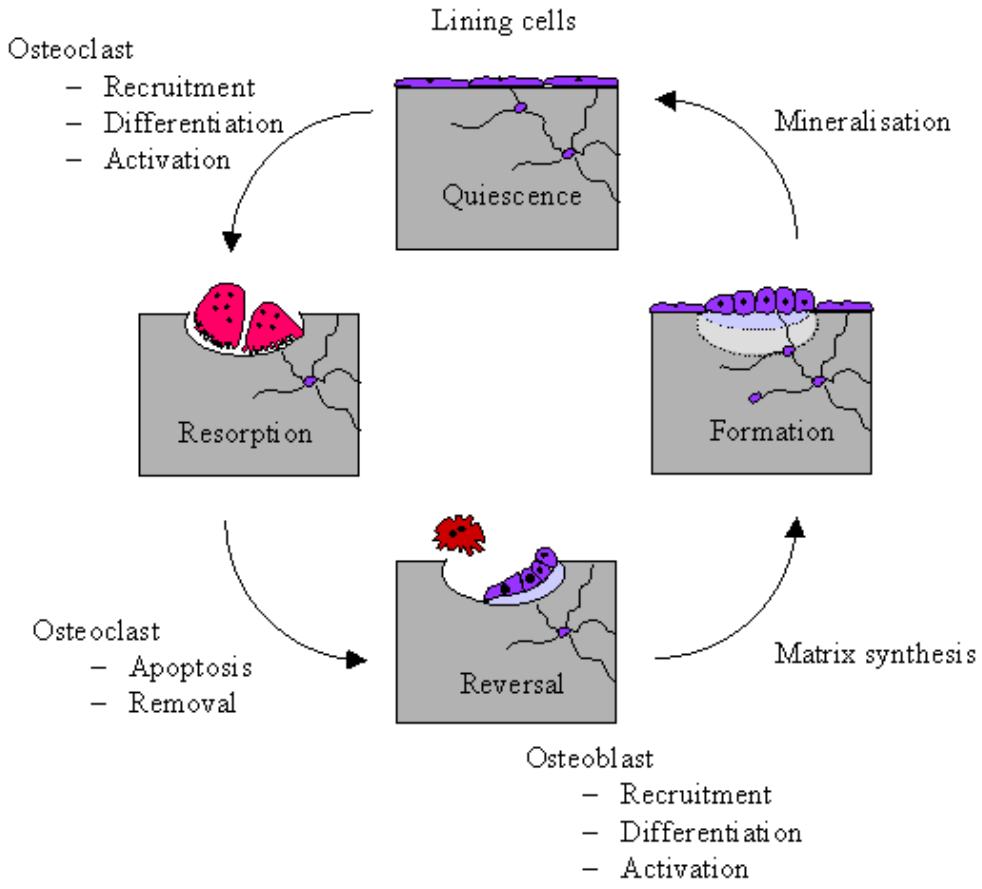

Figure 2.3 The bone remodelling cycle [36]

Adaptation to mechanical stimuli

Wolff's law states that mechanical stress is responsible for determining the architecture of bone and that bone tissue is able to adapt its mass and three-dimensional structure to the prevailing demands of stress-bearing [37, 38]. Various theories exist as to the details of this mechanism, though a complete explanation is yet to be developed [31, 39, 40].

Turner defines three key features of bone adaptation in response to mechanical stimuli [33]:

i. Bone adaptation is driven by dynamic, not static, loading.
ii. Only a short duration is necessary to initiate an adaptive response. Extending the loading duration has a diminishing effect on further bone adaptation.
iii. Bone cells accommodate to a customary loading environment, making them less responsive to routine loading signals.

It has been suggested that bone lining cells are responsible for activating the remodelling cycle, acting in response to biochemical signals from osteocytes [31, 41]. However, the exact role of osteocytes in mechanotransduction remains controversial, as it is not clear how osteocytes actually sense mechanical loading and transduce it into a cellular signal [42]. They are difficult to study as they do not proliferate and are located deep in the bone matrix [42]. Osteoblasts have also been shown to be sensitive to mechanical strain [43]. Stress generated potentials (SGPs) in bone are also thought to act as signals in mechanotransduction [5]. The mechanisms by which these potentials are produced are to be discussed in Section 2.4.

Despite the importance of bone cell responses to grafts, these are not the first cells to respond when a material is implanted. The response of macrophages to biomaterials is critical to their biocompatibility. The following section introduces the role of macrophages in immune and inflammatory responses to biomaterials.

2.1.5 Macrophages

Macrophages are phagocytic immune cells. They engulf, phagocytose or attach to foreign bodies and particles. They also mediate immune and inflammatory responses to foreign objects through the release of cytokines [44]. When a biomaterial is implanted in contact with tissues *in vivo* an interfacial tissue that contains macrophages and foreign-body giant cells may form. In such cases, macrophages have been shown to

represent 60–80% of the local cell population [45]. The presence of activated macrophages in this type of periprosthetic membrane has been linked to osteolysis around total joint replacements [46].

The production of cytokines in response to biomaterials, especially to biomaterial particles, is complex. Figure 2.4 shows potential mechanisms leading to the stimulation of osteolysis identified by Ingham and Fisher in their review of macrophage responses to ultra-high molecular weight polyethylene (UHMWPE) particles [46]. Inflammatory cytokines TNF-α and IL1 were found to play an important role in the differentiation of precursors to osteoclasts. They also stimulate osteoblasts to produce macrophage colony stimulating factor (M-CSF, a promoter macrophage development) and RANKL, leading to the differentiation and recruitment of osteoclasts at the implant site [46].

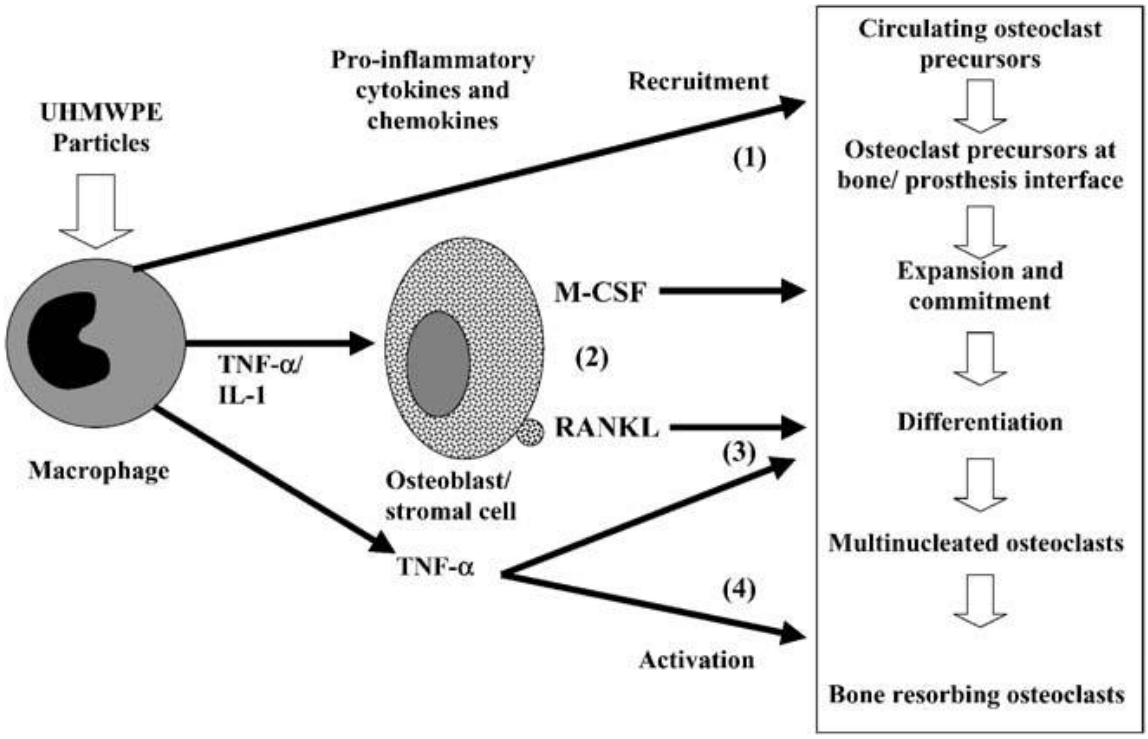

Figure 2.4 Potential mechanisms whereby UHMWPE particle-stimulated macrophages may stimulate osteolysis in total joint replacement [46].

The mechanism for the resorption of, and reaction to, biomaterial particles varies according to their size. Figure 2.5 illustrates the three primary mechanisms of macrophage resorption of biomaterials, namely phagocytosis, engulfment and extracellular degradation. In the case of bulk materials, macrophages may remain on the surface for years. It is therefore desirable for non-degradable materials to induce a lower level of macrophage response [44]. Small particles (0.10-1μm) have been found to be the most reactive in inducing inflammatory cytokine release [46]. However, it has also been shown that macrophages cultured on dense discs of titanium produce more inflammatory cytokines than those cultured with phagocytosable titanium particles (particle diameters 2.6±1.8μm) [47].

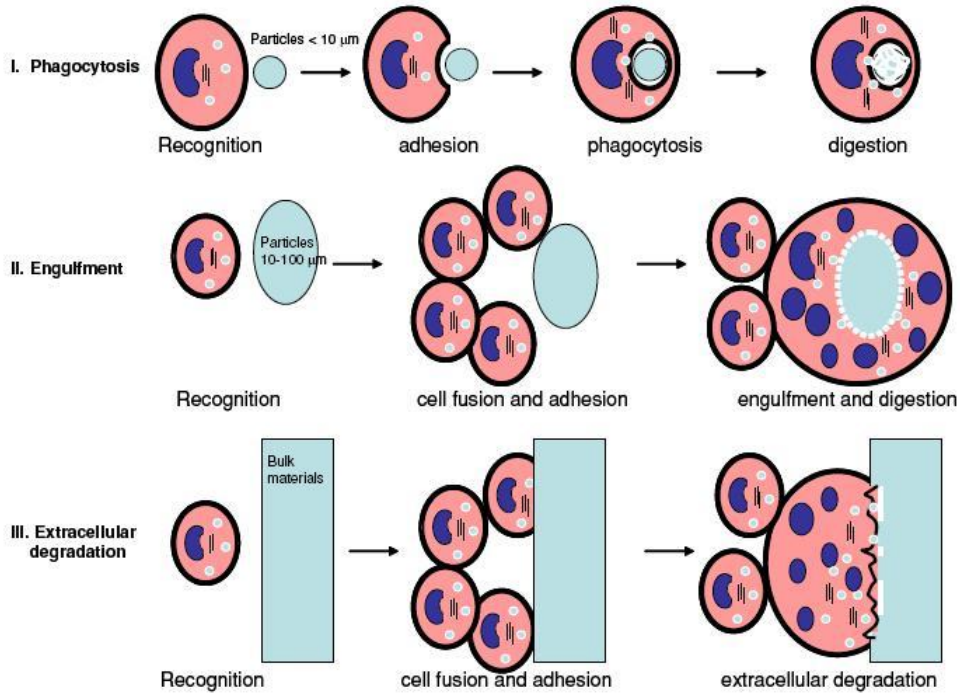

Figure 2.5 The schematic diagram showing macrophage responses to biomaterials. Macrophages respond to small particles (<10 μm) by phagocytosis (I). For large particles, macrophages fused to form foreign body giant cells (FBGC) to either engulf the particles (II) or remain on the surface of bulk materials (III) [44]

In addition to their phagocytic and immune system roles, macrophages are key to the regeneration of tissue in wound healing and osteoinduction. The wound is cleaned via the phagocytosis of debris particles. In bone, macrophages have been shown to produce bone morphogenetic proteins (BMPs), implying that they play an important role in osteoinduction by the promotion of differentiation of mesenchymal stem cells into osteoblasts [48]. In the same study, it was also shown that the presence of TNF-α reduces the expression of BMP-2 in the J774 macrophage cell line. The induction of proinflammatory responses (i.e. the production of TNF-α and IL1) from macrophages should therefore be avoided if the recruitment of osteoblasts to the material surface is desired. Although medium conditioned by culture with J774 cells was found to induce increased alkaline phosphatase production in mesenchymal stem cells, the addition of lipopolysaccharide (LPS) inhibited this effect. This implies that, when stimulated to produce TNF-α, J774 cells do not produce BMP-2 and therefore will not act to recruit osteoblasts. It has been noted that although unlikely, it is possible for biomaterials to be contaminated with endotoxins such as lipopolysaccharide (LPS) [49]. Contamination of this kind could lead to the induction of inflammatory responses in macrophages which are unrelated to the material itself.

Having summarised the structure, composition and biology of bone, the literature review will now focus on bone grafts and their uses.

2.2 Bone grafts

There is a growing need for materials suitable for the replacement of bone lost through trauma or disease and as a result of complications arising from joint replacement surgery. Bone grafts are used in either bulk or particulate form and are inserted into a defect to provide a scaffold for the regrowth of host bone. The following section discusses commonly used types of natural bone graft and potential bone graft substitutes.

2.2.1 Current practice in bone grafting

Nine out of ten bone replacement procedures carried out in the United States use either autograft or allograft bone tissue [1, 50]. Autograft material is considered to be the "gold standard" from a biological point of view [2]. It is taken from a donor site in the patient's own body, usually from the iliac crest. Autograft has the benefit of assured compatibility with the host tissue. It is naturally osteoconductive, osteogenic and osteoinductive. Allograft material is harvested from patients undergoing total joint replacement as a consequence of diseases such as osteoarthritis. The harvested bone is then freeze-dried and stored in bone banks. Both types of bone graft are available in particulate and bulk forms [51].

Each of these sources has its own disadvantages. The use of autograft carries increased risk of infection, pain due to the additional surgical procedure of harvesting the bone and donor site morbidity [2, 52]. Allograft carries the risks of infection and rejection of donor tissue and there are shortages in supply. It is therefore desirable to design artificial bone graft substitute materials, as synthetic bone graft substitutes have no limits on the amount of usable material that can be manufactured. They could be produced in shapes appropriate for specific reconstructions and reduce the risk of complications associated with a second surgical site. These materials are to be discussed in more detail in Section 2.2.3.

2.2.2 Applications of bone grafting

Bone grafts are used in the treatment of a wide range of conditions. Procedures in which they are used include revision of total joint replacement, spinal fusion and maxillofacial surgery. Some of the most common applications are briefly introduced here.

Over 147 000 total hip replacements (THR) and total knee replacements (TKR) were carried out in the UK in 2007 [53]. Unfortunately, it is often necessary to revise total joint replacements and replace lost bone stock. Currently around 10% of THR and TKR surgeries are revisions [53]. In THR revision bone graft is needed to fill the large femoral cavity created by the removal of the original implant. Allograft material is typically used because of the relatively large amount of graft material required for the procedure. It is important for the graft material to be sufficiently mechanically stable to prevent subsidence of the revision implant. Allograft is also used in the majority of acetabular reconstructions [54]. The material may be in the form of morsellised [55] or bulk graft, though the use of bulk graft remains controversial in acetabular reconstruction as the likelihood of failure increases as larger grafts are used [54].

Interbody spinal fusions involve the creation of a bone regenerative bridge between two vertebrae. Cages made from various materials are used to provide mechanical stability and stiffness, with the graft material placed inside the cage. Both autograft and allograft are used in spinal fusion applications, though there is some discussion as to which is preferable [54]. Calcium phosphates in various forms have been used inside cages as an alternative to autograft and allograft substitutes [56, 57]. Other bone graft substitutes available for use in spinal fusion include collagen and biodegradable polymers [57]. Other procedures in which bone grafts are commonly used include repair of fractures [58] and maxillofacial surgery.

2.2.3 Bone graft substitute materials

The ideal bone graft substitute would replace bone temporarily, providing a scaffold for the growth of new bone, blood vessels and soft tissue, being replaced over time by natural host tissue. It would interact with surrounding bone, promoting differentiation of osteogenic stem cells [12, 59].

Materials used as substitutes for natural bone in grafting procedures include ceramics, bioactive glasses, coral derived products, polymers, calcium sulphate, and demineralised bone graft. Calcium phosphates including HA and β-tricalcium phosphate (β-TCP) are among the most commonly used of these ceramics [2]. They are available in the form of granules, blocks in a range of porosities and cements. The reader is referred to a recent review for information on calcium phosphate cements [60].

The following section discusses the nature and medical use of calcium phosphates before summarising approaches which have been undertaken with the aim of improving current calcium phosphate bone grafts.

2.3 Calcium phosphates

2.3.1 Natural calcium phosphates

In the human body, calcium phosphate (CaP) forms the mineral content of bone. It makes up 60-70% of the dry weight of the skeleton, in a form resembling HA ($Ca_{10}(PO_4)_6(OH)_2$) [7]. For replacement of bone, calcium phosphate-based biomaterials require appropriate mechanical properties and porosity as well as biocompatibility [61].

2.3.2 Synthetic calcium phosphates

In general, CaP ceramics are bioactive, biocompatible, osteoconductive and may become osteoinductive when used in conjunction with bone morphogenetic proteins (BMPs) [62]. Osteoconductivity is dependent on the porosity of the graft material [63]. It is necessary to find a compromise between enlarged pore size (for increased osteoconductivity) and the associated reduction in mechanical strength, as porosity characteristics strongly affect the mechanical properties of ceramic foams [64].

CaP ceramics are therefore suitable for a variety of medical applications including use as dental implants, coatings for metallic implants and artificial bone grafts. The exact properties of calcium phosphates depend on the atomic Ca:P ratio, presence of water (both in synthesis and in the environment during use), impurities and sintering temperature [65].

CaP ceramics exist in various phases. HA has a Ca:P ratio of 1.67 and can be referred to as stoichiometric HA. It is bioactive: when in contact with bone an electron-dense layer forms at the interface containing high concentrations of Ca and P ions, permitting the creation of a direct chemical bond between bone and implant [66]. β-TCP ($Ca_3(PO_4)_2$) is resorbable, resulting in a region of free Ca and P ions adjacent to the implant site, stimulating osteoblastic activity and therefore bone growth. When heated to 1180^0C, β-TCP is transformed into α-TCP. The chemical composition of the material remains unchanged but α-TCP has a higher volume (and therefore lower density). Both HA and β-TCP may occur within the same ceramic sample in what is known as biphasic calcium phosphate. This material degrades more quickly than pure HA and is commercially available as a bone graft substitute designed to be mixed with autograft in spinal fusion procedures [2].

2.3.3 Calcium phosphates as bone graft substitutes

The factors important to the success of a CaP ceramic bone graft substitute include:

i. bioactivity
ii. osteoconductivity
iii. mechanical properties.

The mechanism by which bioactive ceramics interact with the biological environment has been studied extensively [67]. The rate at which a bioceramic is resorbed is dependent on its bioactivity. Achieving an appropriate resorption rate is key to

producing a successful bone replacement material [59]. Crystallinity influences the absorption of particles at the surface, altering the ability of osteogenic cells to attach to it [2, 68]. HA resorbs very slowly (e.g. over decades), while β-TCP is resorbed much more quickly (e.g. in months) [2]. In order to produce a calcium phosphate material which is more quickly resorbed, a biphasic CaP or composite of HA with a polymer or collagen may be used [69, 70].

In order to be osteoconductive, a material must have the appropriate pore size and interconnectivity of pores. Osteoid and fibrous tissue ingrowth occurs in pores of 50-150μm, though the minimum pore size allowing new bone formation in the material is 150μm [71, 72]. It is generally accepted that the volume of bone ingrowth increases with pore size [63]. Also, pore sizes between 300 and 500μm are thought to encourage vascularisation [1, 73]. A high level of pore interconnectivity is also highly important in order to allow the development of vasculature, leading to osteogenesis [2, 74, 75] .

Unfortunately, increased pore size and interconnectivity usually leads to a reduction in mechanical strength [76]. Sufficient strength is required to withstand large multiaxial cyclic loads if graft substitutes are to be used in load-bearing applications. For reference, the compressive strength of compact bone parallel to the axis of the bone is 170-193MPa [12], as shown in Table 2.1. A compromise must therefore be reached between these conflicting requirements.

The addition of reinforcing materials to form HA-based composites can go some way towards improving mechanical properties in HA graft materials. Various reinforcements have been used including platelets and whiskers of HA and partially stabilised zirconia [12]. In general, the addition of such materials reduces the bioactivity and biocompatibility of the HA, though this is not the case for HA/bioglass composites [12].

However, HA open porous scaffolds and spinal fusion bioceramics have been manufactured with improved mechanical resistance and structural characteristics compared to a commercially available product. These materials were produced using a foam replication method. The improvement in mechanical properties was achieved by applying sol-gel solutions as low viscosity coatings before sintering to reduce the number of surface defects in the ceramic [64]. Another study of ceramics produced using foam replication measured strengths comparable to that of human bone [72]. This was achieved using a vacuum impregnation technique which substantially filled the foam with slurry before sintering. This study also produced functionally graded materials which mimicked the cortical-cancellous structure of natural bone [72].

2.3.4 Improvements to calcium phosphate bone grafts

Various techniques may be employed to improve the performance of calcium phosphate-based synthetic bone graft materials in terms of their osteoconduction and osteoinduction. Growth factors such as transforming growth factor-β (TGF-β), fibroblast growth factor (FGF) and bone morphogenetic proteins (BMPs) [77] can be synthesised *in vitro* and included in graft materials. The inclusion of BMP-2 in an HA scaffold has been found to increase production of ALP in osteoblast-like cells *in vitro* [78]. Mesenchymal stem cells may be differentiated *in vitro* to form osteoblast-like cells for use in bone graft substitutes but this technique is yet to be used in a commercially available product [77].

Another approach to the improvement of the biological response to calcium phosphates is the inclusion of mineral [79] or silicon ions, producing a material that reproduces more accurately the composition of the mineral phase of bone [80]. Silicon substitution has been shown to significantly improve the bioactivity tested both *in vitro* with human osteoblast-like cells [81] and *in vivo* in ovine models [80]. Similarly, magnesium-substituted HA has induced improved osteoconductivity and resorption *in vivo* in comparison to pure HA [82].

It may also be possible to improve the biological response to HA-based materials through the use of electrical charges or stress generated potentials. The induction of a surface charge on HA has been shown to modify biological responses *in vitro* [83]. A combination of HA with a piezoelectric ceramic component, barium titanate (BT), has been shown to induce an improved bone growth around an implant [6]. The literature indicates that the inclusion of electrically active components to HA bone grafts, in particular adding a piezoelectric component to a CaP graft, is an area that warrants further investigation. The following section gives a brief introduction to electromechanical effects in piezoelectric ferroelectrics and in bone, before discussing in more detail published research on the influence of charged and piezoelectric materials on biological responses in bone, both *in vitro* and *in vivo*.

2.4 Electromechanical effects

It has been known since the 1950s that bone exhibits piezoelectric properties, i.e. that it produces electrical charge when mechanically stressed [84]. Subsequently, streaming potentials (strain-generated potentials produced when a charged fluid flows over a charged surface) have been identified as another source of stress-generated potentials (SGPs) in bone [17, 85]. These phenomena have been linked to the mechanical adaptation of bone in response to loading (Wolff's law) [86-88]. It is therefore of interest to examine these effects, as well as the electromechanical behaviour of potential bone graft substitute materials, in order to make use of them in improving implant performance.

2.4.1 The piezoelectric effect and ferroelectric materials

The piezoelectric effect was first discovered by Pierre Curie in 1880. It is a property of certain crystals whereby an electrical polarisation is produced by the application of a mechanical stress as illustrated in Figure 2.6. This is known as the "direct" piezoelectric

effect. In the "converse" piezoelectric effect a crystal becomes strained when an electrical field is applied.

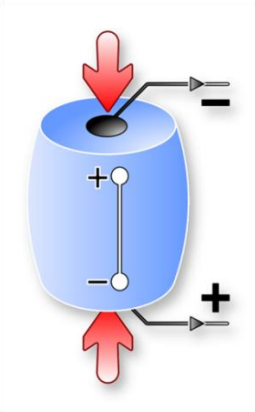

Figure 2.6 The direct piezoelectric effect [89]

2.4.2 Ferroelectrics

Ferroelectricity is a property of certain ionic crystals whereby they exhibit a spontaneous dipole moment. All ferroelectric materials are piezoelectric, though not all piezoelectric materials are ferroelectric. Quartz is a non-ferroelectric piezoelectric material in which the movement of unit cells creates a dipole moment when the material is compressed.

Barium titanate, $BaTiO_3$ (BT) is a ferroelectric material. It has been shown to be biocompatible in canine subjects *in vivo* and to generate electric currents after implantation in bone, though it has not been shown that the growth of bone in these implants was induced by stress generated potentials [90-92].

BT has a perovskite crystal structure and above the Curie temperature is cubic, with atoms of barium at each corner of the unit cell, a single atom of titanium in the centre and oxygen atoms placed in the faces of the cube (see Figure 2.7). These atoms are ionically bonded due to the exchange of electrons. When the crystal is heated above its Curie temperature its crystal structure is cubic and symmetrical. The material is non-

ferroelectric and exhibits no dipole moment. If the material is cooled below the Curie temperature, the structure is tetragonal and the titanium ion moves away from its central position, creating the asymmetrical pattern necessary (tetragonal, for example) for the generation of a dipole moment within the unit cell.

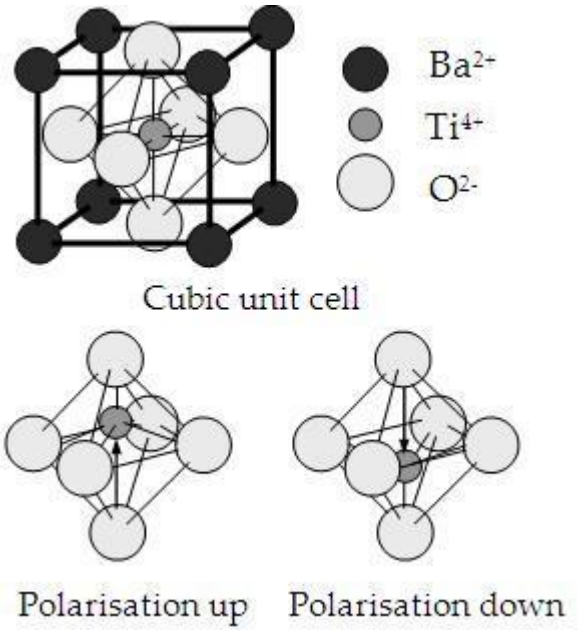

Figure 2.7 Cubic unit cell for BT, illustrating polarisation in two of the six possible polarisation states produced by the displacement of the central cation in the tetragonal phase (Adapted from [93])

Within each crystal, domains (groups of unit cells) occur in which the dipole moments of the unit cells are aligned in the same direction. If the domains in the material are randomly orientated, as in Figure 2.8a, there is no net polarisation. As a result, on the application of a mechanical stress the domains cancel each other out and no charge is generated. In order to align the domains and produce a piezoelectric material it is necessary to "pole" the material.

During the poling procedure, a ferroelectric material is heated to an elevated temperature below its Curie temperature in the presence of a strong electric field (~1-2kVmm^{-1} [94]). This process has the effect of aligning the domains in the direction of

the electric field, meaning that the crystal has an overall dipole moment as in Figure 2.8b. The material is then cooled to room temperature and the electric field removed. The domains remain aligned and the material is now polarised and piezoelectric. In this state, the application of an electric field produces a deformation of the unit cells and therefore the crystal. Conversely, an applied mechanical deformation varies the separation between the various differently-charged parts of the unit cell, creating an internal voltage. The piezoelectric constant (d_{33}, a measure of charge induced per unit force) is dependent on fabrication conditions, but values of d_{33} of between 87pCN^{-1} [95] and 190pCN^{-1} [96] have been reported for BT ceramics. As shown in Figure 2.8c, the material exhibits a polarisation direction along a "poling axis". This is often termed the "3" direction, as in the piezoelectric coefficients in Section 2.4.3.

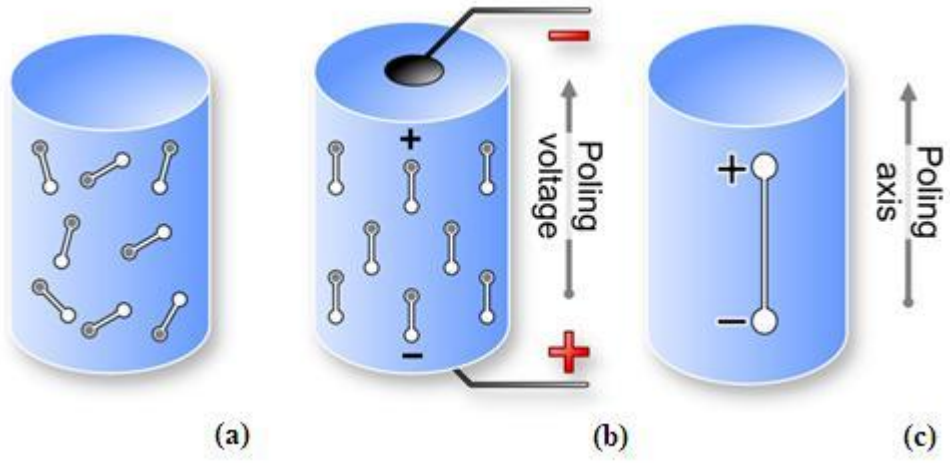

Figure 2.8 The production of piezoelectrics by poling [89]. (a) Initial random domain orientation (b) application of heat and electric field to align domains and (c) cooling and removal of field leaves poled material with poling axis.

2.4.3 Piezoelectric coefficients

The piezoelectric sensitivity of a material is given by the piezoelectric charge coefficient, d_{ij}, where i denotes the direction in which the electric field is developed and j denotes the direction in which the stress is applied. The orthogonal axes used in defining the properties of a piezoelectric material are shown in Figure 2.9.

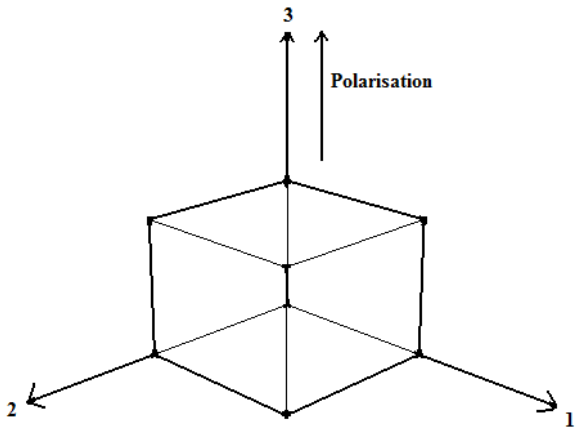

Figure 2.9 The orthogonal axes of a piezoelectric material

Axis 3 corresponds to the direction of poling. The d_{33} therefore corresponds to the charge generated per unit force, with the force applied in the direction of poling. The d_{31} is the charge per unit force, with the force applied perpendicular to the poling direction. The charge coefficient may therefore be defined by the following equation:

$$d = \frac{Q}{F} \tag{2.1}$$

where Q is the charge generated and F is the applied force. The charge coefficient may be defined either as the charge per unit force generated in the material (CN^{-1}) or as the strain per unit of electric field (mV^{-1}) according to the Equation 2.2, where S = strain, E = electrical field strength, D = electrical displacement and T = applied stress. The subscripts indicate the parameter which is kept constant in each case.

$$d = \left[\frac{S}{E}\right]_T = \left[\frac{D}{T}\right]_E \tag{2.2}$$

The piezoelectric voltage coefficient, g_{33}, is the electric field produced per unit of applied stress:

$$g_{33} = \frac{E}{T} \tag{2.3}$$

The g_{33} coefficient may also be calculated the following equation:

$$g_{33} = \frac{d_{33}}{\varepsilon} \tag{2.4}$$

where ε is the absolute permittivity of the material. The electrical displacement (*D*) is the surface charge divided by the surface area (*A*):

$$D(t) = \frac{Q(t)}{A} \tag{2.5}$$

The polarisation (P) may then be calculated by the following equation:

$$P(t) = D(t) - \varepsilon_0 E(t) \tag{2.6}$$

where *E* is the electric field and ε_0 is the permittivity of free space. The relative permittivity (ε_r) of the material is calculated using equation 2.5:

$$\varepsilon_r = \frac{Ct}{A\varepsilon_0} \tag{2.7}$$

where C is the capacitance, t is the distance between the plates, A is the surface area and ε_0 is the permittivity of free space.

The dielectric and piezoelectric properties of barium titanate are known to diminish over time [97]. This occurs due to the relaxation of stresses induced in the poling process [98]. The rate of loss therefore diminishes over time and is expressed in % per time decade. As ageing after poling occurs approximately logarithmically, the majority of ageing occurs in the first hours after poling [99]. The piezoelectric coefficient of a newly-poled material is therefore normally measured 24h after poling.

The piezoelectric properties of a material can be further explained by the examination of its polarisation-field (P-E) curve. This hysteresis effect results from the delay between the application of a voltage to the material and the movement of domain walls within it. It results from the "pinning" of domain walls (the prevention of domain wall movement), caused by inclusions or vacancies in the crystal structure [100]. A typical P-E loop for a typical piezoelectric material is shown in Figure 2.9. Table 2.3 explains the form of the curve.

It is also possible to generate a characteristic strain-field (S-E) curve for each piezoelectric material, as shown in Figure 2.10. The form of the curve, often described as a "butterfly loop" due to its shape, is explained in terms of strain and motion of domains in a piezoelectric ceramic in Table 2.4. At low applied fields domain switching does not occur and the S-E curve is linear. As the piezoelectric coefficient of a material may be expressed as the strain in the material divided by the electrical field (Equation 2.1), the gradient of the low-field (linear) S-E curve is the piezoelectric coefficient in the form of strain per unit of electric field (mV^{-1}).

Typical P-E and S-E loops for BT are given in Figure 2.12. Note the "bias" in the loops for poled BT samples (Figure 2.12b and 2.12d). This is caused by the alignment of domains in the poled material.

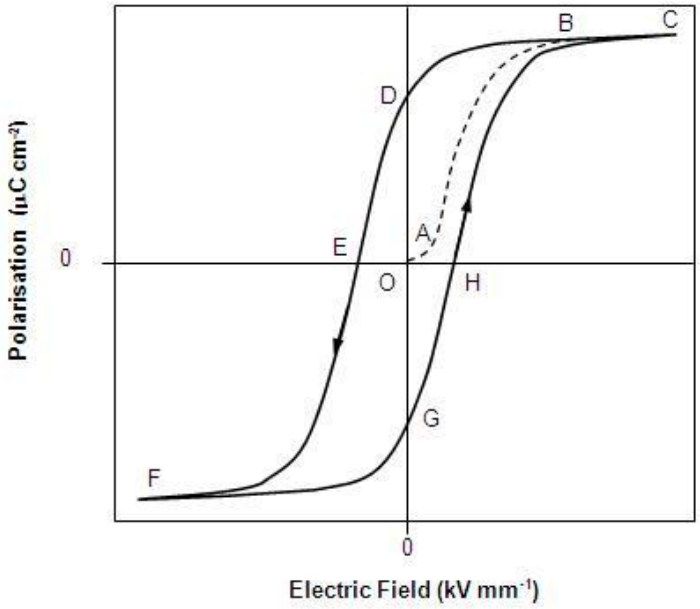

Figure 2.10 Polarisation-field curve for a piezoelectric material [101].

Table 2.3 The relationship between the polarisation-field curve and the movement of domains within a piezoelectric material (Adapted from [101]).

Section of Curve	Process
O-A	The P-E relationship remains linear when the field is small as the material behaves as a linear dielectric
A-B	Domain switching causes a rise in polarisation as the field is increased.
B-C	Once all domains have switched to align in a common direction, saturation occurs.
C-D	As the field is removed, some domains remain aligned, resulting in a remnant polarisation (P_r) when the field returns to zero (point D).
D-E	To remove the remnant polarisation, a negative field must be applied to the material. The strength of field required to return the material to an unpoled state is known as the coercive field (E_c).
E-F	A further increase in the negative field strength causes complete alignment of the dipoles in the opposite direction.
F-G-H	The cycle is completed by reversing the field again.

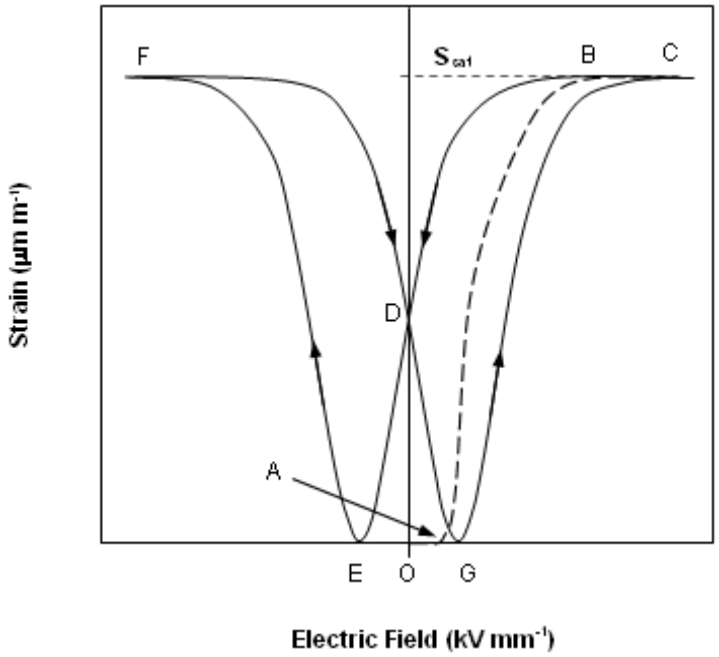

Figure 2.11 Strain-field curve for a piezoelectric material [101]

Table 2.4 The relationship between the strain-field curve and the movement of domains within a piezoelectric material (Adapted from [101] and [102])

Section of Curve	Process
O-A	The strain in the crystal remains at zero because the domains are randomly aligned.
A-B	As the applied field increases, domains begin to align and the crystal expands through the piezoelectric effect.
B-C	Once all domains have switched to align in a common direction, no further increase in strain occurs.
C-D	As the field is removed, some domains remain aligned, resulting in a remnant strain (S_r) when the field returns to zero (point D).
D-E	To remove the remnant strain, a negative field must be applied to the material. The strength of field required to return the material to an unpoled state is known as the coercive field (E_c).
E-F	A further increase in the negative field strength causes complete alignment of the dipoles in the opposite direction.
F-G-H	The cycle is completed by reversing the field again.

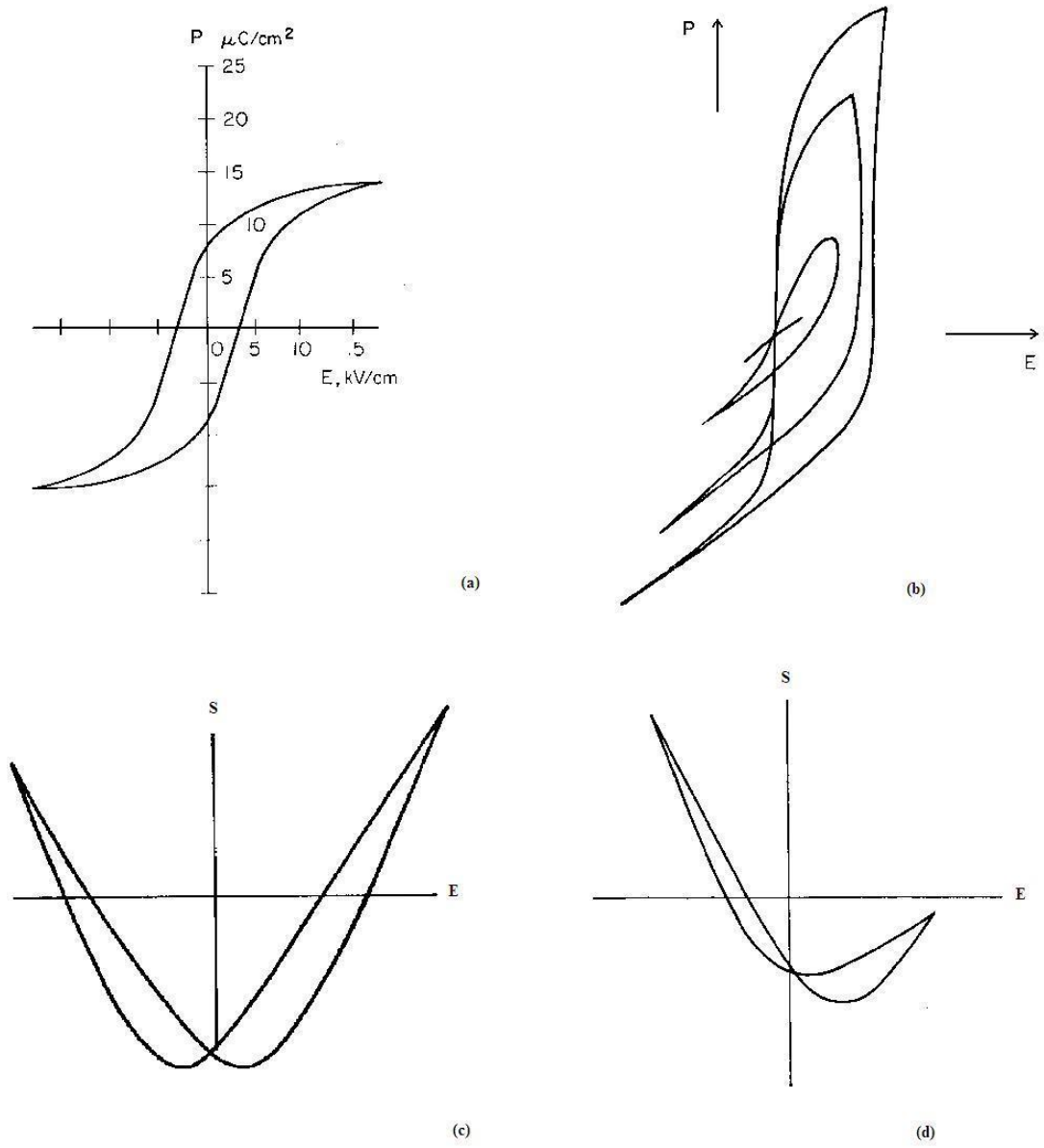

Figure 2.12 (a) Polarisation-field loop for high quality BT (b) Polarisation-field loops for poled BT at applied fields of 1, 2, 5 and 10 kVcm^{-1} (c) Strain-field loop for unpoled BT and (d) strain-field loop for poled BT at a peak field of 10kVcm^{-1} (Adapted from [97])

Lead zirconium titanate (PZT, $Pb(Zr,Ti)O_3$) is another piezoelectric material which has a perovskite structure. It displays significantly stronger piezoelectric properties than BT, with a d_{33} of between 300 and 550pCN^{-1} [95]. However, though PZT does not appear to be toxic to cells (Zomorrodian *et al*, 2001, cited by [103]), there is concern over

using PZT in medical applications due to lead oxide toxicity [103]. There is also European legislation restricting the use of lead based materials [104]. This legislation does not currently apply to implanted medical products, only to "medical equipment systems", however the known toxicity of lead should not be ignored [105].

Most of these materials are polycrystalline and consist of randomly arranged grains. However, some materials (including BT) are available in single crystal form. While being limited in size and shape and therefore unsuitable for direct use in a bone graft replacement, these materials display high piezoelectric coefficients and may therefore be useful in testing the response of bone cells to stress-generated potentials.

In investigating the possible improvement of the biological performance of CaP bone graft materials using piezoelectric components, it is desirable to understand the piezoelectric performance of composites containing electrically inert materials. This is discussed in the following section.

2.4.4 Piezoelectric composites

The piezoelectric properties of hydroxyapatite-barium titanate (HABT) composites containing varying volume fractions of BT were examined by Aba and Erdun [106]. A rapid decline in piezoelectric properties was observed as the volume fraction of HA in the composite increased. No piezoelectric charge coefficient was recorded for composites containing less than 80% BT. The piezoelectric charge coefficient of the BT used in this study, $20pCN^{-1}$, was significantly lower than previously reported values which are in the range of $87pCN^{-1}$ [95] and $190pCN^{-1}$ [96]. The phase stability of composites containing lower proportions of BT (10-20%) was examined. For materials sintered at 1300°C in air, the formation of non-piezoelectric phases ($BaTiO_4$ and calcium titanate) was reported. The authors attribute the absence of piezoelectric properties in the composites to this phase substitution. The composition of the sintered ceramics

was dependent on the sintering conditions used. The reduction of piezoelectric properties in ferroelectric composites may also result from matrix "clamping", whereby the non-ferroelectric component limits the deformation (strain) and therefore the voltage induced in the composite for a given applied force [107].

The permittivity bounds of a random piezoelectric composite may be estimated using following the series and parallel equations:

$$\varepsilon_c = \nu_1 \varepsilon_1 + \nu_2 \varepsilon_2 \tag{2.8}$$

$$\frac{1}{\varepsilon_c} = \frac{\nu_1}{\varepsilon_1} + \frac{\nu_2}{\varepsilon_2} \tag{2.9}$$

where the subscript c denotes the composite, υ_1 and υ_2 are the volume fractions of the two components, and ε_1 and ε_2 are their permittivities. The permittivity of a random composite should fall between these series and parallel bounds, which are illustrated in Figure 2.13.

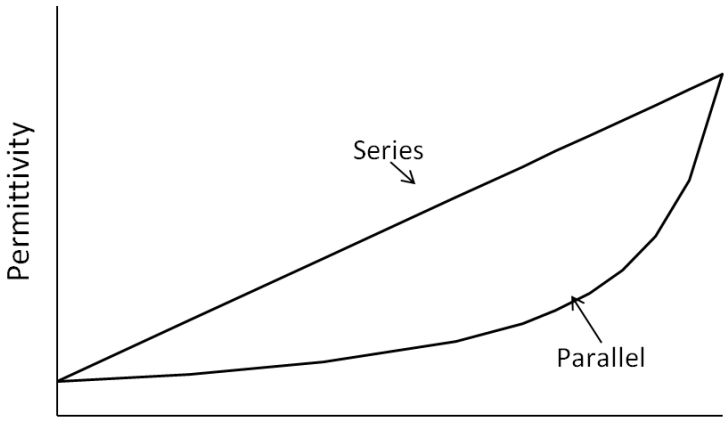

Figure 2.13 The theoretical series and parallel bounds for the permittivity of a piezoelectric composite

2.4.5 Grain sizes in piezoelectric ceramics

In a study of lead zirconate-titanate ceramics, diminishing grain size was found to contribute to a rapid decrease in d_{33} for grain sizes below 1μm [108]. An explanation of this phenomenon is offered by other researchers [109], who found that domain wall motion, and therefore piezoelectric properties, are limited by grain size. Though domain size in BT has been linked to grain size [110], with clamping by adjacent grains hindering domain formation [109], the influence of domain size and grain size on piezoelectric coefficient in BT ceramics remains uncertain when grain sizes are large. In particular, one group measured the piezoelectric coefficients of BT ceramics with grain sizes between 1 and 100μm [10]. They observed no relationship between the grain size and the piezoelectric coefficient, finding high coefficients (d_{33} = 350pCN^{-1}) in a BT-based ceramic with small grains (2.1μm).

The following section will discuss the piezoelectric effects observed in bone.

2.4.6 Electromechanical effects in bone

Fukada and Yasuda were the first to measure and propose a mechanism for piezoelectricity in bone [84]. They suggest that the piezoelectric effect occurs when shearing forces cause collagen fibres in the bone to slip past each other. The origin of the piezoelectric effect is ascribed to the asymmetric collagen molecules within the bone and the development of a dipole (analogous to the asymmetrical unit cell in BT). Collagen fibres are oriented parallel to the long axis of the bone which form helices within the lamellae forming the Haversian stems, oriented at various angles. The overall orientation of the collagen is therefore in the direction of the bone axis and results in the occurrence of the piezoelectric effect and therefore the development of charge on the application of load [111].

Due to the symmetry of the collagen fibres only two constants, d_{14} and d_{25} (equal but opposite to d_{14}), represent the piezoelectric effect in bone. Fukada and Yasuda reported the highest value of d_{14} to be $6x10^{-9}$ c.g.s.e.s.u. ($0.2pCN^{-1}$) [84], though a later study found values as high as $14x10^{-9}$ c.g.s.e.s.u. ($0.7pCN^{-1}$) [112]. These values are notably smaller than those generated in BT ($87pCN^{-1}$ - $190pCN^{-1}$ [95, 96]).

It is generally accepted that the electromechanical properties of wet and dry bone are different and cannot be explained by a single mechanism: both streaming potential and piezoelectricity are thought to occur in live bone [113]. The extracellular bone matrix is negatively charged due to the presence of proteins. The extracellular matrix is deformed in mechanical loading, inducing a flow of positively charged fluid and therefore developing streaming potentials [5]. The site of this mechanism within the bone is under debate, though the interstitial fluids are thought to move within bone canaliculi [114, 115]. Streaming potentials are thought to be part of the mechanosensory mechanisms in bone by which mechanical forces influence bone remodelling [4, 5].

2.4.7 Poling of HA

Though HA is neither ferroelectric nor piezoelectric, it is possible to induce polarisation in HA ceramics. When the ceramic is heated, ion carriers become free to move. Under an applied electric field these carriers are attracted to one surface of the material. The field is left in place until the material has cooled, fixing the ions in place and leaving a residual surface charge. Although the exact nature of the mechanism for the polarisation of HA remains uncertain, these ion carriers are thought to be H^+ ions (protons) moving within the OH^- columnar structure of the material [116, 117]. One published study claims to demonstrate P-E hysteresis data and remnant polarisation for HA [118], however, the data presented shows P-E loops typical of a "lossy capacitor" as opposed to a ferroelectric material [97].

2.5 Electrical effects in biomaterials for bone graft

The influence of electrical charges and voltages on biological responses to bone graft materials has been investigated in a number of studies. The following section discusses the *in vitro* bioactivity testing of charged and piezoelectric materials through submersion in simulated body fluid (SBF) or culture medium before examining both *in vitro* and *in vivo* biological responses to them. In many cases, the piezoelectric properties or surface charges of the materials tested are not given in the literature. Where they are given, details are included in this review.

2.5.1 Bioactivity testing

In one study of CaP formation on BT, samples of BT were immersed in SBF for 30 days [119]. CaP was found to form preferentially on the negative surfaces of the poled samples, as seen in Figure 2.14b, which demonstrates the presence of CaP formation in comparison with Figure 2.14a (the surface before soaking) and Figure 2.14c. The authors suggest that this demonstrates an increased capacity for bone development on negative surfaces. Though the piezoelectric properties are not given, the poling conditions used (poling in a silicon oil bath whilst cooling from 160°C-25°C over 2 hours with an applied field of $5kVcm^{-1}$) were suitable for inducing a piezoelectric coefficient in the ceramic. A similar study by the same group immersed BT in Modified Eagle's Medium (MEM) [120]. Preferential growth of CaP crystals was observed on the negative surface as compared to the positive surface. The authors suggest that Ca^{2+} ions adsorb more rapidly on the negative surface and act as nuclei for the formation of CaP. Similar results were found on both poled HA and poled BT by other authors [121]. In addition, a similar study evaluated CaP formation on BT thin films immersed in MEM [120]. A thicker, more homogeneous layer of CaP formed on negatively polarised BT compared to that on the unpoled film. Positively polarised films were not tested.

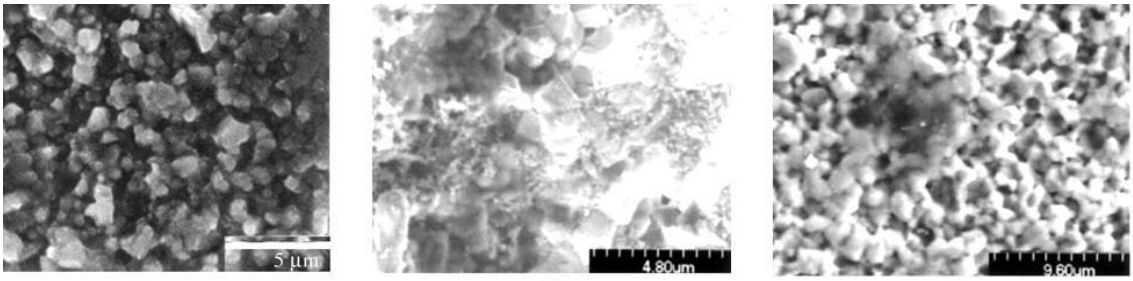

Figure 2.14 Poled BT soaked in SBF for 30 days, (a) before soaking (b) negative surface showing formation of CaP on the surface and (c) positive surface showing no formation of CaP (Adapted from [119]).

A more recent study agreed with the above findings for HA soaked in "stable" SBF solution in which no particles were allowed to form [3]. Deposition of CaP on positive surfaces did occur, however, when "unstable" soaking solutions were used. In these solutions the pH or ionic concentrations were altered to allow the nucleation of CaP in the solution. It may therefore be concluded that the results observed in this type of study are highly dependent on the exact concentration of ions in the soaking solution.

2.5.2 *In vitro* studies

Cell attachment

It has been suggested that the attachment of cells to charged surfaces is mediated by the adsorption of serum protein from the culture medium [122]. It has been concluded that bone cell morphology and subsequent development are affected by the charge of the culture substrate as the nature of the protein population creating the cell-material interface is affected by charge [123]. The proposed differences in cell morphology are shown in Figure 2.15. On positively charged surfaces both the intracellular and cell-substrate spaces are small. The author suggests that the forces between the charged surface and the cell membrane are too large for cells to overcome and limit the

production of extracellular matrix. On negatively spaced surfaces, intracellular spaces and cell-substrate spacing are greater.

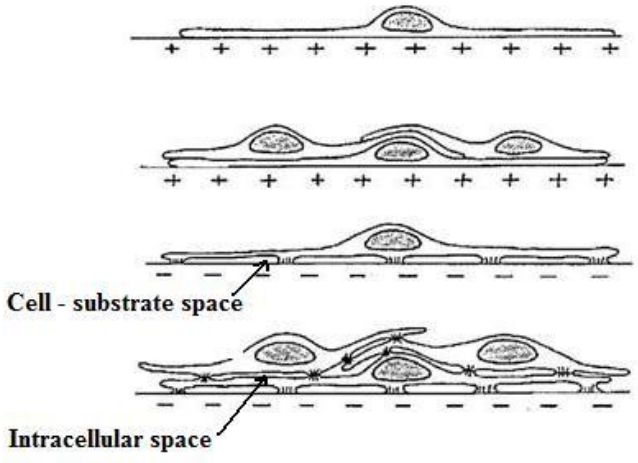

Figure 2.15 The morphological differences associated with the migration of osteoblasts over substrata of differing charge character (Adapted from [123])

This paper also stated that charge carrier species released into solution by the substrate influence the composition of charge double layers (structures that describe the variation of electrical potential near a surface) and therefore alter protein adsorption. However, other research showed an increase in rat marrow stromal cell attachment on positively charged titanium to be independent of serum protein adsorption [124].

These findings support those of published work which highlights the role of hyaluronan, an extracellular matrix component, in cell adhesion [125]. It gives the cell a negative surface charge and has been shown to mediate the first contact between osteoblasts and metal surfaces. The authors link an observed increase in osteoblast adhesion on positive titanium surfaces (zeta potential +7.7mV) to the negative charge of the hyaluronan. These findings are in turn contradicted, however, by others who have repeatedly observed reduced attachment of osteoblasts to positively charged HA surfaces [83].

A study of cell attachment to charged titanium also examined responses to negatively charged surfaces with surface potentials of 0.2-0.5V [124]. No significant difference ($p<0.001$) was found between cell responses on the neutral and negative surfaces in either serum-free or complete medium, though in serum-free culture the number of attached cells on the negative surfaces was marginally higher than that on the neutral surface. Data for the cultures in complete medium was not shown. The results were found to be dependent to some extent on the magnitude of the voltage.

While higher cell numbers have been found on negatively charged HA surfaces 48 hours after seeding, no increase was noted on these surfaces in comparison with unpoled HA controls at 24h after seeding [83]. As no error bars were included for the data, it is not possible to assess the significance of the trends shown. However, improved attachment of osteoblast-like cells to negatively charged HA surfaces has been reported [126]. In this study, ten times more cells attached to the charged material than to the electrically neutral surface.

In contrast, increased osteoblast attachment has been found on charged hydrogels with both positive and negative surface charges in cultures grown with and without serum [127]. The largest numbers of cells were found on the positive gels, but attachment on the negative materials remained better than that on the neutral gels.

The *in vitro* biocompatibility of BT-containing piezoelectric polymer films have been examined [128]. The adhesion of cells to poly(vinylidene-trifluoroethylene)/barium titanate (P(VDF-TrFE)-BT) composites was found to be improved compared to that on a commercially available polymer control (e-PTFE). Interestingly, the cell adhesion to the e-PTFE was very low (around 25% of the seeded cells) with adherence on the piezoelectric material around 70-80%. This study examined both poled and unpoled materials without detecting significant differences [129]. The d_{33} of the material was 25-

$30pCN^{-1}$ and the remnant polarisation was $33\mu cm^{-2}$, though the values cited for remnant polarisation do not concur with the P-E loop given in the same paper [130].

Longer term effects *in vitro*

A study was carried out to investigate the proliferation of cells on P(VDF-TrFE)-BT composites up to 10 days after seeding [128]. Cultures were tested for alkaline phosphatase (ALP) production and matrix mineralisation up to 21 days of incubation. The composite was found to encourage an increase in cell numbers, ALP and matrix mineralisation as compared to the commercially available material. No difference was found between poled and unpoled materials [129]. The authors conclude that the piezoelectric film had better *in vitro* biocompatibility than e-PTFE.

In addition to their CaP deposition study, one group analysed the response of mouse fibroblast cells to BT thin film materials [120]. The cells were found to attach (tested three hours after seeding) and proliferate (tested three days after seeding) on the material surface, showing preference for the negatively charged areas. Despite the differences in their assessment of cell behaviour on neutral and negative materials, this work supports the conclusions of the study on P(VDF-TrFE)-BT composites [128] in suggesting that barium titanate is not cytotoxic to murine cells.

The two studies [83, 120] do, however, concur in finding greater number of cells on negatively charged HA surfaces compared to neutral surfaces three to four days after seeding. A further study is also in agreement, reporting a 1.6 times increase in cell proliferation on negatively charged HA [126]. One of these studies went further by also examining cell responses to positively charged HA and reported reduced cell attachment to the positive surface compared to the neutral surface [83]. The mechanism proposed by the authors for the reaction between charged surfaces and the biological environment is shown in Figure 2.16, showing how the exchange of ions and proteins on the surfaces may affect cell attachment. This model includes a mechanism

for reduced cell attachment on positively charged surfaces, apparently contradicting the proposed model for increased cell attachment on positive surfaces [125].

This image is available upon request from the University of Bath library.
The author requests that readers without access to the image via the University of Bath library refer to the original source as cited in the figure legend.

Figure 2.16 Schematic drawing of the interaction between the polarized charge and environmental materials contributing to cell adhesion. Inorganic ions, organic ions, amino acids, and proteins float around the HA ceramics, and then these materials are adsorbed to the O-surface. Cations and positively charged ionic groups are actively adsorbed on the negatively charged surface of HA ceramics, and Ca^{2+} ions contribute to the formation of the bone-like layer growing on the HA surface (N-surface). Anions and negatively charged species are actively adsorbed on the positively charged surface of HA ceramics, which fail to nucleate crystal growth (P-surface) [83].

A later study continued to work on charged HA surfaces and found that soaking polarised HA in complete culture medium for 24h before seeding did not significantly alter cell proliferation patterns [131]. On both soaked and non-soaked samples, increased cell numbers were found on the positively charged HA compared to the negatively charged material two days after seeding. Fewer cells were counted on the negative surface than the neutral surface at both time points. This data appears to contradict the findings of earlier work on the same material. Morphologically, the cells were described as being "flattened" on the negative surface.

Despite the increased cell attachment and spreading morphology observed on positive titanium surfaces at 24h after seeding, the majority of cells on this surface three days after seeding were round in shape, indicating reduced quality of cell attachment and function [124]. Those on the negative surface exhibited a well spread morphology. The ability of cells to spread was suppressed on the positive surfaces at this time point, as was the production of ALP, indicating limited cell differentiation. Changes in cell behaviour were enhanced by increases in the surface voltage. No corresponding long-term differences were noted on the negative surface. The authors suggest that an increase in substrate surface potential increases the electrical field in the double layer, modifying the local environment in the vicinity of the cell membrane and affecting the intra- or extracellular ion concentrations, altering cell development.

In vitro studies, with or without cells, may give indications of the biocompatibility of an implant material. However, these tests cannot currently replicate the mechanical loading, chemical and cellular environments surrounding an implant *in vivo*.

The following section summarises work that has been published to date examining the influence of charged and piezoelectric materials in orthopaedic applications *in vivo*. It should be noted that while piezoelectric materials will develop a charge in response to loading, poled HA is non-piezoelectric and is not expected to produce a stress induced potential.

2.5.3 *In vivo* studies

Enhanced osteoblast activity has been observed to result from both positive and negative polarisation of HA plates implanted in calvarial bones of rats [132]. This was coupled with a decrease in osteoclast activity. The authors attributed the increase in bone formation on the negative surfaces to the accumulation of Ca^{2+} ions on the surfaces. On the positive surfaces, the observed differences were attributed to the adhesion of molecules such as fibronectin, osteocalcin and BMPs, improving osteoblast migration. This is contrary to the findings of an alternate study which found reduced cell spreading on positive surfaces *in vitro* [124].

A feasibility study examining the possibility of using piezoelectric barium titanate as a bone implant material was carried out [90]. Ceramic samples with porous surfaces and a voltage coefficient (g_{33}) of approximately $9x10^{-3}mVN^{-1}$ were implanted into canine femora (specifically, into the cortex of the femoral midshaft). Subjects were sacrificed at 16 and 86 days. Analysis of explanted femora showed larger voltages produced under compression in samples implanted for the longer period. This was attributed to an increase in osseointegration and therefore improved load transfer to the implants over the course of the experiment.

However, a subsequent study compared bone responses to poled and unpoled barium titanate ceramics [92]. The implantation method was the same as that used in the previous experiment. Subjective assessment of bone ingrowth at the bone-implant interface showed no differences between poled and unpoled samples. In addition, bone-implant interface strengths also showed no difference between the two groups. The authors concluded that the geometry of the holes drilled to house the implants may have restricted loading of the samples, leading to an absence of stress generated voltages in the piezoelectric implants.

Similar problems were encountered in a later study [133]. This assessed the biological response to lead-based piezoceramics ($Pb(TiZr)O_3$) with a voltage coefficient (g_{33}) of $11x10^{-3}mVN^{-1}$ in avian subjects. No difference was found when comparing poled and unpoled samples. As with the Park *et al* study, the authors state that experimental design is likely to have lead to insufficient loading on the implants to produce a piezoelectric signal. In this case, the piezoelectric signal was limited by the low body weight of the test subjects and the properties of the piezoelectric material. It is concluded that, given the lack of piezoelectric response in the materials, the absence of influence on bone response in these studies is unsurprising. Although the poled materials must have retained some remnant surface charge resulting from poling it is possible that this charge was of a smaller magnitude than that of charged materials found by other studies to exert an influence on biological responses. Neither the piezoelectric coefficient nor the remnant polarisation of this material was given.

A later study in a small animal model used an implantation method previously shown to ensure loading of implants [134]. In this study, bone responses to chemically identical piezoelectric and neutral polyvinlyidene fluoride (PVDF) films with a piezoelectric charge coefficient of $17pCN^{-1}$ were investigated. Films were implanted in the interosseous membrane of the anterior tibia of rats. Histological analysis of explanted materials showed improved osteogenesis on the piezoelectric films from seven days to six weeks. An increased periosteal response was also noted in the first week. The authors speculate that this periosteal response indicates an increase in production in bone cells in response to the piezoelectric signal, resulting in improved osteogenesis. In agreement with earlier work, increased ossification was found on piezoelectric films made from PLLA in a rabbit model [135].

A further study showing an improved biological response to piezoelectric materials was carried out by Feng *et al* [6]. As with the earlier studies [90, 92], BT-containing ceramics were implanted in canine subjects. In this case, the piezoelectric material was

in the form of a hydroxyapatite-barium titanate (HABT) composite. The exact composition and properties of the material are not given. The piezoelectric coefficient was given as $6pCN^{-1}$, though in an earlier paper [136] it was reported as $60pCN^{-1}$. The values given for the permittivity of the materials used are also inconsistent, with the relative permittivity of the composites (4864) much higher than that of BT used to manufacture them (1700). This is contrary to the parallel and series equations for the permittivity of a composite (Equations 2.8 and 2.9), given that reported values of relative permittivity of HA vary between 4 [137] and 57 [138].

The biocompatibility of the HABT material was investigated by the culture of L929 mouse fibroblast cells in medium in which samples of the ceramic had been soaked [136]. This "leaching test" did not detect any cytotoxic effect caused by the composites. Later, HABT samples were implanted in the jawbones of dogs, to be loaded during chewing. Histological analysis showed improved bone tissue growth on HABT samples compared to HA controls. Bone growth was also found to be direction dependent, being aligned with the direction of poling. The authors claim that these results demonstrate a link between osteogenesis and stress generated potentials in the piezoelectric materials. However, the possible effects of residual surface charge are not considered in this analysis and loading of samples is not quantified.

A later study investigated the promotion of ossification by piezoelectric PLLA films implanted on the periosteum of rabbit tibiae. Newly formed osteoid was detected at one week, maturing over six to eight weeks following insertion. Significantly more new bone was formed on the piezoelectric polymers compared to electrically inert films [135].

More recently, responses to PVDF in rats were analysed [139]. The polymer was in the form of tubes with negative inner surface. Bone was found to grow preferentially on the inner surfaces of the tubes. In this study the authors question whether remnant

surface charge, rather than a stress generated potential difference, could be responsible for improved biological responses. The hydrostatic piezoelectric coefficient (d_3h) was $2.5pCN^{-1}$.

In vivo responses to P(VDF-TrFE)-BT composites, studied previously *in vitro* [128], were also examined [130]. Membranes containing 10% BT were implanted into rabbit tibiae and the animals were sacrificed 21 days postoperatively. Although bone growth and vascularisation indicated the biocompatibility of the material, the authors make no comment on the influence of the remnant polarisation or stress-generated potentials in the material on bone growth.

As stated in Section 2.1, macrophages are the first cells to respond to an implanted biomaterial [44]. None of the proposed piezoelectric bone graft materials have been tested *in vitro* using macrophages. Those tested *in vivo* would have been exposed to macrophages while *in situ*, though no specific information on macrophage responses is given. Macrophage-osteoclast differentiation and bone resorption have been shown to be independent of the surface charge of biomaterial particles [140]. *In vitro* studies have, however, been carried out examining macrophage responses to calcium phosphates, which are to be the base materials for this study. A brief review of this work is given in the following section.

2.5.4 Macrophage responses to calcium phosphates

The J774 macrophage cell line was cultured on stainless steel with and without an HA coating [141]. Though no IL1 or IL6 was found, an increased level of TNF-α was found in non-coated samples, leading the authors to speculate that HA coating "may improve the surface properties" of metallic materials and increase cytocompatibility. Despite the reduced TNF-α expression in cells cultured on the HA coated samples, it should be noted that a measurable inflammatory response was still found. This is significant as HA is generally accepted to be a highly biocompatible material. The production of TNF-α in response to HA was confirmed by a later study which linked the level of cytokine expression to the size of the HA particles with which they were cultured. Particles in the range of 1-15μm were used, with the highest level of TNF-α produced by cells cultured on the smallest particles [142]. This work was further confirmed in an *in vivo* study in rats in which calcium phosphate particles were found to induce inflammation [143]. In contrast with previous studies [141, 142], this inflammation is interpreted by the authors as being beneficial to the healing process and osteogenesis. A strong, but brief, inflammatory reaction associated with micro-particles is interpreted as being indicative of a massive release of cytokines and therefore favourable to the bone healing process.

In addition to examining the influence of biomaterials on macrophages *in vitro*, research has been carried out using co-cultures of macrophages and osteoblastic cells. These two cell types are known to interact *in vivo* and it has been shown that osteoblast response influences the release of cytokines by macrophages *in vitro* [144]. Co-cultures of macrophages and osteoblasts have also been used to assess the biocompatibility of calcium phosphates. Primary human macrophages and osteoblasts were cultured on granules of biphasic calcium phosphate particles containing different ratios of HA/TCP over a 7 day culture period, measuring LDH and cytokine release at 1, 4 and 7 days. Differences in surface chemistry were found to be the most influential factor in determining cell adhesion. The authors suggest that CaP-rich areas on the material

surfaces may lead to the formation of intramitochondrial CaP crystals, causing mitochondria lysis and cell death. Materials with increased levels of TCP were found to induce an augmentation in IL1-β production. This increase in cytokine production was not found to correspond to any difference in free calcium levels in the culture medium [145].

No *in vitro* testing of barium titanate ceramics using macrophages has been published. However, in their *in vivo* study, Feng *et al* noted that no inflammation was observed around the HABT, suggesting an absence of detrimental macrophage response to the implant [6].

2.5.5 Discussion

There is no consensus in the literature as to whether positive or negative surface charges are more beneficial to biological response. It is clear, however, that the application of a surface charge may influence the biological response to an implant material. It appears that responses to different charges vary depending on the material in question and the time scale considered. The mechanisms proposed for cell attachment of positively [125] and negatively [83] charged surfaces (Figure 2.16) are not mutually exclusive. These mechanisms, along with a conclusive definition of the influence of surface charge on biological response, for HA and other materials, are yet to be proved.

Some apparent contradictions between studies may stem from variations in the experimental methods employed. For *in vitro* studies, cell types and analytical methods are not consistent. *In vivo*, the use of a wide range of animal models, implant sites and durations of implantation renders direct comparison of studies difficult.

In general, for piezoelectric materials, in those studies in which implants were deemed by the authors to have been appropriately mechanically loaded, improved biological

responses were observed [6, 134]. In those studies where implants were not loaded [92, 135], piezoelectric implants did not perform better than electrically inert controls. Consequently, it appears that remnant polarisation, along with the resulting remnant surface charge, is not sufficiently strong to induce the improved biological response seen on some charged materials. However, the choice of control materials and lack of non-loaded controls in some studies means that any influence from remnant polarisation cannot be considered separately to that of stress-generated potentials. The studies are not directly comparable due to differences in the protocols used. No one study has effectively isolated the influence of surface charge from that of the piezoelectric effect for a particular material. Direct comparison of the different piezoelectric materials studied is also difficult due to the lack of consistency in reporting of piezoelectric properties.

Existing work on P(VDF-TrFE)BT composites [129, 130] suggests BT may be a suitable material to induce osteogenesis. Feng *et al* provide a basis for improving the performance of HA grafts using BT [6] but, while providing promising results, do not elaborate on the composition of the sintered material and do not sufficiently establish the biocompatibility of HABT ceramics. Consequently, further testing is justified to investigate the chemistry and piezoelectric properties of and biological responses to HABT ceramics. The effect of poling of theses composites and of mechanical loading on the biological response may also be examined.

A range of techniques is available for the testing of biological responses to HABT ceramics. The following section introduces current practices for testing the biocompatibility and efficacy of biomaterials.

2.6 Biomaterials testing *in vitro*

The success or failure of any implant material is highly dependent on the response of the surrounding tissue. It is therefore necessary to understand the biocompatibility of, and potential for bone growth on, any new implant material.

Biocompatibility is defined in William's Dictionary of Biomaterials as "the ability of a material to perform with appropriate response in a specific application" [146]. According to the British Standard for biological evaluation of medical devices, the biocompatibility of a ceramic bone graft can be assessed in terms of cell response, cytotoxicity and absence of inflammation in the host tissue [147]. Cytotoxicity tests are used to confirm that a material or device will not cause abnormal cell death and therefore induce an unfavourable tissue response. Cell response tests establish to what extent cells behave in their normal manner when in contact with the material.

Analysis of biocompatibility may be carried out *in vivo* using animal models of various types. *In vitro* analysis may be carried out with or without the use of cell culture. *In vitro* experiments carried out without the use of cells may be seen as an assessment of the bioactivity of the material rather than its biocompatibility, commonly measuring the deposition of calcium phosphates on the surface of materials in simulated body fluid [119]. In the work presented in this thesis study, the biocompatibility of electrically active ceramics is to be assessed using *in vitro* cell culture techniques. The rationale behind the choice of cell types and analysis methods for this study is discussed in the following sections.

2.6.1 Cells for biocompatibility testing

Cell types

Though non-human animal cells, particularly mouse and rat cells, are widely used for *in vitro* experimentation on biomaterials [148-151] it is important to select a clinically relevant cell type when using cell cultures to predict *in vivo* cytotoxicity. Human cells have also been successfully used in biomaterials evaluation research [152, 153] and, as the materials to be investigated in the current study are intended for implantation in humans, may be considered to be more clinically relevant than cells of non-human origin [151].

Cells used in biocompatibility testing of materials for use in bone are commonly either stem cells (pluripotent cells that are capable of self-renewal) or osteoprogenitor cells. Osteoprogenitor and osteoblast-like cells can be maintained and propagated outside the body for prolonged periods [154], making them suitable for *in vitro* experimentation. Cells may be either primary cultures (obtained directly from a living subject) or secondary cultures (also known as continuous cell lines). A primary culture becomes a cell line after the first passage but will grow for a limited number of generations. It has been suggested that the use of bone-derived cells in biocompatibility analysis is preferable to the use of other cell types as these are the cells to which implant materials are exposed *in vivo* [155]. Continuous cell lines, however, are often obtained from cancerous tumours and are referred to as "immortal". Use of continuous cell lines is convenient in a laboratory setting though they may display differences in growth and both genotype and phenotype may change over time [156].

Though the phenotypes of osteosarcoma cell lines are not identical to those of osteoblasts, some cell lines have been well characterised and are considered to be good models of osteoblastic behaviour [157]. It is necessary to understand the characteristics of the cells used in any study in order to draw appropriate conclusions about cell behaviour from the data. In a study comparing three cell lines (MG63, Saos-2 and U2

OS) to primary osteoblasts, the osteosarcoma cells were found in general to be 1/6 of the size of osteoblasts (20-30μm [157]). Unlike osteoblasts, osteosarcoma cells were not found to change their size dependent on cell density. Doubling times of osteoblastic cells were 2-3 times faster than that of osteoblasts [157]. The MG63 and Saos-2 cell lines were found to be appropriate models for primary osteoblast behaviour. Both cell lines are commonly used in the testing of orthopaedic biomaterials.

Saos-2 is a human osteosarcoma cell line isolated from an 11 year old Caucasian female. They are polygonal in shape and have been shown to display a more mature osteoblastic profile that of MG63s [157]. These cells have been shown to maintain an osteoblast phenotype for up to 40 days post-confluence in the presence of ascorbic acid. It is accepted that Saos-2 cells produce measurable amounts of ALP and deposit a collagen matrix that is able to mineralize in the presence of β-GP [158]. They express the osteoblastic markers osteocalcin and procollagen I [157]. Production of ALP by Saos-2 cells was, however, not shown to be entirely representative of osteoblastic ALP production. In the cultures tested, only 30% of primary osteoblasts showed positive ALP activity while all Saos-2 cells produced ALP. Like primary osteoblasts and in contrast with the MG63 cell line, Saos-2 cells do not produce collagen III, a type of collagen not normally produced by primary osteoblasts. Production of osteonectin, a protein involved in the binding of collagen and calcium, by Saos-2 cells has been reported [41]. Saos-2 cells have been used extensively in the study of biomaterials. The behaviour of Saos-2 cells on ceramics [159], polymeric materials [160] and metals [161] has been studied. They are therefore suitable for use in the current study.

Where inflammatory or immune responses to a material are to be tested, primary macrophages or macrophage-like cell lines may be used [44]. The cell line J774.2 was obtained from the European Collection of Cell Cultures (ECACC No. 85011428). The cells are described by the ECACC as mouse monocyte macrophages. They are semi-adherent, with some cells growing in suspension. It has been well characterised, is

easy to use and is known to express appropriate cytokines for the measurement of inflammatory responses to biomaterials *in vitro* [162, 163].

Osteoblast behaviour on biomaterials *in vitro*

The sequence of osteoblast attachment, proliferation and differentiation on a biomaterial surface is illustrated in Figure 2.17. The initial adhesion phase involves non-specific electrostatic forces and ligand-receptor bonds, followed by cell spreading and the development of anchoring sites and reorganisation of the cytoskeleton from [164]. Proliferation and differentiation phases follow at later culture times. The exact time scales for these phases of development differ between cell lines and according to culture conditions. For Saos-2 cells, it is common to measure cell attachment up to 24h [165], proliferation from 24h up to 14 days [166-168] and differentiation at 7 days and longer culture periods[160, 168].

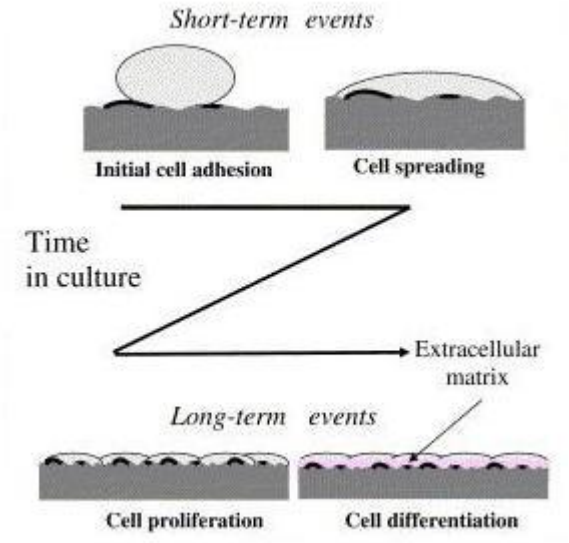

Figure 2.17 The phases of cell development on a biomaterial surface (Adapted from [164])

Analysis of cell proliferation

In order to analyse the results of cell proliferation assays, it is important to understand the standard cell growth curve. *In vitro*, the growth of a population of cells occurs in three main phases. After an initial lag phase, the cells enter a growth phase before, in the third phase, the number of cells in the population stabilises. These phases are seen on the standard growth curve (a log plot of cell population against time) seen in Figure 2.18.

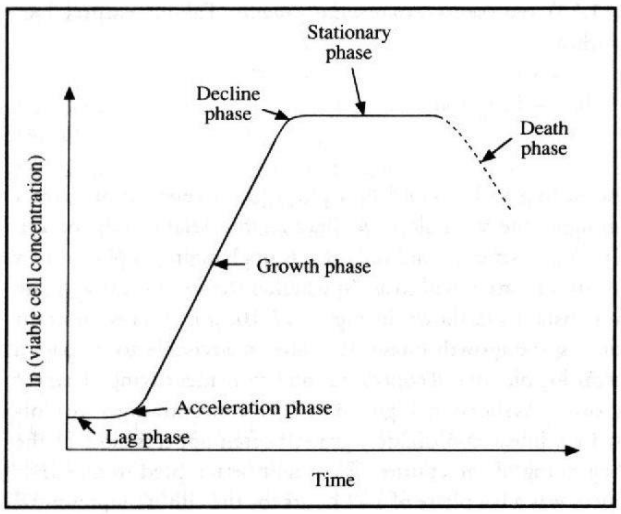

Figure 2.18 Typical batch cell growth curve [180]

Using a curve such as the one shown above, the growth rate (μ) and doubling time (t_d) of the population can be established. The maximum growth rate (cells/day) is found from the maximum gradient of the straight line (growth phase) section of the graph. The doubling time is then calculated according to the following equation:

$$t_d = \frac{\ln(2)}{\mu} \tag{2.10}$$

2.6.2 Analytical methods

A wide range of methods is used to assess cell behaviour and tissue growth in the analysis of orthopaedic or dental biomaterials. Commonly, these include measurement of cell attachment, proliferation, differentiation and function. Stains are used in order to reveal the presence of various cell secretions when examined under an optical microscope. Table 2.5 gives an overview of common techniques used in the assessment of cell behaviour.

It has previously been suggested that two factors determine cell responses to an implant material: the three-dimensional topography (size shape and texture) and the physico-chemical properties of the surface [154]. The physico-chemical properties (chemistry and electrical states) of possible graft materials are to be varied in this study. An understanding of the influence of surface characteristics on *in vitro* biomaterials testing is therefore needed in order to properly interpret the results. The following section is an introduction to the influence of variations in substrate surfaces on bone cell behaviour.

Table 2.5 Common assessment techniques used in the assessment of cell behaviour

Substance/ characteristic tested	Stain or test method	References
Cell population size	Haemocytometer	[169]
	Picogreen	[170] [171] [172]
	Lactate dehydrogenase	[173]
Cell viability	Trypan blue	[169]
	Dimethylthiazol-2-yl)-2,5-diphenyltetrazolium bromide (MTT) assay	[174, 175]
Cell morphology	Haematoxylin and Eosin	[176]
	Electron microscopy	[169]
Alkaline phosphatase production	p-nitrophenol assay	[149, 177]
	Immunostaining	[176]
Osteocalcin	Immunoenzymatic assay (ELISA kit)	[169, 176, 177]
	Immunoenzymatic assay (Novocalcin enzyme kit)	[178]
Calcium deposition	Alizarin red	[149, 177]
Collagen I	Immunostaining	[177, 179]
	Hydroxyproline reaction	[170]

2.6.3 The influence of surfaces on *in vitro* outcomes

Bone cells have been shown to be sensitive to both general topography [181] and nanotopography, responding to features as small as 10nm [182]. Physico-chemical properties affecting biocompatibility include surface charge and surface energy, though it has been found that surface charge is the more important element in influencing osteoblast behaviour (Moller *et al* 1994 cited by [154]). Cell proliferation [2], differentiation, matrix production and morphology have all been shown to be affected by surface roughness and topology [183, 184]. Increased surface roughness has been shown to improve human bone marrow cell adhesion and advance proliferation. This study found no significant differences in ALP production on the different surfaces. The influence of changes in surface on cell morphology is shown in Figure 2.19. On the smooth surface (Figure 2.19a) the cells are flattened with numerous filopodia while the cells on the rougher surface (Figure 2.19b) are less flattened with some globular cells visible [165]. The average roughnesses of the smooth and rough materials are given as Ra=0.30 and Ra=0.94.The units of measurement are not stated, though it is usually to give values of roughness in μm.

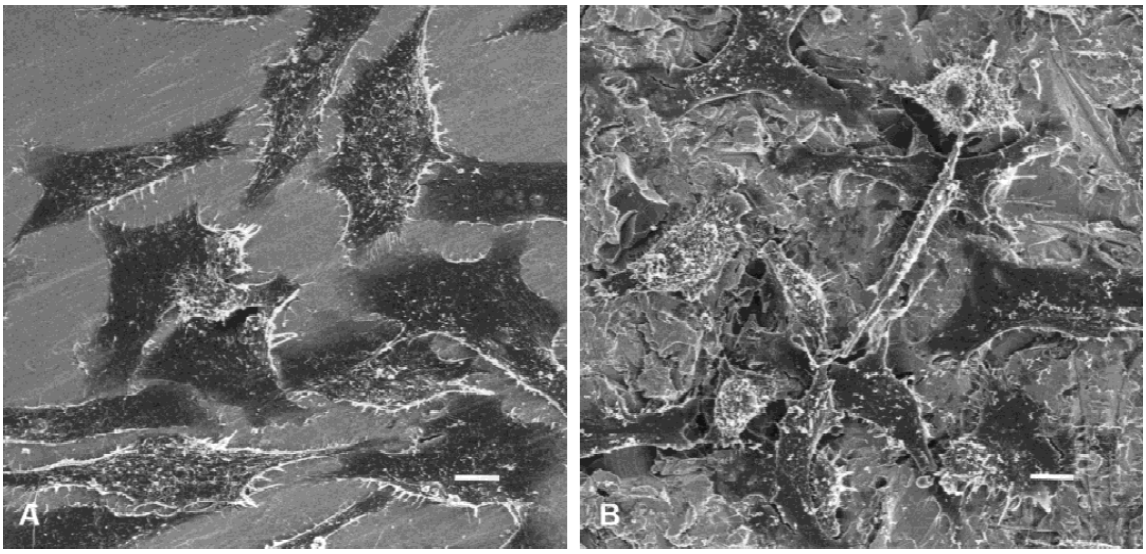

Figure 2.19 Saos-2 cells in culture on (a) non-sandblasted titanium and (b) sandblasted titanium. Scale bar = 10μm [165]

A later study did, however, find an increase in ALP production associated with an increase in surface roughness when comparing materials with average roughnesses of 5.6μm (smooth) and 21.2μm (rough) [185]. Significant differences have been found in the behaviour of Saos-2 cells cultured on smooth and rough surfaces. Cells were cultured on polished (Ra=0.92μm) and acid-etched (Ra=3.3μm) titanium samples. Cells on the smoother samples were found to attach and migrate less effectively than those on rough surfaces [43].

The shape of surface features (e.g. grooves, pits, steps, pores), as well as surface roughness, has been found to influence cell behaviour on biomaterials *in vitro* [186]. The exact influence of substrate morphology, as with any individual aspect of cell-material interaction, is difficult to assess from the published literature due to differences in experimental procedures (e.g. feature sizes observed, cell types used). A number of studies have reported the alignment of cells to nano- or micro-scale grooves on substrate surfaces. The size of features has also been shown to influence cell attachments. In a study of 0.5μm depth grooves spaced at 2, 5 and 10μm, cells were found to align with the smaller grooves, but not those spaced at 10μm [187]. In a later study, cavities of various sizes (10-100μm) were created in a substrate surface. Cell adhesion and behaviour varied depending on the size and spacing of the cavities. The authors noted, however, that on surfaces with features of 10μm diameter, cells did not conform to the material, instead forming focal attachments allowing them to suspend across the features [188].

2.7 Conclusions

A need exists for the development of bone graft substitute materials. A large proportion of the synthetic bone grafts which are currently commercially available are based on HA. Published studies indicate that piezoelectric materials can induce enhanced biological responses. It may therefore be possible to improve biological responses to HA grafts by introducing a piezoelectric component. In particular, there is a lack of understanding of the influence of the microstructure, piezoelectric properties, permittivity and sintered composition of HABT composites. An investigation of HABT composites is needed to determine their composition, structure and piezoelectric properties, as well as their biocompatibility and effectiveness.

It is important to understand the mechanism by which a material influences biological responses. In order to determine the cause of any change in biological response to HABT composites in comparison with commercially available HA, they must first be tested, in both electrically inert and poled states, in the absence of mechanical loading.
A range of biomaterials testing techniques are available. The cell lines, incubation times, assays and evaluation techniques used varies greatly amongst the published studies, making comparison of results difficult. A need therefore exists for the establishment of a consistent set of protocols for the measurement of the biocompatibility. Later work may then determine the influence of stress-generated potentials independently of that of remnant polarisation in the piezoelectric materials.

Saos-2 osteoblast-like cells are an appropriate model for the determination of osteoblast responses to biomaterials. The J774.2 cell line may be used for the investigation of inflammatory response to the ceramics.

The objectives of the current study are to:

i. manufacture a range of HABT composites
ii. determine their piezoelectric properties, composition and structure
iii. select an appropriate HABT composite material for biological testing
iv. determine the influence of adding BT to HA on its biocompatibility
v. determine the influence of poling on *in vitro* biological responses to HABT composites.

The determination of biological responses will be separated into three investigations. These will include studies of osteoblast-like cell attachment, osteoblast-like cell development and inflammatory responses to HABT ceramics. The following chapter details the materials and experimental and analytical methods used in this study.

3 Materials and methods

3.1 Introduction

This chapter outlines the materials and methods used for the experimental work presented in this thesis. Initially, details of the materials used and the manufacture of ceramic samples are given. Subsequent sections detail the measurement of the electrical properties of the samples, cell culture and analytical techniques used to investigate biological responses. These sections are, for the most part, arranged in the order in which the results will be presented. In cases where one technique has been used in a number of separate experiments, it is described in general here, with additional details given where relevant in Chapters 4 and 5. A schematic diagram of the methods used is shown in Figure 3.1, showing the various preparation and analysis techniques used throughout the study.

3.2 Materials

Hydroxyapatite base powder (Grade 130) was supplied by Stryker Orthopaedics (Limerick, Ireland). It was manufactured by Thermphos International BV (Oldbury, UK). Barium titanate powders were manufactured by Ferro (Haverhill, UK), supplied by Morgan Electroceramics Ltd. (Wrexham, UK).

Both the Saos-2 and J774.2 cells lines were obtained from the European Collection of Cell Cultures (ECACC No. 89050205 and 85011428 respectively). Full details of materials, equipment and consumables used can be found in Appendix A.

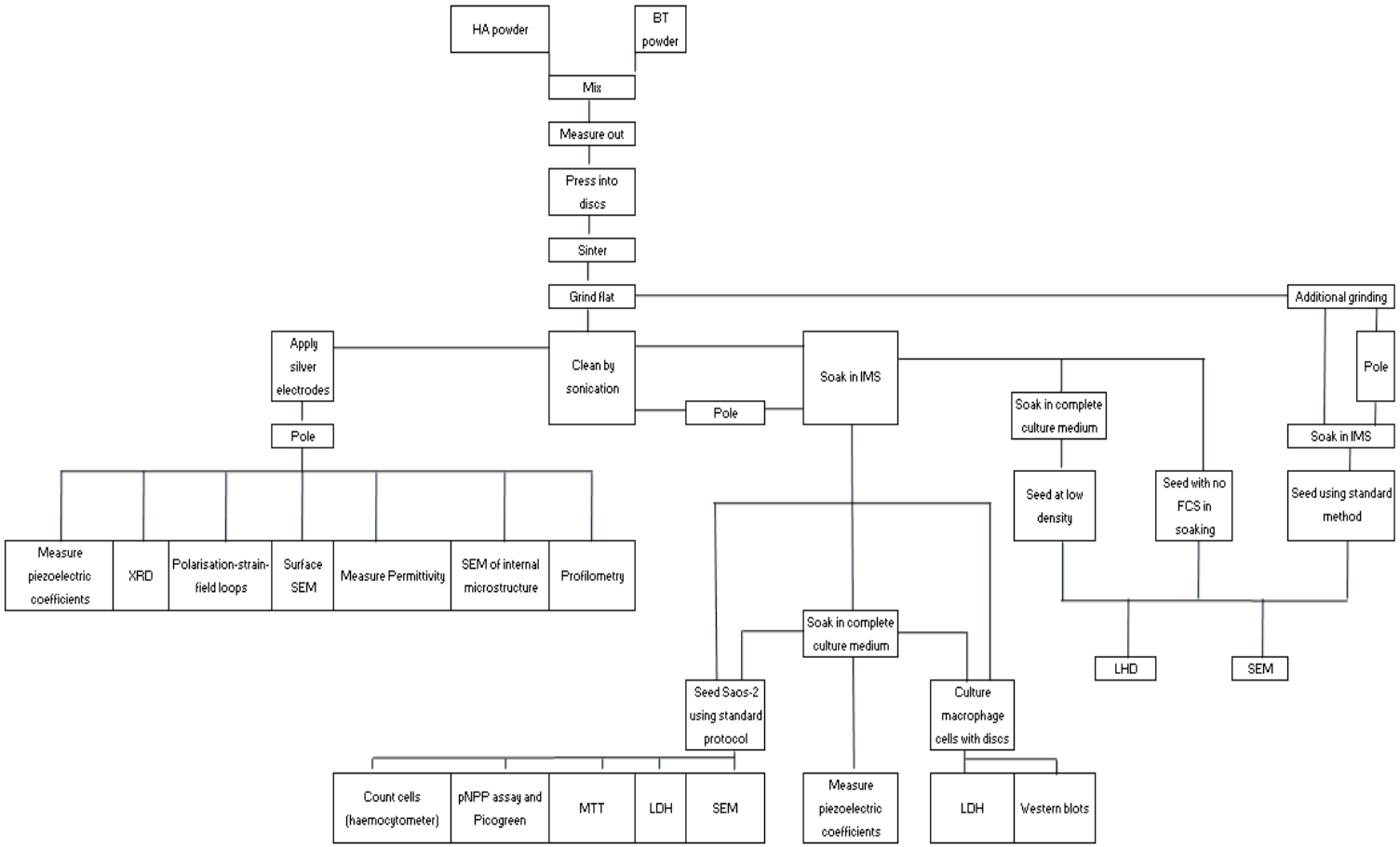

Figure 3.1 Schematic chart of methods for ceramic manufacture and testing

3.3 Ceramic disc manufacture and preparation

3.3.1 Disc manufacture

Ceramic powders were intimately mixed in order to produce sets of discs in a range of compositions (0-100% BT by volume) as shown in Table 3.1. Relative quantities of each powder were determined according to volume fraction calculations given in Appendix B. For the remainder of this thesis, each composite will be named according to the percentage of BT included in the powder mixture (see Table 3.1). Sufficient powders for fifty discs in each set were weighed out and mixed. Sufficient powder for an individual disc was then measured out by volume from this mixture. Discs were cold pressed in a 15mm diameter die, being held at 100MPa for 5 seconds.

Table 3.1 Compositions of HABT discs

Volume % of HA in powder mixture	Volume % of BT in powder mixture	Composition name
100	0	HA
80	20	20% BT
60	40	40% BT
40	60	60% BT
30	70	70% BT
25	75	75% BT
20	80	80% BT
15	85	85% BT
10	90	90% BT
5	95	95% BT
0	100	BT

The discs were then sintered in air at 1300°C for 2.5 hours with a heating and cooling rate of 60°C/h. After sintering, the tablets measured 13mm in diameter (see Figure 3.2) and 2-3mm in thickness. The density of the discs was 85-90% of the theoretical density. The surface of each disc was ground using P600 silicon carbide paper and finished using P1200 silicon carbide paper in order to achieve a uniform surface finish. The

discs were then sonicated in two changes of 100% ethanol for 10 minutes to remove grinding debris and were dried in air.

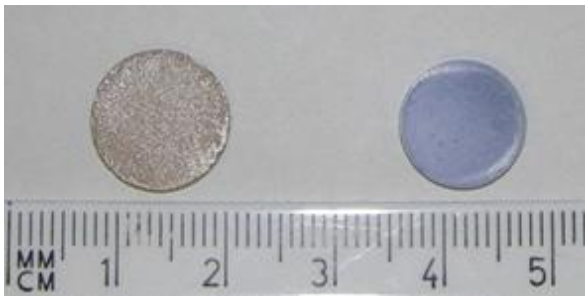

Figure 3.2 Barium titanate and hydroxyapatite discs before grinding.

Ceramic particles

For macrophage experiments using particles of the sintered ceramics, two discs of each ceramic to be tested were ground in a pestle and mortar and the resulting powder was passed through a sieve with a 100μm mesh. These powders were sealed in glass bottles and sterilised in an autoclave at 121°C for one hour.

Reuse of discs

Due to the large numbers of ceramic samples required for testing, discs used for short cell culture studies (1 or 3 days) were sterilised and reground and before reuse in later experiments. These discs were sterilised in an autoclave at 121°C for one hour. The surfaces were then reground using P600 silicon carbide paper, finished using P1200 silicon carbide paper and sonicated in two changes of ethanol for 10 minutes to remove grinding debris and dried in air. Measurements were taken to ensure that the discs were ground back sufficiently to produce a new surface using this process. Details are given in Appendix C.

3.3.2 Poling

As described in Section 2.4, the ferroelectric domains within BT must be aligned by poling in order for it to exhibit piezoelectric properties. In this study, samples were poled using corona poling. The poling apparatus (as constructed and tested by Panteny [94]) is shown in Figure 3.3. During poling, an electrical field is generated between the needle and the earthed base, resulting in the ionisation of the air inside the poling chamber. The ions generate a high static potential difference across the thickness of the samples, causing the domains to be re-oriented.

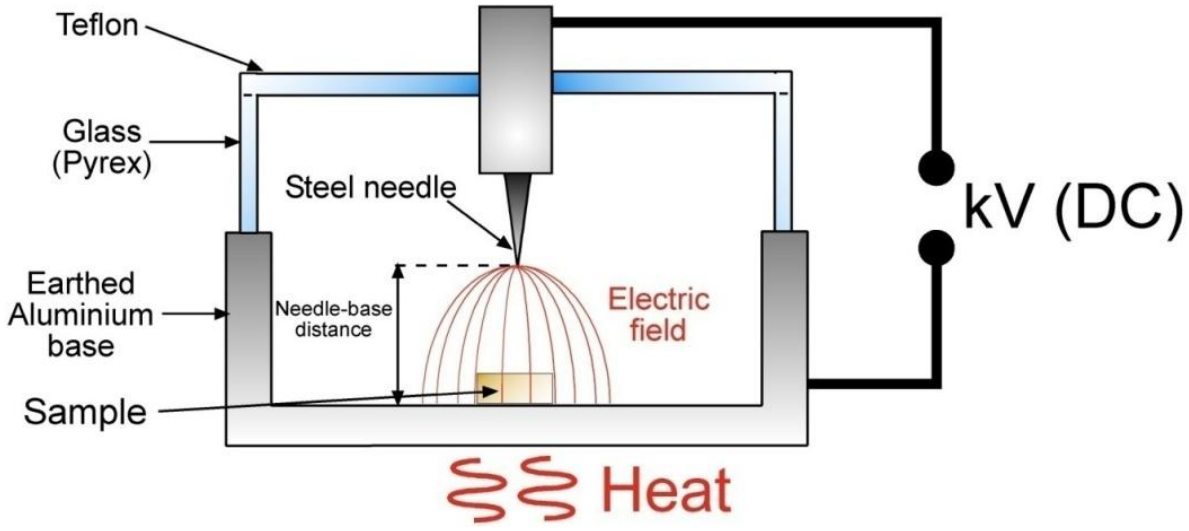

Figure 3.3 Corona poling equipment [94]

The equipment was set to generate an electrical field of 25kV, while the discs were heated to 130^0C. The samples were allowed to cool to room temperature in the presence of the electric field. The height of the poling needle (the needle-base distance shown in Figure 3.3) was maintained at 55 mm.

3.4 Measurement of electrical properties and structure

In preparation for measurement of electrical properties, electrodes were applied to the circular faces of discs using silver conductive paint. Discs were then poled according to the method described in the previous section.

Piezoelectric coefficients

The piezoelectric coefficients in the poled and orthogonal directions of the sample, d_{33} and d_{31} (described in Section 2.4.2), were measured using a Berlincourt piezometer (Take Control Piezoemeter System PM25). This meter applies a small alternating force (0.1N) and measures the piezoelectric charge generated via conducting metal studs in contact with the material surface. The size and shape of the studs varies according to the geometry of the sample.

The system was calibrated using a PZT reference sample with a d_{33} of 330pCN^{-1}. Measurements were carried out 24h after poling since the piezoelectric properties are known to degrade as a result of minor domain relaxation. For each composition tested (see Table 2.1), six discs were used. Three measurements are taken per disc. Values reported are the mean and standard deviations over all measurements for each composition.

Permittivity and voltage per unit stress

The permittivity (ε) was measured at varying frequencies of applied current using a Solartron 1260 Impedance Analyser and a 1296 Dielectric Interface at 1 V_{rms}. Measurements were taken at room temperature at frequencies ranging between 0.1Hz and 1MHz. The piezoelectric voltage coefficient (g_{33}) was then calculated using Equation 2.5. Nine compositions (0, 20, 40, 60, 80, 85, 90, 95 and 100% BT) were tested.

Polarisation-Strain-Field measurements

The polarisation-field (P-E) and strain-field (S-E) responses of the ceramics were measured using a system designed at the National Physical Laboratory, Teddington, UK. Briefly, an oscillating voltage was applied to the ceramic and the strain in the sample was measured using a capacitance sensor linked to the ceramic surface by a leaf spring. The output of the sensor was linearly related to the displacement of the spring. The polarisation state of the material was determined by measuring the current flowing through the sample, this was then converted to a voltage. The input voltage waveform, generated voltage and capacitance data were recorded by the control computer.

Measurements were undertaken at 10Hz with the electric field magnitude increasing in $0.25 kVmm^{-1}$ increments up to $2 kVmm^{-1}$ in order to observe the switching of ferroelectric domains in response to the applied electric field as described in Section 2.4.

Composition

The composition of the sintered ceramics was analysed using X-Ray Diffraction (XRD). Discs were crushed to powder and studied in a Philips X-Ray Diffractometer using Cu α radiation with a wavelength of 1.54° and a graphite monochromator. X ray intensity was measured for angles in the range $20^{o} < 2\theta < 60^{o}$ with a step size of 0.01°. The diffraction patterns produced were then compared with existing data using PDFC 2.00 database software. To identify the phases present, the location of peaks in the XRD profiles were compared to reference spectra [189].

Surface roughness

Six samples each of HA and 90% BT were prepared as described in Section 3.3. A Scantron Proscan 2000 profilometer with a step size of 1μm was used to produce 3 dimensional micro-topography plots. The area of the disc surface to be analysed was selected at random. The average roughness (R_a, the average deviation of the profile

from the mean line), maximum roughness (R_{max}, the maximum peak to valley height) and ten-point height (R_z, the average of the five highest peaks and the five lowest valleys) were then calculated using the Proscan 2000 software. An S5/03 chromatic sensor with a resolution in the z axis of 0.01μm was used.

Surface topology and microstructure

Discs of each composition used for cell culture (HA and HABT) were prepared as described in Section 3.2, sputtered with gold in order to avoid the build up of electrical charge on their surface and examined using scanning electron microscopy (SEM).

For the analysis of microstructure, discs were sectioned vertically and the exposed faces were polished, followed by chemical etching using 10% hydrofluoric acid for 60 seconds. Samples were then coated with gold to ensure the conductivity of their surface. A Jeol JSM6310 microscope operating with an accelerating voltage of 10-20kV was used to examine the prepared surfaces of the ceramics. Two samples were examined for each composition tested (see Table 2.1). During the examination of the microstructure of the discs, energy dispersive x-ray analysis (EDAX) was used to map the ions present at selected points on the surface of the viewed area of the specimen.

3.5 Biological testing using osteoblast-like cells

HA and HABT discs were manufactured as previously described (Section 3.3). For the biological evaluation of poled HABT discs, poling was carried out without the application of silver electrodes to the discs in order to avoid contamination of the cell cultures.

3.5.1 Saos-2 cell culture

The Saos-2 cell line was selected for use in this study as discussed in Section 2.6. Though experimentation using primary cells obtained from human tissue may produce

results more closely replicating *in vivo* responses, no facility for the derivation and use of these cells was available at the start of this study.

The cells were cultured in McCoy's 5A medium supplemented with 2mM L-glutamine and 10% foetal calf serum (FCS). All cells used in this work were between passage numbers 16 and 25. They were seeded at 20 000 cells/cm^2 in T75 flasks and grown to confluence at 37 °C with 5% CO_2 before subculture. The culture medium was changed every 2-3 days. All cell culture procedures were carried out under sterile conditions within a category II laminar flow hood.

Subculture

Media was removed from the flask and cells were rinsed twice with 10ml phosphate buffered saline (PBS). 2ml of trypsin-EDTA (ethylenediaminetetraacetic acid) were then added and the flask was incubated at 37^0C and 5% CO_2 until cells detached from the flask surface. 8ml of complete culture medium (as described above) was then added to inactivate the trypsin-EDTA. The cells were transferred to a 50ml centrifuge tube and spun at 1500xg, for five minutes at 20^0C before being resuspended in 5ml of complete medium. A 10µl sample of this suspension was mixed in a 1:1 volume ratio with trypan blue and pipetted into the chamber of a haemocytometer. The cells in the sample were counted and, based on this cell count, an appropriate volume of cell suspension to give a seeding density of 20 000 cells/cm^2 was transferred to a number of new T75 flasks. Complete culture medium was added to give a total volume of 10ml per flask. The flasks were then incubated at 37^0C and 5% CO_2.

Freezing

At confluence, cells were detached from their flasks using trypsin as described above. The suspension was centrifuged at 1500xg, for five minutes at 20^0C. The liquid phase was then discarded and the cells were resuspended in FCS to a concentration of 5 x 10^6

cells/ml[1]. 900µl of the cell suspension and 100µl of dimethyl sulfoxide (DMSO) were added to each freezing vial. The vials were then placed in an isopropyl freezing vessel to freeze at -1^{0}C min^{-1} and placed in a -80^{0}C freezer. After 24h vials were transferred to a liquid nitrogen store.

To defrost cells, a vial was removed from the -80^{0}C freezer and placed in warm water until the contents were liquid. The contents of the vial were added to a T25 flask with 10ml media. The vial was rinsed with 1ml media which was then added to the flask, which was placed in an incubator at 37^{0}C and 5% CO_2. After eight hours the media was exchanged for fresh media to remove the DMSO from the flask. After 24h the medium was removed from the flask and cells were rinsed twice with 5ml PBS. 1ml of trypsin-EDTA was then added and the flask was incubated at 37^{0}C and 5% CO_2 for 10 minutes, until cells detached from the flask surface. 9ml of complete culture medium was then added to inactivate the trypsin-EDTA. The cells were transferred to a T75 flask and culture continued as described above.

3.5.2 Seeding of Saos-2 cells onto ceramics

Standard seeding method

Before use in cell culture, the ceramic discs were kept for 24h in 70% industrial methylated spirit (IMS) at 4°C, rinsed in sterile 1ml of PBS per well and soaked in 500µl of complete culture medium overnight. Discs were then allowed to dry in air in a 24-well plate, one disc per well with the ground surface (prepared as detailed in Section 3.3.1) facing up. Confluent cells were then removed from the T75 flasks using trypsin. These were centrifuged, resuspended and counted as described for subculture before being seeded onto the surface of the discs at 20 000 cells/cm^2 in 25µl of complete culture medium. Cells were seeded onto the tissue culture plastic of the 24-well plate as a control at 20 000 cells/cm^2 in 38µl of complete culture medium, accounting for the difference in surface area between the control and the sample. The 24-well plates were

incubated for 90 minutes at 37°C with 5% CO_2 in order to allow cells to adhere to the ceramic surface before 1ml of complete culture medium was added to each well. In addition, cell-free controls containing ceramics in culture medium and culture medium alone were included. The culture plates were then incubated for up to 14 days as required. The culture medium was changed every 2-3 days. For cultures of 7 and 14 days, 1% antibiotic-antimycotic solution was added to the culture medium in order to reduce the risk of infection associated with longer term cell culture.

Modifications to standard method

In some studies, as indicated in Chapter 5, the standard seeding method was modified. Three modifications were used. (1) For low seeding density experiments, cells were seeded onto the ceramic discs at a reduced density of 10 000 cells/cm^2 in 25µl of complete culture medium. (2) In the case of seeding "without serum", the discs were soaked overnight in culture medium without FCS. The cells were suspended in serum-free medium for seeding. 1ml of complete culture medium (containing 10% FCS) was then added after the initial 90 minute cell attachment period. (3) The surface finish of the ceramics was varied by the addition of a final grinding stage before sonication, finishing the surfaces by polishing for 10 minutes using a 1µm polycrystalline diamond suspension in order to achieve a smoother surface finish. The roughness of these discs was measured for comparison with the properties of those produced by the standard preparation method (the roughness measurements of these materials are described in Section 5.2).

3.5.3 Analysis of Saos-2 cultures

SEM

In preparation for analysis of cell morphology by SEM, culture medium was removed from the wells containing the discs and the wells were washed with 500µl serum-free culture medium. After the medium was removed, 500µl fixative solution containing gluteraldehyde (2.5% by volume) and potassium ferrocyanide (1% by weight) in serum-free culture medium was added to each well. The culture plate was then incubated at 37^0C and 5% CO_2 for two hours. The discs were washed with serum-free medium and 500µl osmium tetroxide 1% solution was added and the plate was kept at room temperature for one hour. This was followed by washing the discs twice with distilled water before the discs were transferred to glass petri dishes. The samples were then dehydrated in serial concentrations of acetone (50, 70, 90 and 100%, two five-minute treatments per concentration). A 1:1 mixture of acetone and hexamethyldisilazane (HMDS) was then applied for 15 minutes. The samples were soaked in 100% HMDS for 15 minutes before being allowed to dry. This procedure was carried out in a Class II fume hood. Samples were stored, until required, in an airtight container at room temperature (maximum storage three days). The discs were sputter coated with gold and examined using SEM as described in the previous section.

Estimates of cell sizes were obtained using Image-Pro MC software to measure the longest dimension and the area of the cells growing on the various ceramic surfaces. Two images (x500 magnification) of each material type were assessed, with four cells measured from each image giving a total of eight measurements per material (n=8).

Cell counts

At the end of the relevant incubation time, the culture medium was removed from the wells, which were then rinsed twice with sterile PBS. Trypsin (500µl, 0.1%) was added to the wells and the culture plates were incubated at 37^0C and 5% CO_2 for 10 minutes.

The contents of the well were then mixed using a 250µl pipette. A 10µl sample of this suspension was mixed in a 1:1 ratio with trypan blue and pipetted into the chamber of a haemocytometer. The live and dead cells in the sample were counted and the number of cells in the well was calculated according to the following equation:

$$proportion\ of\ viable\ cells = \frac{number\ \ of\ live\ cells}{number\ \ of\ live\ cells + number\ \ of\ dead\ \ cells} \qquad (3.1)$$

This figure was then normalised by the surface area of the control or sample. The efficacy of this method was tested using repeated counts and verified using SEM. Further information on this testing is included in Appendix C.

Determination of cell population and viability

In order to obtain an indication of the total number of cells present, a lactate dehydrogenase (LDH) assay was carried out according to the principle outlined by Haslam *et al* [173]. At the end of the required incubation time 100µl of 20% triton-X was added to each well to lyse the cells. A 100µl sample was then taken from each well and from negative control wells containing no cells. All samples were then analysed using an LDH detection kit (Cytotoxicity Detection Kit, Roche) according to the manufacturer's instructions. Fluorescence readings were taken using a FLOstar OPTIMA plate reader from BMG Labtec. The background values obtained from the negative control wells were subtracted from the test readings before data analysis.

Determination of cell metabolic activity

Cell metabolic activity was determined by measuring the reduction of 3-(4,5-Dimethylthiazol-2-yl)-2,5-diphenyltetrazolium bromide (MTT) into purple formazan crystals in the mitochondria of living cells. This assay was carried out using a Cell Growth Determination kit (CGD-1, Sigma) adopting a modified protocol. At the end of the required incubation time, the culture medium was removed from the wells and

cells were rinsed twice in sterile PBS. Serum-free culture medium (500µl) was then added to each well. MTT solution (50µl) was added to each well and the plates were incubated for 4 hours at 37^0C and 5% CO_2 after which the culture medium was removed from the wells and replaced with 200µl MTT solvent. The solvent was mixed using a 250µl pipette to ensure the complete dissolution of the formazan crystals. The solution from each well was transferred to a clean well in a 96-well plate and the absorbance was read in a plate reader at 570nm with a 690nm reference wavelength.

Assessment of cell differentiation

The amount of alkaline phosphatase (ALP) present in the cell cultures was used to determine the level of differentiation in the cell populations. Quantities of ALP present in the cultures were determined using a colorimetric protocol. In this assay, the substrate (4-nitrophenyl phosphate) is dephosphorylated by the alkaline phosphatase present in the sample, forming 4-nitrophenol. This reaction product is yellow and can be read by an absorbance plate reader with a wavelength of 405nm.

An assay buffer was prepared by combining 2ml of alkaline buffer solution with 30µl of igepal in 10ml distilled water. The assay substrate was prepared by adding 0.04g of 4-nitrophenyl phosphate to 10ml of alkaline buffer solution and 20ml of distilled water. Standards were prepared by the serial dilution of 4-nitrophenol solution in the assay buffer, producing solutions containing 0, 10, 50, 100, 200, 500 and 1000nmolml^{-1} 4-nitrophenol. Standards were tested in triplicate, with 100µl standard per well in a 96-well plate.

After the required incubation period, the culture medium was removed from the cell cultures and 500µl 0.05% triton-X solution was added to each well. The plates were then frozen at -80°C for one hour and defrosted at 37°C to ensure cell lysis. For cultures tested at 7 days incubation, two 10µl samples from each well were transferred to a 96-well plate. For cultures tested at 14 days incubation, a 10µl sample from each

well was diluted in 90µl assay buffer and then two 10µl samples was transferred to a 96-well plate. This dilution was accounted for in the final calculation of total 4-nitrophenol present in the sample. 90µl assay substrate was then added to each test well and the plate was incubated at 37^0C and 5% CO_2 for 10 minutes after which 50µl of sodium hydroxide (0.5M) was added to each well to stop the reaction. Following this, the reaction was measured in a plate reader at 405nm. The amount of 4-nitrophenol in each sample was determined by comparison with the standard curve. These results were normalised by the amount of DNA present in the sample, determined using a Picogreen assay as described below.

Determination of quantity of DNA

The Picogreen assay was used to determine the total DNA present in the lysate samples prepared for the alkaline phosphatase assay. Undiluted samples were stored at -80°C until the assay was performed using a Quant-IT Picogreen kit according to the manufacturer's instructions.

3.6 Biological testing using macrophages

3.6.1 J774.2 cell culture

The J774.2 murine macrophage cell line was cultured in Dulbecco's Modified Eagle Medium (DMEM)-F12 supplemented with 2mM L-Glutamine, 10% FCS and 1% antibiotic-antimycotic solution. All cells used in these experiments were between passages 9 and 15. Cells were seeded at 300 000 cellsml^{-1} in 30 ml of complete culture medium in T150 flasks and grown to confluence at 37 °C with 5% CO_2 before subculture. The culture medium was changed every 3 days.

Subculture

Cells were detached from the flask into the culture medium using a cell scraper. The cell suspension was transferred to a 50ml centrifuge tube and spun at 1500xg, at 20^0C for five minutes before being resuspended in 10ml of complete medium. A 10µl sample of this suspension was mixed in a 1:1 volume ratio with trypan blue and pipetted into the chamber of a haemocytometer. The cells in the sample were counted and, based on this cell count, cells were seeded into fresh flasks.

3.6.2 Seeding of macrophage cells onto ceramics

Before use in cell culture, the ceramic discs were kept for 24h in 70% industrial methylated spirit (IMS) at 4°C and rinsed in sterile PBS. Some discs were soaked in complete culture medium overnight, as described in Section 5.3. Discs were then allowed to dry in air in a 24-well plate, one disc per well, with the ground surface uppermost.

For the testing of biological responses to ceramic particles, samples of the particles were measured out by volume (10µl) and transferred to the 96-well plates using a spatula. As some particles of the ceramic were in suspension in the culture medium, with others remaining in the bottom of the well, the retrieval of all of the particles from soaking medium proved difficult. The powders were therefore not soaked in culture medium before cell seeding.

Confluent cells were then detached from the T150 flasks using a cell scraper. The cell suspension was transferred to a 50ml centrifuge tube and spun at 1500xg at 20^0C for five minutes before being resuspended in 20ml of complete medium. A 10µl sample of this suspension was mixed in a 1:1 volume ratio with trypan blue and pipetted into the chamber of a haemocytometer. The cells in the sample were counted and, based on this cell count, cells were seeded into the wells at 800 000 cellsml^{-1}, with 1ml of suspension

per well. Cells were also seeded directly onto the tissue culture plastic of the 24-well plate as a control. In addition, two types of cell-free controls (ceramic discs in culture medium and culture medium alone) were included. The culture plates were incubated at 37°C with 5% CO_2 for 24h before analysis of cell responses.

3.6.3 Analysis of macrophage cultures

Cytotoxicity

In order to assess the cytotoxicity of the materials to J774.2 cells a 50µl sample of culture medium was taken from each well of the 24-well plate containing a disc, as well as controls, and transferred to a 96-well plate. 100µl of 20% triton-X was added to each well of the 24-well plate to lyse the cells. A 50µl sample was taken from each well and transferred to the 96-well plate. These samples were then analysed to determine the amount of LDH present in the sample as described in Section 3.5.3. From the data obtained, the percentage of total LDH present in the culture before lysis was calculated, providing an indication of the percentage of cells in the well that were viable before lysis.

Cytokine expression

The production of inflammatory cytokine IL1β was examined using gel electrophoresis and western blotting. Two additional control wells were seeded with J774.2 cells. These wells were both primed with LPS (1µgml^{-1}) 18 hours after seeding. Thirty minutes before the end of the 24 hour incubation, ATP (1 mM) was added to one of these controls. A 200µl sample of culture medium was taken from all test and control wells, concentrated in cut-off filters and transferred to a 1ml Eppindorf tube. A 20% triton-X solution (80µl) was then added to all wells to lyse the cells and a further 200µl sample of the resulting supernatant was transferred to a second 1ml Eppindorf tube. All samples were diluted 2x with sample buffer to solubilise the proteins, heated for 5min at 80°C and stored at -20°C until testing.

Before testing, samples were allowed to defrost at room temperature. 25µl of each sample was loaded into a gel for electrophoresis. One lane per gel was loaded with a protein standard to allow the estimation of protein sizes. Samples were electrophoresed at 200V in running buffer for 40 minutes using the Bio-Rad Mini Protean II system (Bio-Rad, UK).

The proteins in the gels were transferred onto nitrocellulose membrane by electroblotting in transfer buffer for 1h at 30V. Membranes were incubated in blocking buffer for 60 minutes at room temperature under agitation, then incubated overnight at 4°C under agitation in blocking buffer containing Mouse IL-1β antibody (MAb 1:5000). After 3 washes (5 minutes each) in wash buffer, membranes were incubated for a further 60 minutes at room temperature in blocking buffer containing polyclonal rabbit anti-mouse IgG/HRP antibody (1:10 000). The membranes were washed (6 x 5 minutes) and treated with Amersham™ ECL Advance™ western blotting detection agent according to the manufacturer's instructions. Finally, membranes were exposed to X-ray film, which was developed in an X-ray film processor.

3.7 Statistical methods

Data was plotted as mean ± standard deviation. The number of samples was 6 (n=6) unless otherwise stated. For the comparison of means, data was first tested for normality using Lilliefors test for normality at a 5% significance level. One way analysis of variance (one way ANOVA) with simultaneous confidence intervals was used to assess the significant difference ($P<0.05$) between three or more independent samples. Where data was not normally distributed, the samples were compared using a Kruksall-Wallis test.

4 Characterisation of HABT composites

4.1 Introduction

Though previous studies have shown HABT ceramics to have properties that may result in enhanced biological responses in canine subjects [6], little information is available on the composites themselves (see Section 2.5.3). For example, details of the composite microstructure, phase composition, HA and BT content and polarisation-strain-field loops for the composites were not given. For these materials to be used as bone graft substitutes, it is important for their post-sintering composition, structure and electrical properties to be properly assessed. Subsequently, the optimal proportion of BT to be included in the HABT composite can be determined.

This chapter examines the ferroelectric properties (d_{33}, d_{31}, permittivity, polarisation-field and strain-field loops), microstructure and chemical composition of HABT composites of various compositions (0-100% BT by volume) using methods described in Section 3.4. Based on the results of these tests, an HABT composite is selected for *in vitro* assessment of biological responses in Chapter 5.

4.2 Results

4.2.1 Piezoelectric coefficients

HABT composite discs were manufactured and poled and their longitudinal and transverse piezoelectric coefficients (d_{33} and d_{31}) were measured as described in Section 3.4. As demonstrated in Figure 4.1, no piezoelectric coefficient was found in ceramics containing less than 70%BT (d_{33} and d_{31} =0).

In ceramics containing 70% or more BT, both piezoelectric coefficients varied according to the proportion of BT in the ceramic up to a maximum of d_{33}= 108.5 ± 12.5pCN^{-1} and d_{31} = - 45.0 ± 5.3pCN^{-1} for discs made with 100% BT powder.

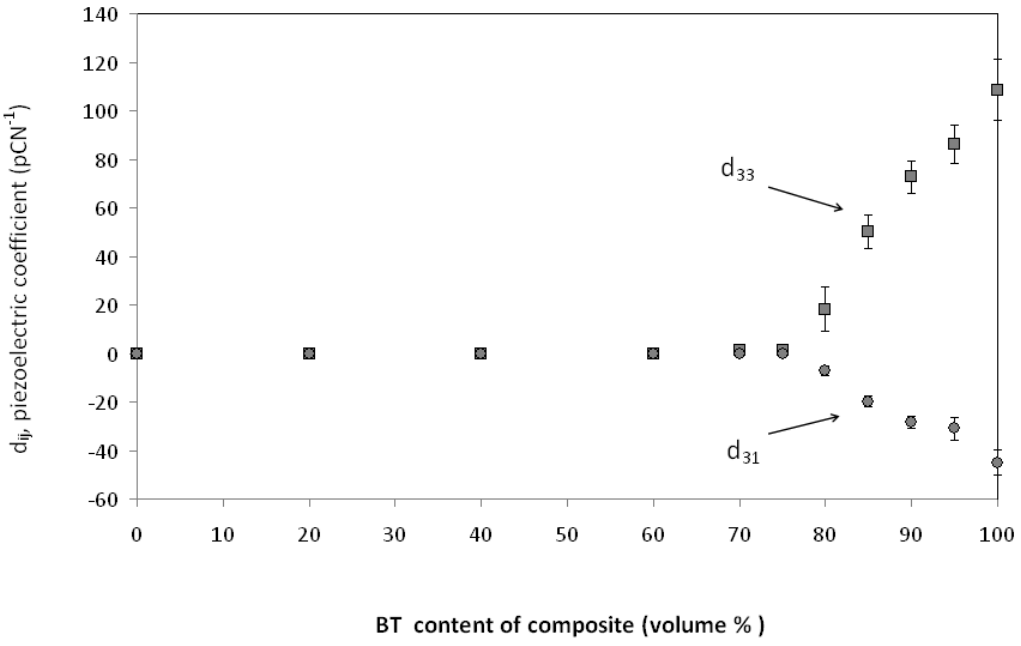

Figure 4.1 Piezoelectric charge coefficients of HABT composites

4.2.2 Permittivity

Figure 4.2 shows the relative permittivity of the composites at a range of frequencies. Some frequency dependence (dielectric dispersion) was found for all compositions, particularly at low frequency. The degree of dispersion decreased as the proportion of the BT in the material was reduced, though a small amount of dispersion was exhibited by the HA (0% BT) ceramic. Similarly to the piezoelectric coefficient, the relative permittivity of the HABT composites was dependent on the amount of BT in the composite; permittivity increased as the volume fraction of BT was increased.

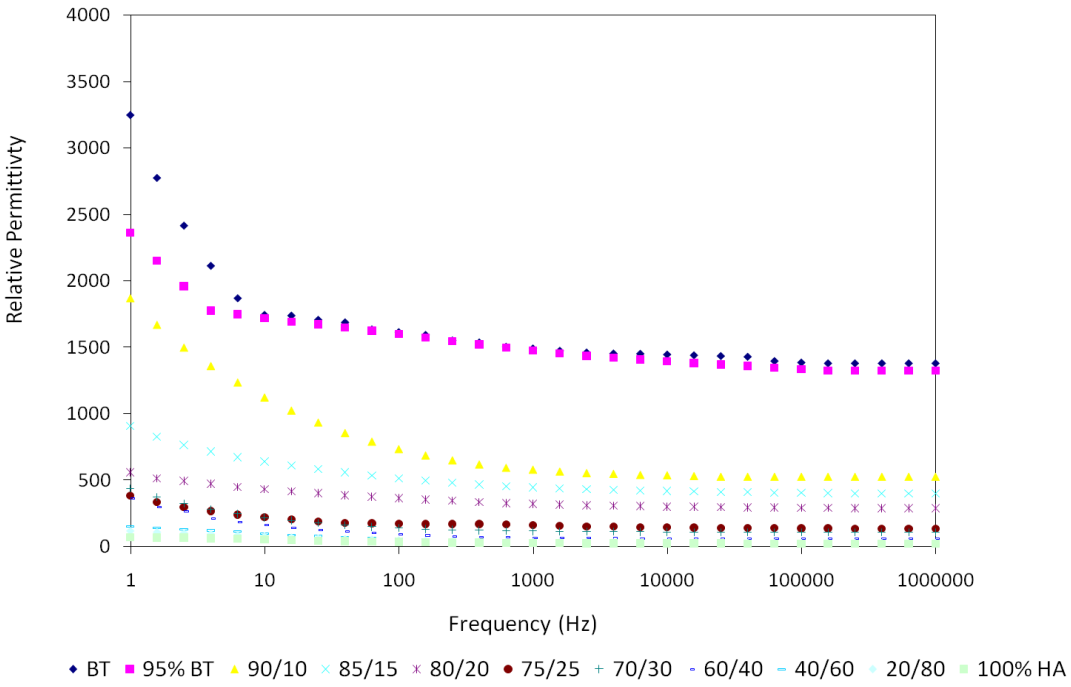

Figure 4.2 The frequency dependence of the permittivity of HABT composites

It is standard practice to cite the relative permittivity of a material measured at 1kHz, as shown in Figure 4.3. At this frequency, the relative permittivity of the composites remains within the bounds set by those of the pure materials (BT and HA). For example, with a relative permittivity of 26 for HA and 1490 for BT, the series and parallel permittivity values (Equations 2.8 and 2.9) for 90% BT are 1346 and 225 respectively, with an actual value found of 581. The relative permittivity of the composite containing 95% BT was very close to that of the 100% BT ceramic.

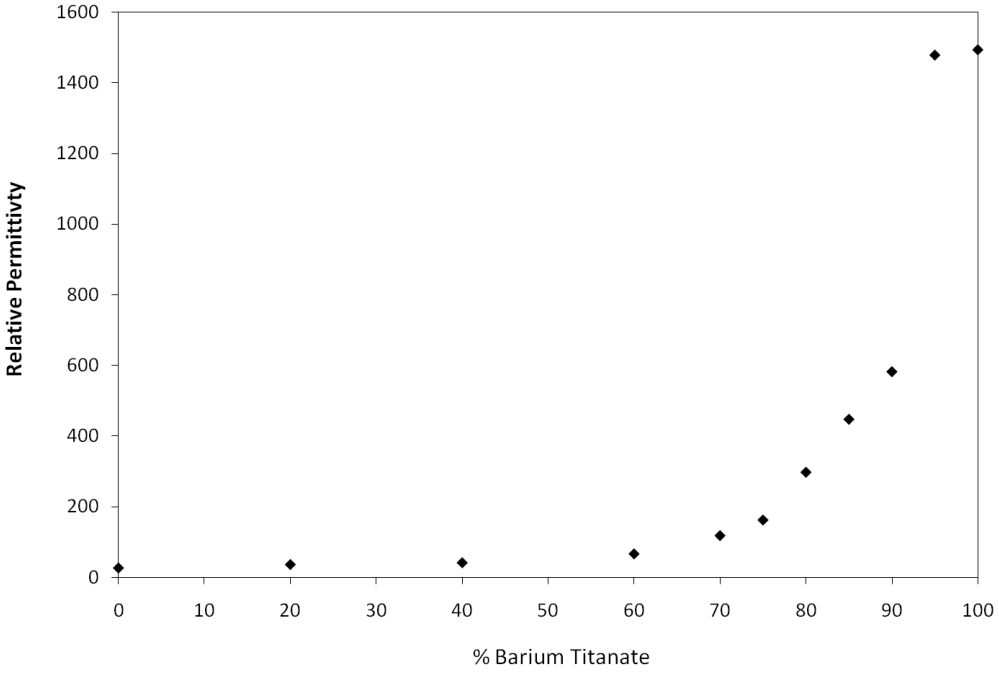

Figure 4.3 The piezoelectric voltage coefficients of HABT composites

Using Equation 2.5, the piezoelectric voltage coefficient (g_{33}, the electric field induced per unit stress) was calculated for each composite (Figure 4.4). The highest piezoelectric voltage coefficient was approximately $14x10^{-3}Vm^{-1}Pa^{-1}$, found in the 90% BT composite. Using Equation 2.10, it can therefore be shown that the application of a 1MPa stress on a sample of the 90% BT composite of 1mm thickness would generate a potential of 1.4V.

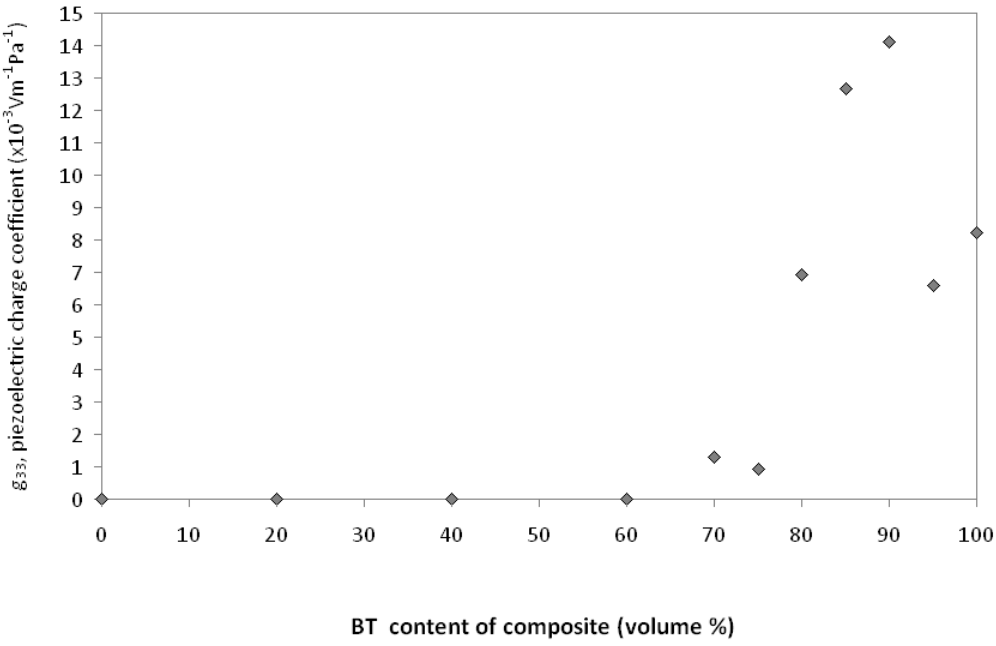

Figure 4.4 The piezoelectric voltage coefficients of HABT composites

4.2.3 Polarisation-field and strain-field loops

Polarisation-field (P-E) and strain-field loops (S-E) loops were generated for two samples of each of BT, HABT discs containing 95, 90, and 80% BT and HA. The results for the pairs of samples were comparable in all cases and representative curves for each material are shown in Figures 4.5 to 4.9. The P-E loops show data from low (small loops) to high (large loops) applied electric fields with a maximum field of 2kVmm^{-1}, as at higher electric fields there is a risk of dielectric breakdown of the sample. The mean remnant polarisation (calculated from $P_r(1)$ and $P_r(2)$ as shown Figure 4.5a, the equivalent of points D and G in Figure 2.10) and mean coercive field (calculated from $E_c(1)$ and $E_c(2)$) at the maximum applied field for each ceramic are give in Table 4.1 along with the piezoelectric charge coefficient calculated from the gradient of the strain-field loop.

Figure 4.5a shows the change in polarisation in a BT disc subjected to an increasing applied field. At low a low applied field, domain switching did not occur, and so the P-E loop appears small and elliptical in shape. The absence of domain switching at low fields is confirmed by Figure 4.5b, which shows that the peaks in current known to be characteristic of domain switching do not occur. At higher applied fields (2kVmm^{-1}) the polarisation of the BT was comparable with that given in the literature (see Section 2.4), and showed the material to be ferroelectric. The linear S-E relationship shown in Figure 4.5c clearly confirms that at low fields no domain switching occurred at low applied fields (0.5kVmm^{-1}). In this region the dipoles are expanding and contracting in response to the applied electric field, resulting in a linear S-E relationship. At higher fields (Figure 4.5d) the characteristic "butterfly" shape of the S-E loop is observed due to domain switching and shows the material to be ferroelectric.

The characteristic P-E loop for BT is also comparable to those obtained for the HABT composites containing 95 and 90% BT, as seen in Figures 4.6a and 4.7a. The polarisation, and therefore remnant polarisation, of the composites decreased the

proportion of HA in the composite increased (note the difference in scales between Figures 4.5a and 4.6a as well as the decreasing remnant polarisation values given in Table 4.1). As with the BT, domain switching was not observed at low applied fields the 95 and 90% BT composites, as shown by the lack of peaks in the I-E curves (Figures 4.6b and 4.7b) and the linear low field S-E curves (Figures 4.6c and 4.7c). At higher fields the I-E curves (Figures 4.6b and 4.7b) and "butterfly" shaped S-E curve (Figures 4.6d and 4.7d) confirm that the composites were ferroelectric and that domain switching occurred. The development of strain in these composites was asymmetrical, unlike that observed in the 100% BT ceramic (Figure 4.5d).

The HABT composite containing 80% BT, showed no piezoelectric or ferroelectric properties, as shown in Figure 4.8. The P-E relationship remained linear (Figure 4.8a), the current measured showed no "domain switching" peaks (Figure 4.8b) and no strain was induced at either low (Figure 4.8c) or high applied field (Figure 4.8d).

The results found for the 80% BT composite resemble those found for HA (Figure 4.9). Again, the absence of polarisation (Figure 4.9a), current peaks (Figure 4.9a) and induced strain (Figure 4.9c and d), indicate that HA is neither ferroelectric nor piezoelectric. The I-E loops for both the 80% BT composite and the HA were small in comparison with those obtained from the piezoelectric materials and were elliptical in shape.

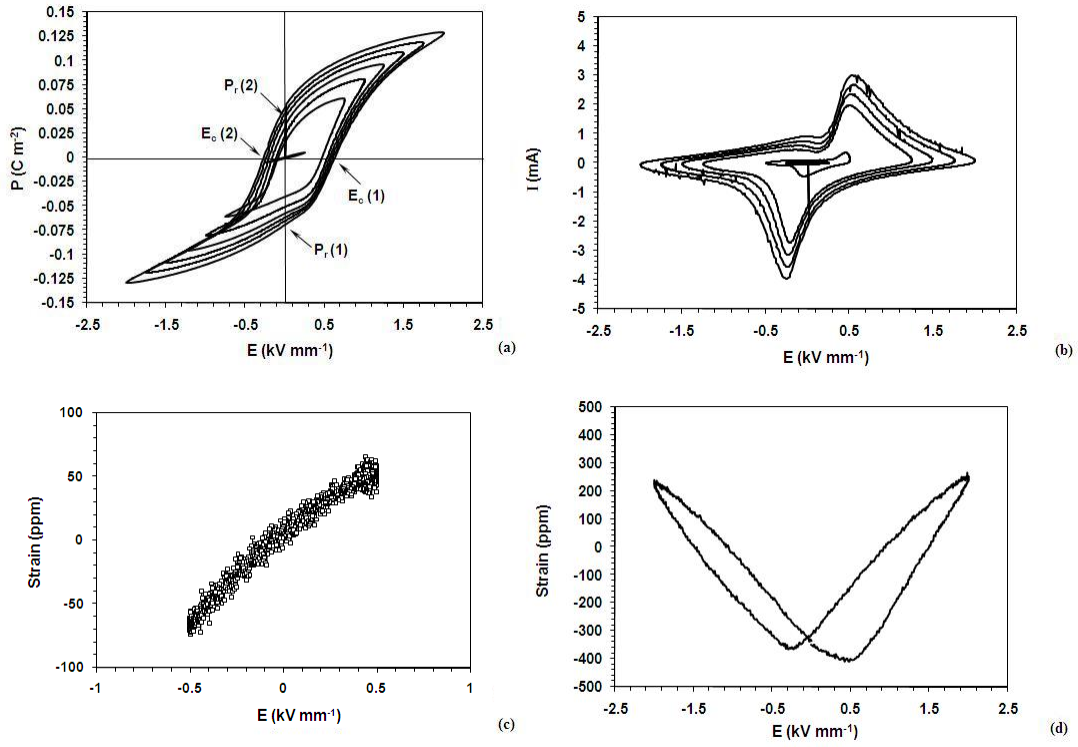

Figure 4.5 Hysteresis loops for poled BT – (a) Polarisation-field loop, (b) Current-field loops for increasing applied electric field, (c) Strain - field loop for low applied field (0.5kVmm^{-1}), (d) Strain - field loop for high applied field (2kVmm^{-1})

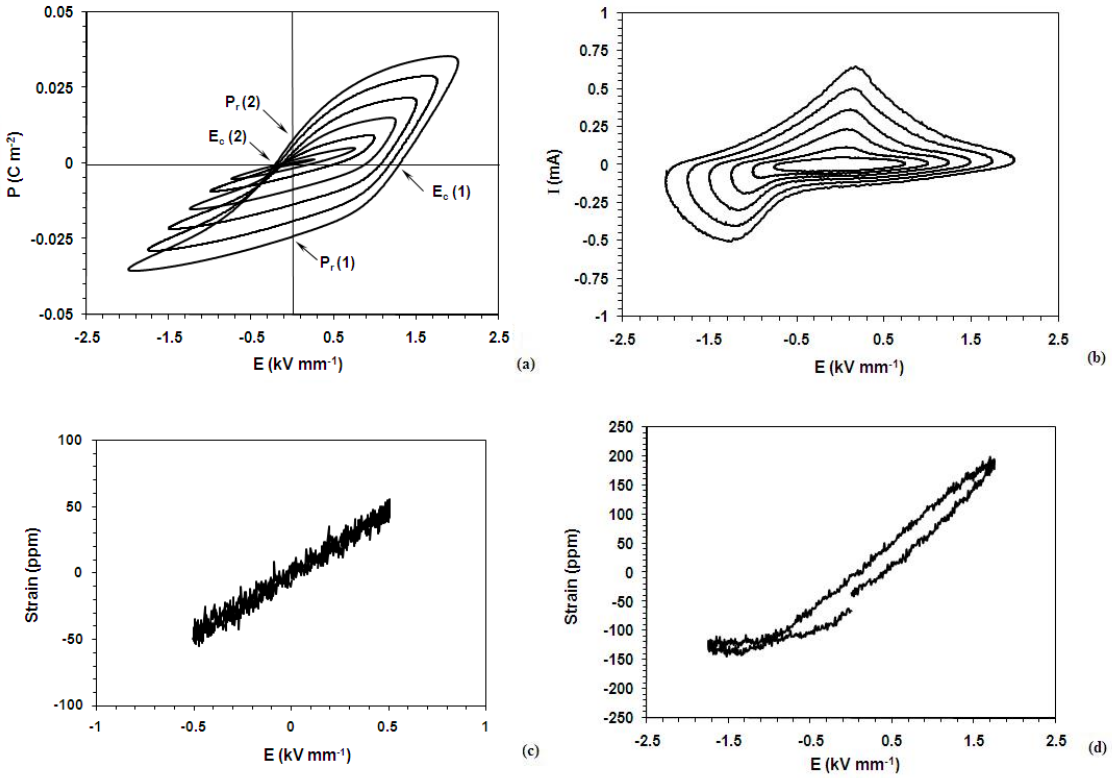

Figure 4.6 Hysteresis loops for poled 95% BT – (a) Polarisation-field loop, (b) Current-field loops for increasing applied electric field, (c) Strain - field loop for low applied field (0.5kVmm^{-1}), (d) Strain - field loop for high applied field (2kVmm^{-1})

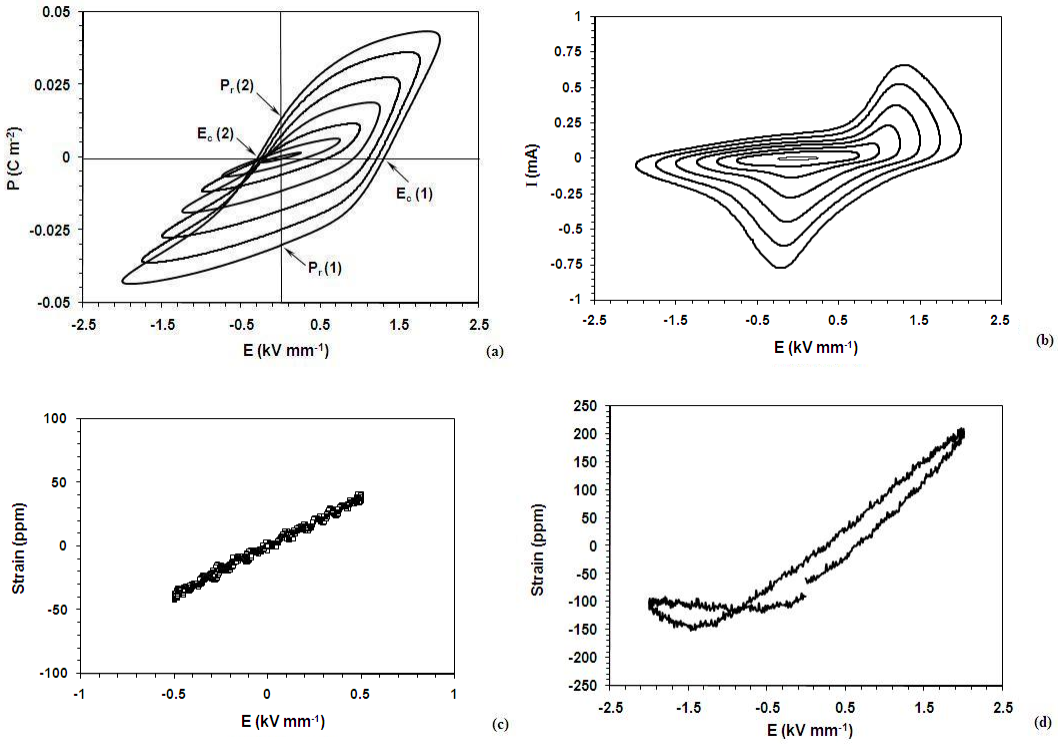

Figure 4.7 Hysteresis loops for poled 90% BT – (a) Polarisation-field loop, (b) Current-field loops for increasing applied electric field, (c) Strain - field loop for low applied field (0.5kVmm^{-1}), (d) Strain - field loop for high applied field (2kVmm^{-1})

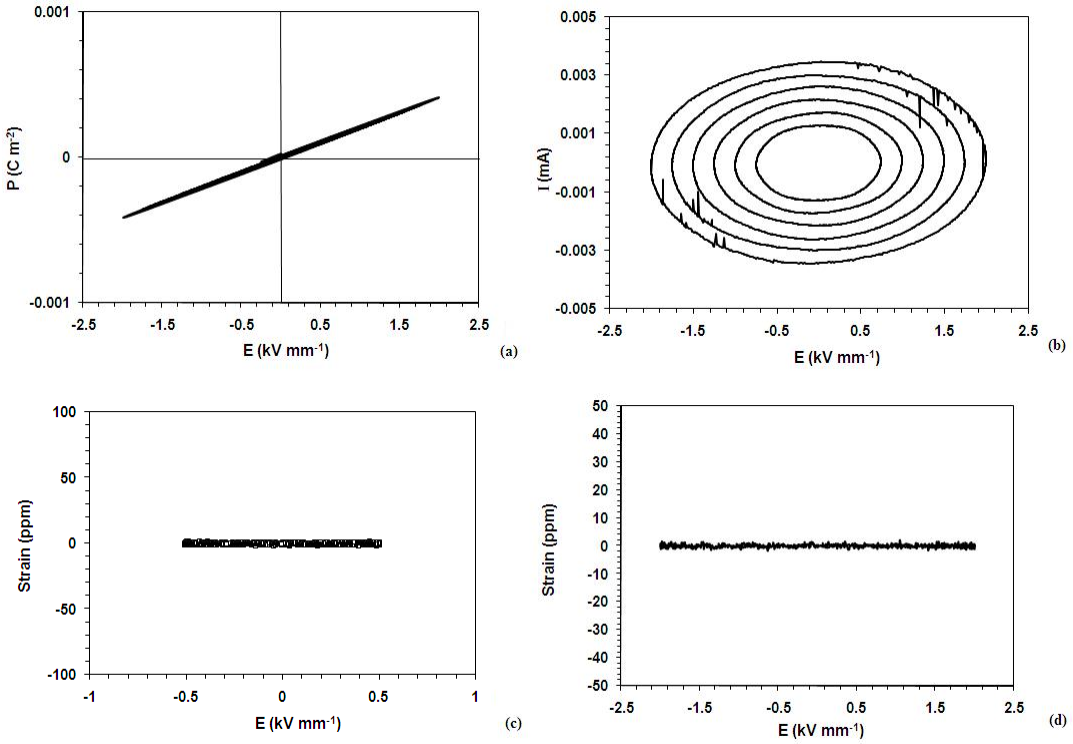

Figure 4.8 Hysteresis loops for poled 80% BT – (a) Polarisation-field loop, (b) Current-field loops for increasing applied electric field, (c) Strain - field loop for low applied field (0.5kVmm^{-1}), (d) Strain - field loop for high applied field (2kVmm^{-1})

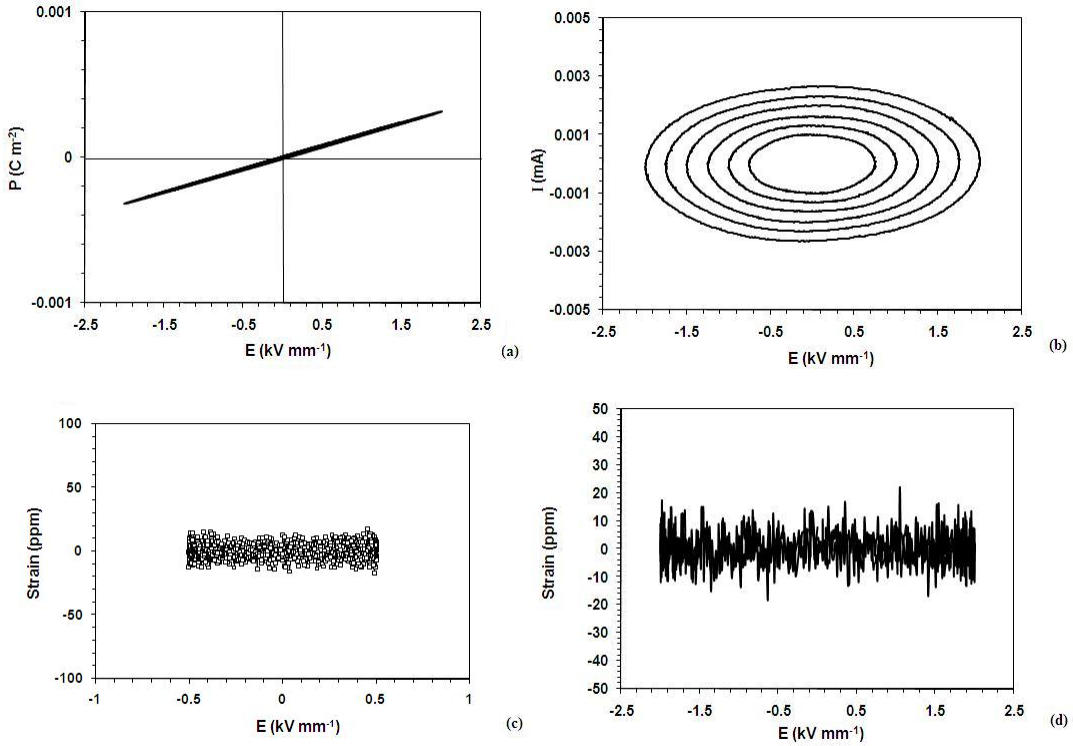

Figure 4.9 Hysteresis loops for HA - (a) Polarisation-field loop, (b) Current-field loops for increasing applied electric field, (c) Strain - field loop for low applied field (1kVmm^{-1}), (d) Strain - field loop for high applied field (2kVmm^{-1})

Table 4.1 Remnant polarisation, coercive field and piezoelectric voltage coefficient of HABT composites

Material	Mean remnant polarisation (Cm^{-2})	Mean coercive field ($kVmm^{-1}$)	Piezoelectric charge coefficient (pmV^{-1})
BT	0.060	0.45	149
95% BT	0.016	0.76	110
90% BT	0.008	0.66	95
80% BT	0	0	0
HA	0	0	0

4.2.4 Microstructure

Unpoled discs of a range of compositions were sectioned and prepared for examination using SEM as described in Section 2.4. In Figure 4.10a the typical fine grained (2-3μm) polycrystalline structure of HA is clearly apparent. Figure 4.10b shows 100% BT, on which surface striations indicated the boundaries of ferroelectric domains, as indicated by the arrow. Ferroelectric domains are also visible, though less clearly, in the 95% BT ceramic (indicated by an arrow in Figure 4.11a). In discs containing 90% BT ferroelectric domains were no longer apparent (Figure 4.11b). Qualitative observation showed the ceramic grain size decreased from 30-50μm in pure BT to 10μm in 95% BT. This trend continued the proportion of HA in the composite was increased, with grain sizes in 90% BT reduced to 1-2μm.

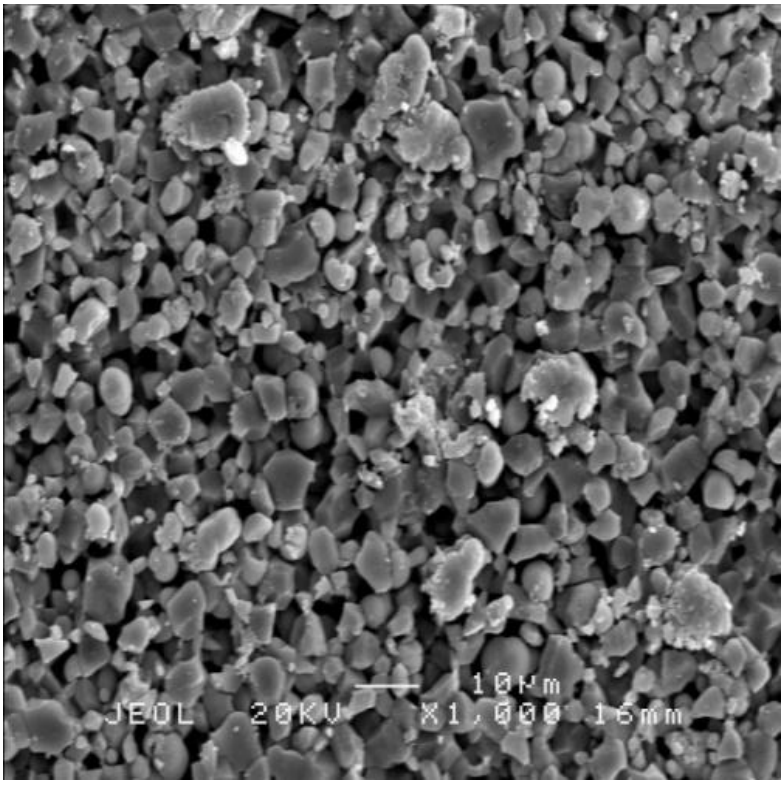

(a)

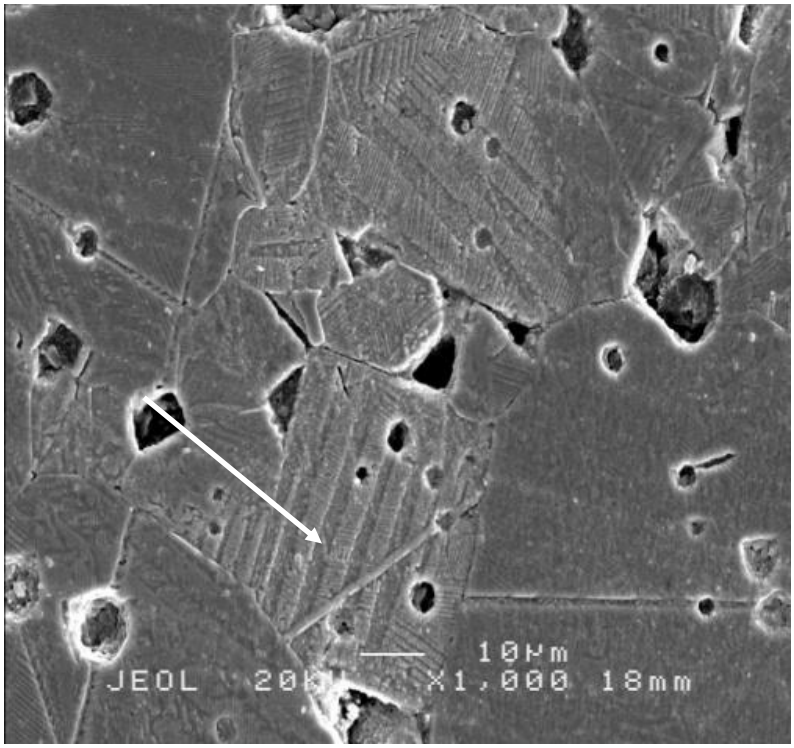

(b)

Figure 4.10 Microstructure of (a) HA and (b) BT with an arrow indicating the ferroelectric domains

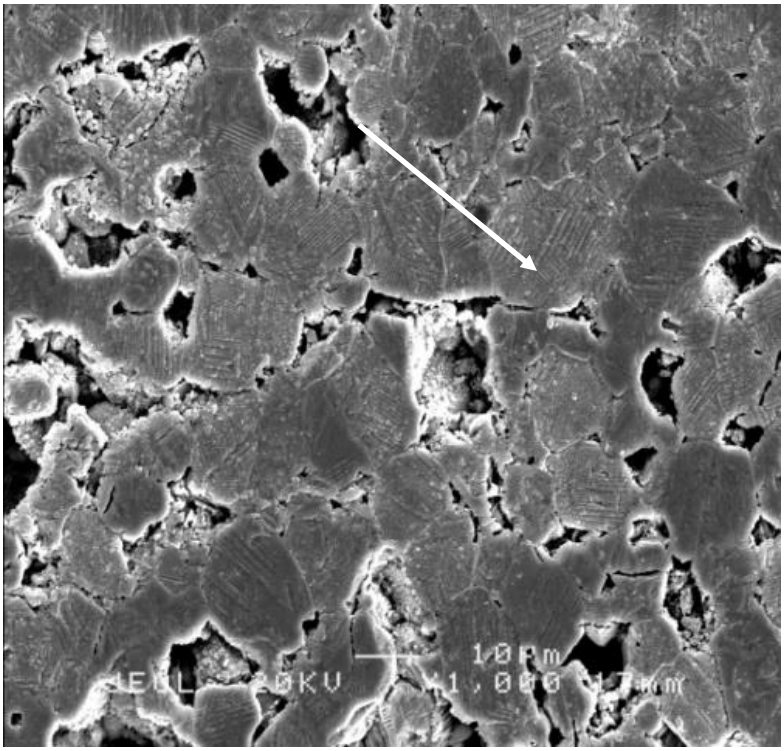

(a)

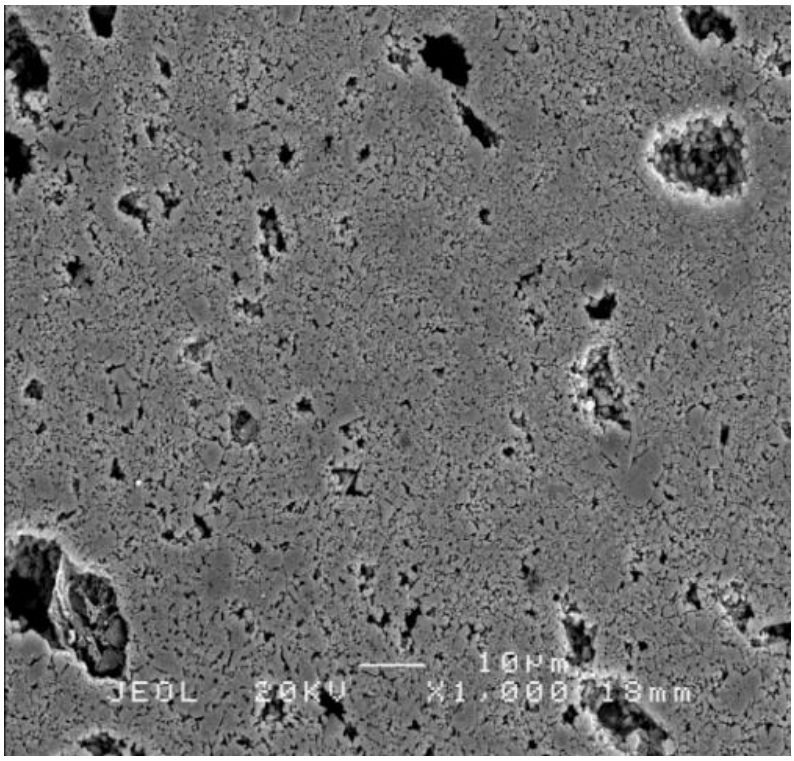

(b)

Figure 4.11 Microstructure of (a) 95% and (b) 90% BT with an arrow indicating the ferroelectric domains

4.2.5 Composition

XRD

In order to assess any chemical reactions occurring between the HA and the BT during the sintering of the ceramics, the composition of sintered discs was examined by XRD. Figure 4.12 shows XRD spectra for HA and BT ceramics as well as for three compositions of HABT composite which displayed piezoelectric properties. The spectra are offset in the figure for clarity and each spectrum has been normalised by its maximum intensity to facilitate comparisons. The major characteristic peaks of HA included those at 31.8, 32.2, 32.9, 39.9 and 46.7°. These correspond to lattice planes 211, 112, 300, 310 and 222 respectively [190]. Those for tetragonal BT were at 31.5, 38.9 and 45.4°, corresponding to lattice planes 110, 111 and 200 [191]. These peaks concur with published data for these ceramics [189]. The clarity of the peaks in the BT and HA tested indicates a high crystallinity in the ceramics and an absence of contamination.

For the most part, the composites did not generate distinct peaks other than those characteristic of HA and BT. However, four small peaks were evident, at 2θ angles of 41°, 43°, 47° and 59° respectively, which were not present for either HA or BT. The size of these peaks increased as the proportion of HA in the composite was raised. To show this in more detail, the XRD spectrum for HABT containing 70% BT is shown in Figure 4.13. The major peaks are labelled to show those attributable to the presence of HA and BT in the material, with unidentified peaks marked with an asterisk.

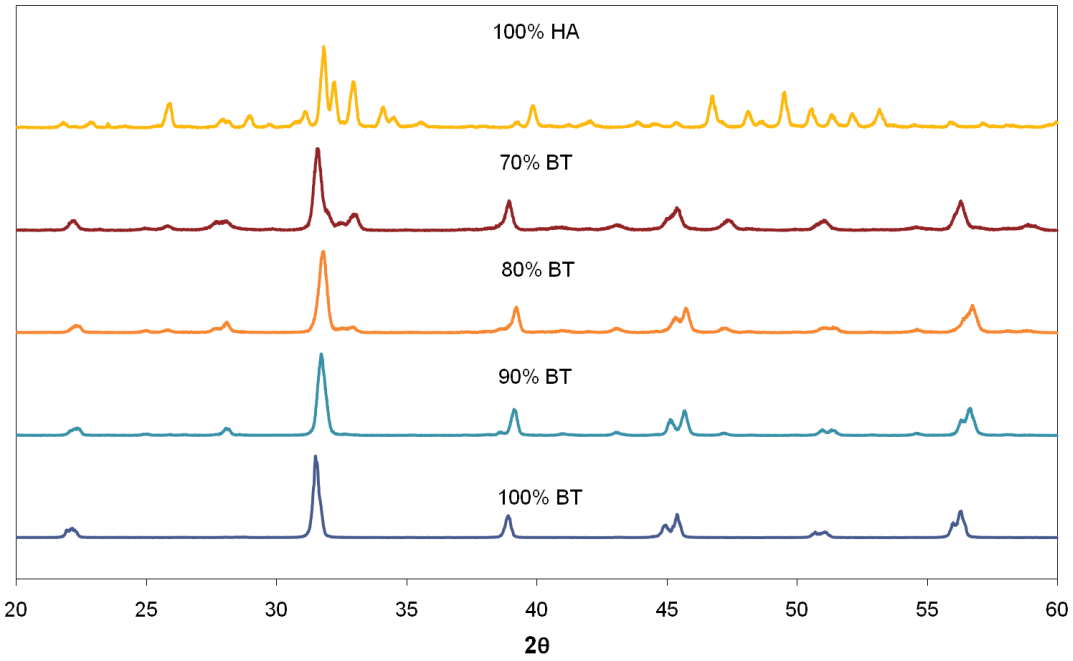

Figure 4.12 X-Ray diffraction spectra of HA, BT and HABT ceramics

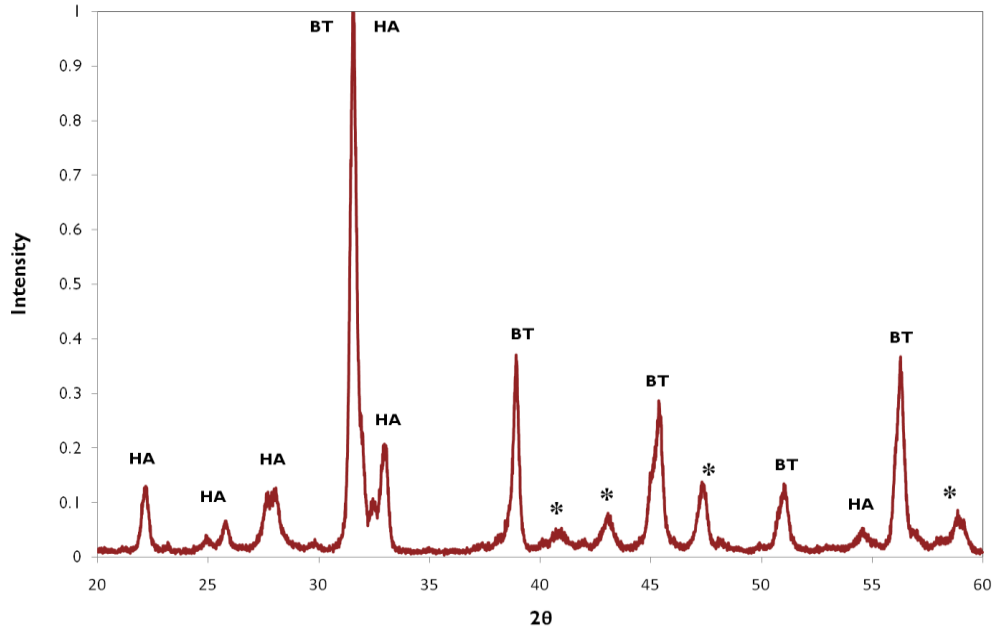

Figure 4.13 X-Ray diffraction spectrum of 70% BT

EDAX

In addition, X-ray maps were taken of samples examined by SEM to analyse the distribution of barium, calcium and titanium ions in the composite materials. In general, the barium, titanium and calcium ions measured were found to be well distributed throughout the material. However, some examples were found of areas in which a large amount of calcium and some titanium but little barium was present. These areas appeared to form clusters around the internal edges of pores in the ceramic, as shown in Figure 4.14.

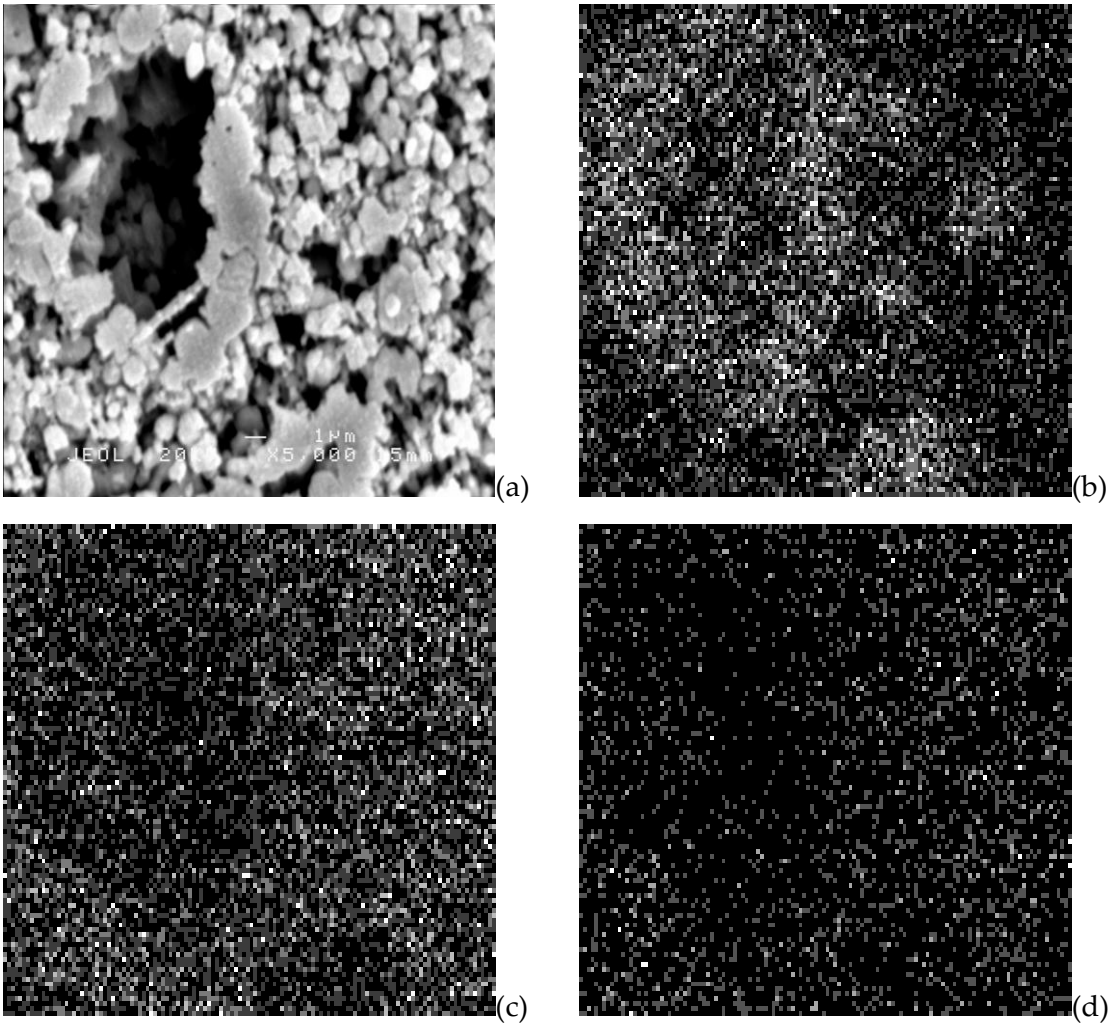

Figure 4.14 (a) SEM image of 85% BT ceramic, x5000 magnification, pore size approximately 10μm and maps of (b) map of calcium ions, (c) titanium ions and (d) barium ions corresponding to the same image

4.3 Discussion

The piezoelectric charge coefficients found for HABT ceramics containing 80% or more BT were in a range which, based on the findings of previous studies (see section 2.5.3), could be expected to induce an improvement in biological response. For comparison, the HABT composites containing 80 and 90% BT had piezoelectric charge coefficients of 18 and 72pCN^{-1}, respectively. Improved biological responses to materials with charge coefficients of 6pCN^{-1} [6] and 17pCN^{-1} [134] have previously been reported. Based on the current results, the HABT ceramic studied by Feng *et al* must have contained a minimum of 80% BT. The coefficients were significantly higher than the 0.2-0.7pCN^{-1} measured in bone [112, 192], though *in vivo* additional stress generated potentials are produced by streaming potentials, as discussed in Section 2.4.6.

The absence of piezoelectric coefficients in HABT composites containing less than 70% BT indicates that these materials are neither ferroelectric nor piezoelectric. For composites containing more than 70% BT the piezoelectric charge coefficient varied according to the amount of BT in the ceramic. This may result from matrix "clamping", in which the non-piezoelectric component restricts the piezoelectric component during the poling process, preventing it from developing a strain. This phenomenon has been previously documented in composites of ferroelectrics and polymers [107]. As HA is stiffer than the polymer examined in that study, the clamping effect may be more apparent than that induced by the polymer. The elastic compliance of the polymer is given as 257×10^{-12} m^{2}N^{-1}, which corresponds to a modulus of elasticity of 4GPa [107]. The modulus of elasticity of HA has been reported as 89GPa [193].

The piezoelectric charge coefficients in the HABT composites compare favourably with reported values [106], which suggested a low d_{33} (2pCN^{-1}) for HABT composites containing 90% BT. The trend of decreasing d_{33} with increasing HA content observed in the current study resembled that reported previously [106], albeit with a significantly

higher maximum d_{33}. The current study produced a d_{33} of 108pCN^{-1} for 100% BT, compared with 20pCN^{-1} reported in the published study [106]. The cause of this variance in coefficients may be the BT used in the composite, as the d_{33} of the 100% BT ceramics differed significantly between the two studies. As previously stated, reported piezoelectric charge coefficients for BT range from 87 [95] to 190pCN^{-1} [96].

The relative permittivities of HA and BT (26 and 1490 respectively) are comparable to published data. A relative permittivity of 1500 has been measured for BT at room temperature [97]. The permittivity of HA is highly variable, depending on fabrication techniques. Values between 4 [137] and 57 [138] have been reported. These results call into question the materials properties reported by Feng *et al*, who gave a value of relative permittivity for their HABT composite (4864) which was significantly higher than for the BT used in its fabrication (1700) [136].

The relationship between the g_{33} (which, as shown in Equation 2.6, may be given by the relationship $g_{33} = d_{33}/\varepsilon$) and the BT content of the ceramic was non-linear. This resulted from differences in the rate at which the d_{33} and permittivity of the composites, used to calculate the voltage coefficient (g_{33}), decreased as the amount of HA in the material increased. The material displaying the highest voltage coefficient was the 90% BT composite. This may be related to the amount of calcium in the composites, as the doping of barium titanate ceramics with calcium has previously been reported to modify the dielectric constant [194].

Though the ferroelectric domain boundaries were not visible in ceramics containing 90% BT and below as they were in 100% and 95% BT, the piezoelectric nature of the materials is confirmed by the measurement of the PSE loops and piezoelectric coefficients. The asymmetry of the P-E loops for the BT, 95% BT and 90%BT discs resulted from the poling of the material before testing. This "biased" loop shape is typical of poled BT [97], as shown in Figure 2.11b. The slope of the tops and sides may

indicate variation in grain size within the materials as a high degree of "squareness" in P-E loops has been linked to homogeneity and uniformity of grain size [93]. The coercive field (E_c) did not increase linearly with the amount of HA in the composite. The lower E_c for 90% BT in comparison with 95% BT may indicate a higher level of domain pinning, a process by which vacancies and inclusions within the crystal structure limit the deformation of the domain walls [195], occurring in the 95% BT ceramic. The peaks in the I-E curves for these materials confirmed that ferroelectric domain switching occurred.

The piezoelectric coefficients calculated from the gradient of the low field S-E loops are generally slightly higher than, but comparable to, the values measured with piezometer. The reduction in size of the loops as BT content decreased concurred with the trend found by measuring the d_{33} using the piezometer (as seen in Figure 4.1).

While the S-E loop for BT displayed a classic "butterfly" loop, those for the ferroelectric HABT composites were asymmetrical. Asymmetrical strain development has been linked in the literature to domain pinning [195], suggesting that the addition of HA to BT introduce inclusions in the material which limit the deformation of the domain walls. It is also possible that matrix clamping may affect strain within the composites.

The remnant polarisation of ferroelectric materials does not depend on mechanical loading. The growth of cells on the surfaces of a poled material may be affected by the remnant surface charge in the absence of stress-generated-potentials. The remnant polarisation of $0.06 Cm^{-2}$ and coercive field of $0.45 kVmm^{-1}$ observed for BT are comparable with published data, which gave a remnant polarisation of ~$0.12\ Cm^{-2}$ for a field of $2 kVmm^{-1}$ [196]. These values are lower are lower than the $0.33 Cm^{-2}$ reported for a P(VDF-TrFE)/BT [130]. However, the results in this paper were inconsistently reported as the stated remnant polarisation for the composite ($0.33 Cm^{-2}$) does not match that displayed in the accompanying figure (~$0.14 Cm^{-2}$).

The absence of piezoelectric properties in HA was confirmed by the absence of strain under the applied electrical field. The I-E and S-E curves confirm that the HA discs were not ferroelectric. The I-E loops for these materials are circular because they behaved as capacitors, discharging as the polarisation of the applied field switched. As the response of the material lagged behind the applied field, a current was recorded at 0 field, with no current at the full applied field. The linear P-E relationship, typical of a capacitor [97], does not concur with the conclusions of a previous study that HA shows P-E hysteresis at comparable applied fields [118]. The P-E loops given for HA in the earlier study are typical of a "lossy capacitor" and do not indicate ferroelectric properties in the HA [97, 197]. Both the data included in the earlier work and the current study show HA to behave as a capacitor, albeit with less losses in the current material.

The 80% BT composites exhibited a measureable d_{33} when analysed with the piezometer. No evidence of piezoelectricity was found, however, in the P-E and S-E loops. This may indicate some manufacturing variability in the ceramics, rendering the 80% BT discs unsuitable for use in biological testing as they may not display piezoelectric properties.

The microstructure of the ceramics changed as the composition was altered. In particular, the size of grains was found to decrease as the proportion of HA in the composite increased. Grain sizes were up to 98% in the 90% BT composite than in the BT ceramic. It is possible that this reduction in grain size contributes to the observed decrease in the piezoelectric coefficients of the composites, as discussed in Section 2.4. The grain sizes for some of the composites displaying a piezoelectric coefficient (90% and above BT) were not sufficiently small to limit the piezoelectricity of the ceramic, as previous studies have shown no link between grain size and piezoelectric properties in materials with grain sizes between 1 and 100μm [10]. Other factors must therefore

have influenced their piezoelectric properties. However, as the amount of HA in the ceramic as increased, the grain size decreased below 1μm. As previously reported for lead zirconate-titanate ceramics with comparable grain sizes, grain size may have been a factor in limiting the piezoelectric properties of these materials [108].

The XRD spectra for HA and BT match those from with published data (PDF 09-0432 and PDF 05-0626 respectively) [189]. The peaks seen in the HABT composites which do not match peaks for HA or BT may indicate the presence of different phases. Table 4.2 lists compounds which contain the same elements as HA and BT and have peaks corresponding to those observed in the HABT ceramics.

Table 4.2 Possible compounds in HABT composites

2θ	Compound	PDF File [189]
40.5 – 41.1	β - TCP	PDF 09-0169
	Barium phosphate	PDF 25-0028
	Calcium barium hydrogen phosphate	PDF 88-0042
42.9	Barium phosphate	PDF 25-0028
	Barium titanium phosphate	PDF 12-0684
47.3	β - TCP	PDF 09-0169
	Calcium barium hydrogen phosphate	PDF 88-0042
	Barium phosphate	PDF 25-0028
	Barium titanium phosphate	PDF 12-0684
	Calcium titanium oxide	PDF 14-0151
58.5-59.0	Calcium barium hydrogen phosphate	PDF 88-0042
	Calcium titanium oxide	PDF 14-0151

It is not possible, based on the available data, to definitively distinguish which, if any, of the above compounds were present in the composites. XRD analysis does not identify either phases making up small proportions (approximately 2% or less) of the total mass of the sample or any amorphous phases [198]. It is clear, however, that the main phases present were HA and BT. The quantification of amounts of each compound present in the material was not possible due to the significant overlap of the

main peaks of HA and BT on the XRD spectra. The sharpness of the peaks in the spectra indicated a high level of crystallinity in the ceramics.

Previously reported XRD analysis of HABT ceramics was carried out on composites containing significantly lower proportions of BT than those examined in the current study (10-20% BT) [106]. It is not, therefore, directly comparable with results obtained here. The published study does, however, indicate that the absence of piezoelectric properties in composites containing low proportions of BT may result from the formation of non-piezoelectric phases in the ceramics during sintering. It may be possible to preserve a larger proportion of piezoelectric BT in a composite by varying the sintering conditions to limit the formation of non-piezoelectric phases during sintering [106].

4.4 Conclusions and key findings

A range of HABT ceramics containing a range of proportions of BT was manufactured. Composites containing 80% or more BT by volume were ferroelectric. The highest piezoelectric voltage coefficient detected was $14x10^{-3}$ $Vm^{-1}Pa^{-1}$, in the 90% BT composite. The highest piezoelectric charge coefficient (d_{33}) was $86pCN^{-1}$, in the 95% BT composite. This is higher than the piezoelectric coefficient of other materials shown to induce an improved biological response. The ferroelectric behaviour of the composites also varied according to the proportion of BT in the ceramic and was found to remain within the bounds set by the permittivities of HA and BT. The piezoelectricity of the 95 and 90% composites was confirmed by the P-E and S-E loops.

The structure of the composites was dependent on their composition, with significant reductions in grain size noted as the proportion of HA in the ceramic increased. XRD analysis showed the composites to be mainly composed of HA and BT, but with small amounts of reaction phases. The reduction of the piezoelectric properties as the HA content increased is attributable to these two factors as well as to the "clamping" effect.

It may be possible to increase the piezoelectric properties of composites containing a lower proportion of BT by varying the sintering conditions. In contrast with the suggestion of some previous literature [118], it is clear that HA is not ferroelectric.

The 90% BT composite displayed a high d_{33} and the highest g_{33} of all the composites tested. Its piezoelectric properties were shown to be consistent by examination of its polarisation-field and strain-field loops. The 90% BT composite was therefore the most suitable composite of those manufactured for use in biological testing.

Key findings:

i. HABT composites containing more than 70% are ferroelectric in nature and display piezoelectric coefficients when poled.
ii. The piezoelectric properties (d_{33}, g_{33}, ε and PSE loops) of HABT composites are dependent on the proportion of BT in the ceramic.
iii. It is possible to produce HABT composite with piezoelectric properties sufficiently strong to induce an improved biological response, with a d_{33} in excess of those shown in previous studies to induce improved biological responses.
iv. The variation in the piezoelectric properties of HABT ceramics as HA content increases may be caused by matrix "clamping", reduction in grain size and the presence of non-piezoelectric phases in the material.
v. 90% BT was identified as the most suitable HABT composite to take forward to biological testing.

5 *In vitro* biological responses to HABT ceramics

Hydroxyapatite-barium titanate (HABT) ceramics may be useful as bone graft substitute materials. While the biocompatibility of HA is well established, little information is available on the influence of adding BT to the ceramic on this biocompatibility. One study has examined biological responses to HABT ceramics of undefined composition in canine subjects [6]. Firstly, this chapter discusses the effect of adding BT to HA on the osteoblast-like cells cultured on the ceramic surface *in vitro*. The influence of poling the ceramic on cell attachment is also considered. Subsequently, an investigation of the experimental conditions used in these studies is presented in order to confirm the validity of the results obtained. The influences of the addition of BT to the ceramic and of the poling of HABT on cell proliferation and behaviour at longer incubation times are then discussed. Finally, a preliminary study into macrophage responses to HABT ceramics is presented. Where the responses to HA and HABT are compared, the composites were tested in an unpoled state.

5.1 Attachment of osteoblast-like cells to HABT ceramics

HABT ceramic discs containing 90% BT were manufactured and their microstructural and ferroelectric properties and phase composition were characterised as described in Chapters 3 and 4. For the remainder of this thesis, this material will be referred to as HABT. Discs were also manufactured containing HA powder alone, in order to compare the cell responses to the two ceramics. Saos-2 cells (see Section 2.6.1) were seeded onto the ceramics at 20 000 cells/cm^2 and their number, viability, morphology and metabolic activity were assessed 24h later as described in Section 3.5. This process was then repeated, comparing the behaviour of cells on unpoled HABT with that on the positive and negative surfaces of poled HABT discs.

In all cases, the data for cells cultured on tissue culture plastic controls are given in addition to the data for cells cultured on the ceramics. The quantitative cell culture experiments described in this section were performed in duplicate, with six samples of each material tested in each run of the experiment. Results included in the figures shown here are from the first experiment in each case, with any differences between the two runs detailed and discussed in the text. The data for each experiment is normalised by the surface area of the sample or tissue culture well as appropriate and is given as mean ± standard deviation.

In the investigation of experimental conditions, the roughness and topology of the surfaces of HA and HABT ceramics were characterised. The substrate surface roughness has been shown to influence the attachment of osteoblast-like cells *in vitro* [199, 165] therefore it is necessary for the surface roughness of the materials in question to be comparable for any change in cell behaviour to be attributable to surface chemistry or charge.

The surface chemistry, electrical state and roughness of the substrate are not the only factors which may affect the response of cells to the substrate on which they are grown. Variation of the initial seeding density of osteoblast-like cells *in vitro* has been shown to influence cell proliferation and differentiation [200]. Although the pre-soaking of biomaterials in complete culture medium (i.e. medium containing fetal calf serum) is not uncommon [201-203], it is possible that a protein layer deposited during this process may mask any influence of the substrate surface chemistry [204].

Therefore, in addition to the assessment of the surface roughness of the ceramics, a cell attachment study was carried out in which three key seeding conditions (the surface roughness of the substrate, the cell seeding density and the presence of FCS in the soaking medium) were varied and the number and morphology of cells present were

assessed 24h after seeding. Finally, the piezoelectric coefficient of HABT discs as prepared for cell culture was measured, without the presence of electrodes on the discs (as in the materials testing).

The following section describes the results obtained in these experiments, followed by a discussion of their implications. Details of the cell seeding, analytical and statistical methods used are given in Sections 3.5.2, 3.5.3 and 3.7 respectively. Firstly, the influence on the biological response of adding BT to the HA is considered. The effect of poling the HABT ceramics is then examined.

5.1.1 Results

5.1.1.1 Cell morphology on HA and HABT ceramics

The morphology of the cells was examined by SEM as described in Section 3.5.3. Typical cell morphologies are shown in Figure 5.1. 24h after seeding, cells were grouped together on some parts of the ceramic surface, leaving other areas of the surface vacant, as indicated by the white arrow in Figure 5.1a. The cells displayed a flattened morphology and appeared to be in intimate contact with the surface of the ceramic. No major differences were noted in the morphologies of the cells on the HA and HABT. Cell migration was evident, with lamellipodia and filopodia visible on some cells, as indicated by the arrows in Figure 5.1b.

Estimated cell sizes showed cells on HA to be bigger than those cultured on HABT. The longest dimension of cells on HA was approximately 57μm, while those on HABT cells measured 48μm. The mean surface area of cells was approximately 1300μm^2 and 900μm^2 respectively.

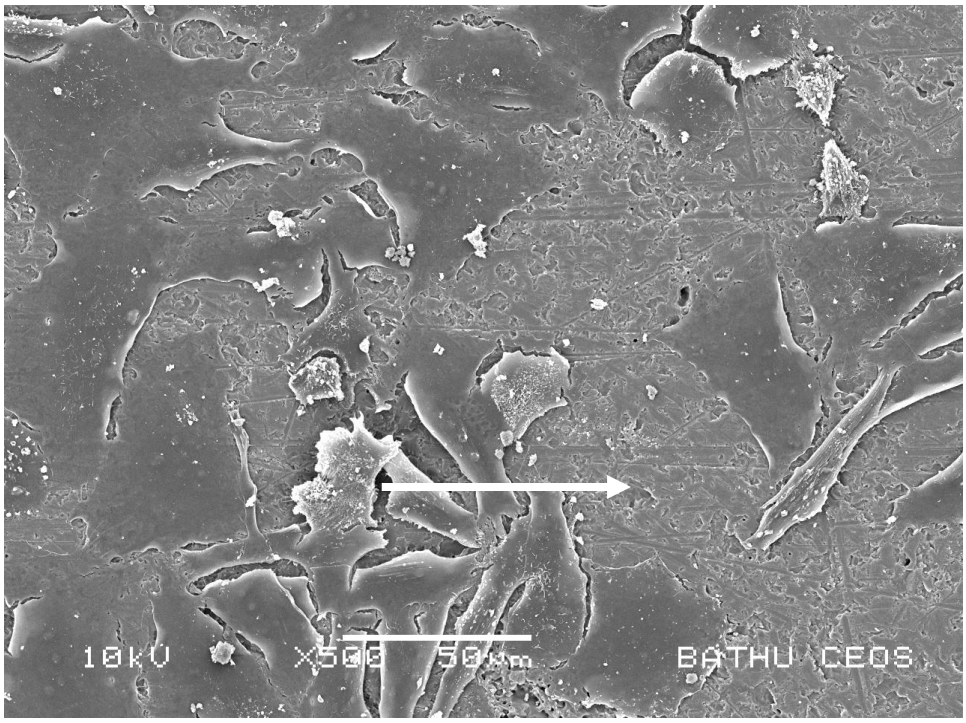

(a)

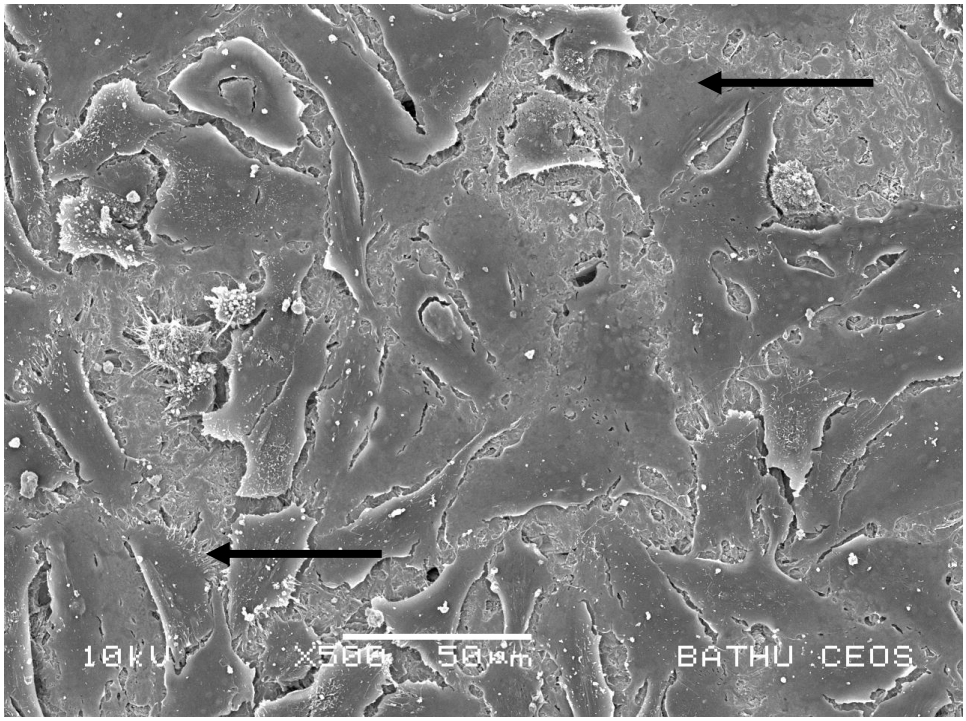

(b)

Figure 5.1 Cells cultured for 24h on (a) HA and (b) HABT. A white arrow indicates space between cells and black arrows indicate the presence of lamellipodia (upper arrow) and filopodia (lower arrow)

5.1.1.2 Cell numbers and viability on HA and HABT ceramics

In order to determine whether the presence of BT influenced the attachment of cells to the ceramic surface, Saos-2 cells were seeded on the two ceramics (HABT and HA) and were incubated for 24h before being counted. The viability of these cells was also tested using trypan blue in order to evaluate any cytotoxic effect that may have occurred.

At 24h after seeding, cells were found to have attached in greater numbers to the tissue culture plastic controls than to the unpoled HA and HABT ceramics. However, no significant differences ($p<0.05$) were found either in the numbers of cells growing on the two ceramics or in the viability of those cells. The cell population on HA was in the order of 16 500 cells/cm^2 on the HA discs and around 15 500 cells/cm^2 on the HABT discs as shown in Figure 5.2. The cell viability, illustrated in Figure 5.3, varied between 87 and 97% as calculated using Equation 3.1.

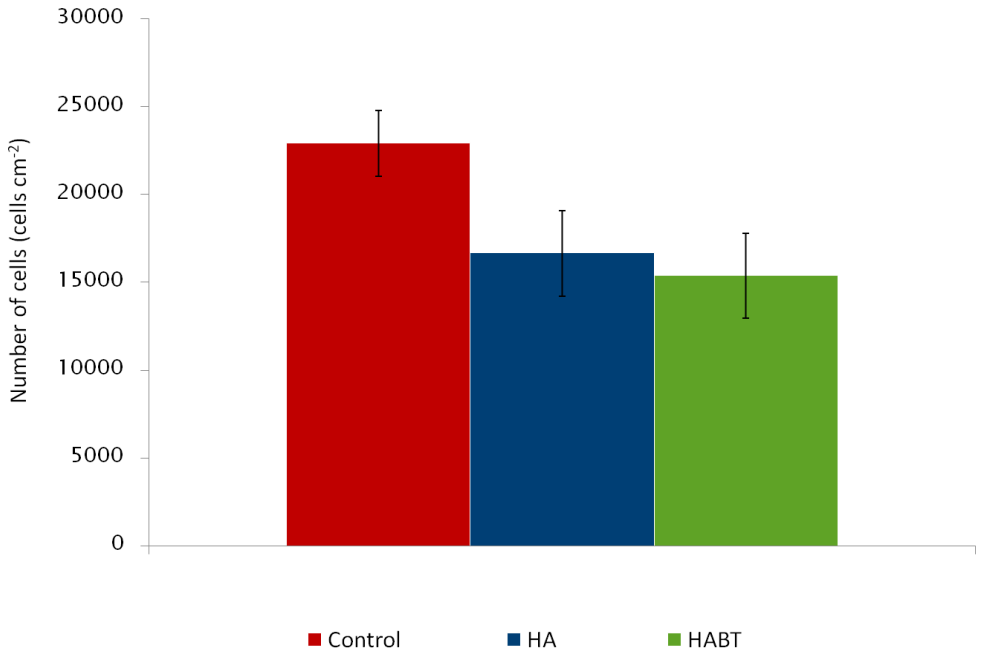

Figure 5.2 Cell numbers 24h after seeding

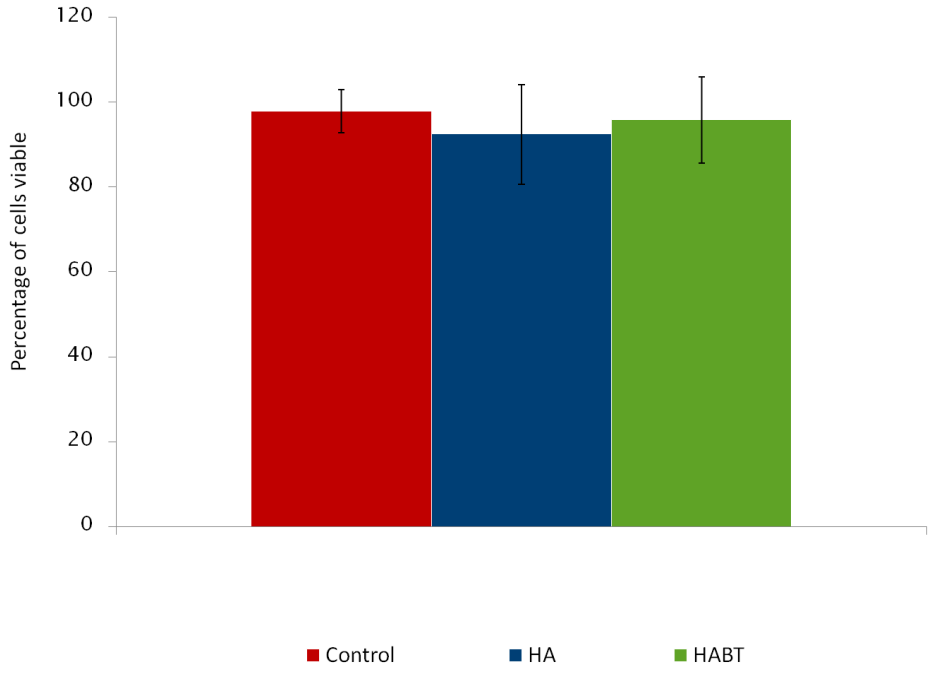

Figure 5.3 Viability of cells 24h after seeding

5.1.1.3 Cell activity on HA and HABT ceramics

In addition to the number of cells present, it is necessary to assess the condition and function of the cells in order to assess the biocompatibility of the HABT composite compared to that of HA. To that end, the metabolic activity of the cells was determined using the MTT assay. Although lower numbers of cells were found on the HA and HABT ceramics when compared to the tissue culture plastic controls (Figure 5.2), the results of the MTT assay, given in Figure 5.4, showed cells on the ceramics to be significantly ($p<0.05$) more metabolically active than those on the tissue culture plastic. There was, however, no significant difference ($p<0.05$) between the relative metabolic activities of the cells growing on the two types of ceramic, with values of 0.065±0.004 $ODcm^{-2}$ on HA and 0.071±0.009 $ODcm^{-2}$ on HABT.

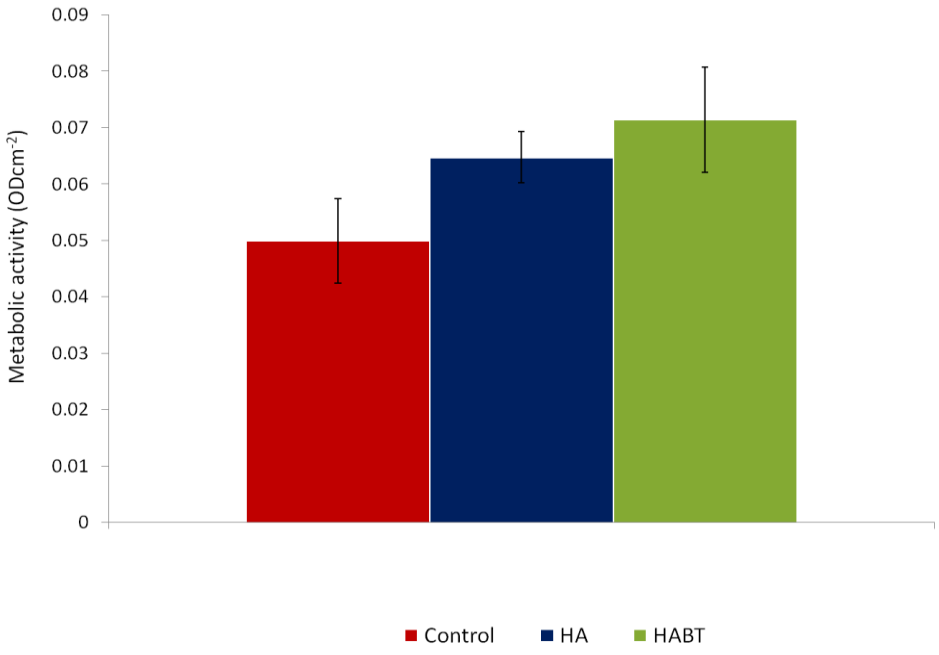

Figure 5.4 Cell metabolic activity 24h after seeding

Having shown the results obtained comparing the HABT and HA ceramics, the outcome of the experiments showing the influence of poling the HABT discs on biological response are presented in the following sections.

5.1.1.4 Cell morphology on unpoled and poled HABT ceramics

The morphology of cells cultured on HABT in various electrical states, i.e. the unpoled material and the positive and negative surfaces of the poled ceramic, was examined in order to determine the influence, if any, of the residual surface charge created by the poling process on the attachment of cells to the material.

No differences were found in cell morphology between the two poled states (Figure 5.5) and the unpoled material (Figure 5.1b) at one day after seeding. The cells were again found to be spread unevenly across the surface of the material. Where cells were present, the majority were flattened and in good contact with the material. Filopodia and lamellipodia were visible, indicating cell attachment and migration.

The remnant surface charge resulting from polarisation (detailed in Section 4.2.3) did not appear to influence the longest dimension of cells on HABT. The surface area of individual cells was found to vary widely on each ceramic. The average surface area of cells on the negatively charged HABT (~1200μm^2) was similar to that on HA (~1300μm^2) rather than that on unpoled HABT (~900μm^2).

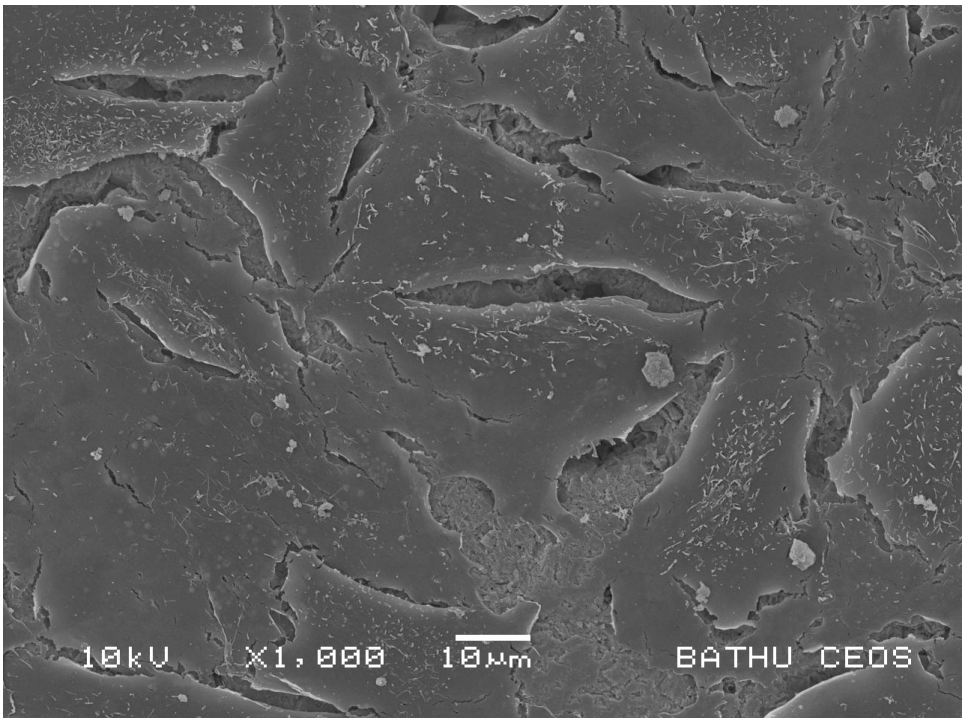

(a)

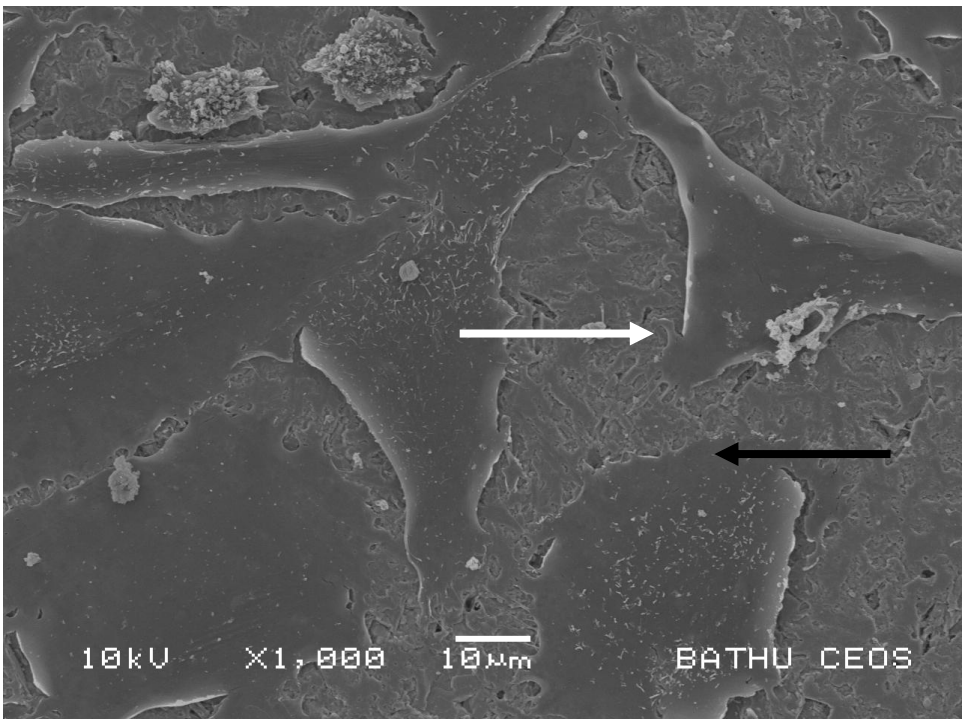

(b)

Figure 5.5 Saos-2 cells cultured for 24h on (a) positive and (b) negative HABT. The black and white arrows indicates indicate the presence of lamellipodia and filopodia respectively.

5.1.1.5 Cell adhesion on unpoled and poled HABT ceramics

As shown in Figure 5.6, at 24h after seeding, cell numbers were higher on the poled ceramics compared to the unpoled material and the control, with around 15 500 cells/cm^2 on the unpoled material and 23 700 and 27 000 cells/cm^2 on the positive and negative surfaces respectively. There was no significant difference ($p<0.05$) between the cell numbers on the positive and negative surfaces of the poled HABT ceramic. Cell viability, given in Figure 5.7 was found to be comparable on all materials examined, varying between 92 and 98% as calculated using Equation 3.1.

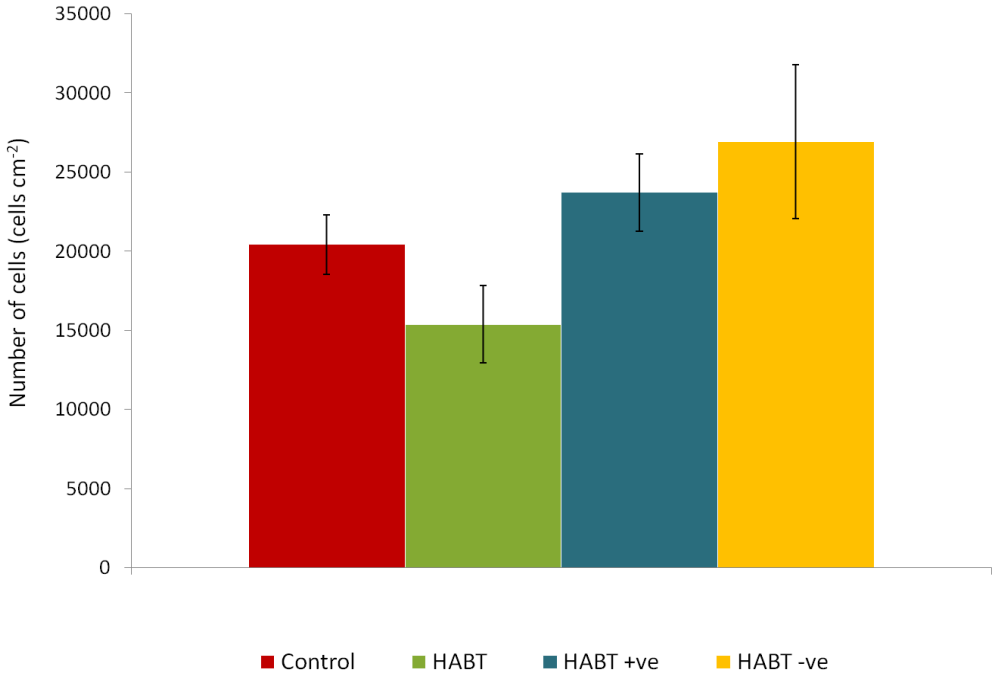

Figure 5.6 Cell numbers 24h after seeding

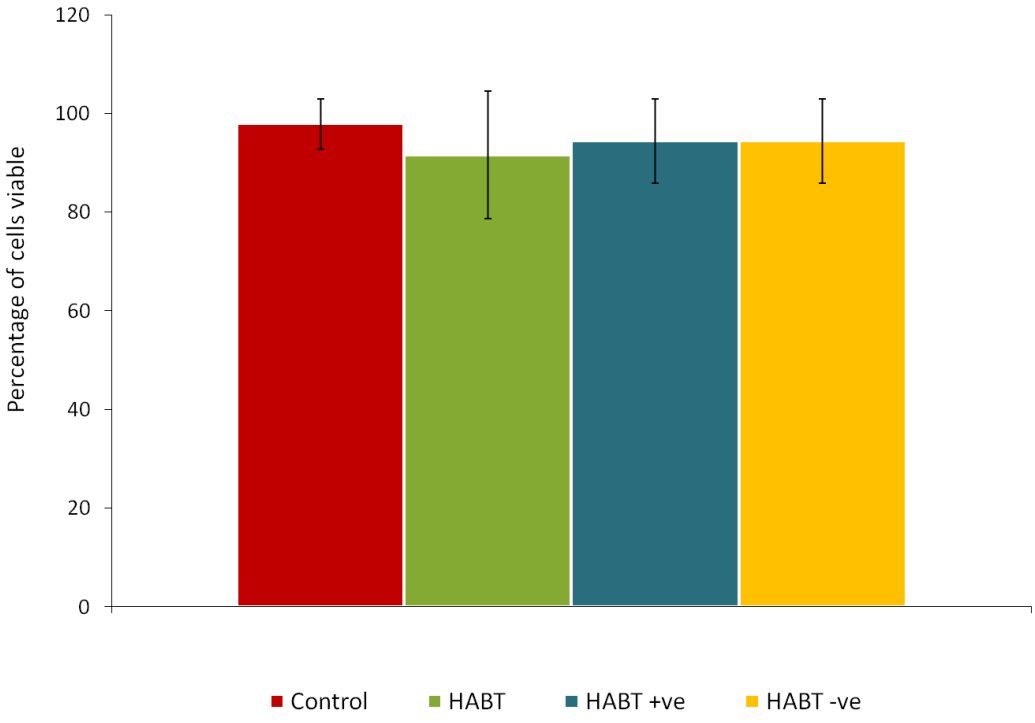

Figure 5.7 Viability of cells 24h after seeding

5.1.1.6 Cell activity on unpoled and poled HABT ceramics

The influence of poling on the functioning of cells grown on the HABT ceramic was examined using the MTT assay to study metabolic activity. Although the previous experiment (Section 5.1.1.4) showed increased cell numbers on the surfaces of the poled ceramics, the analysis of the metabolism of the cells (Figure 5.8) showed values of 0.061-0.072 $ODcm^{-2}$, with no significant increase ($p<0.05$) in cell activity on the ceramics at this incubation time. This implies that the metabolic activity of each cell was lower on the poled HABT than on the unpoled material.

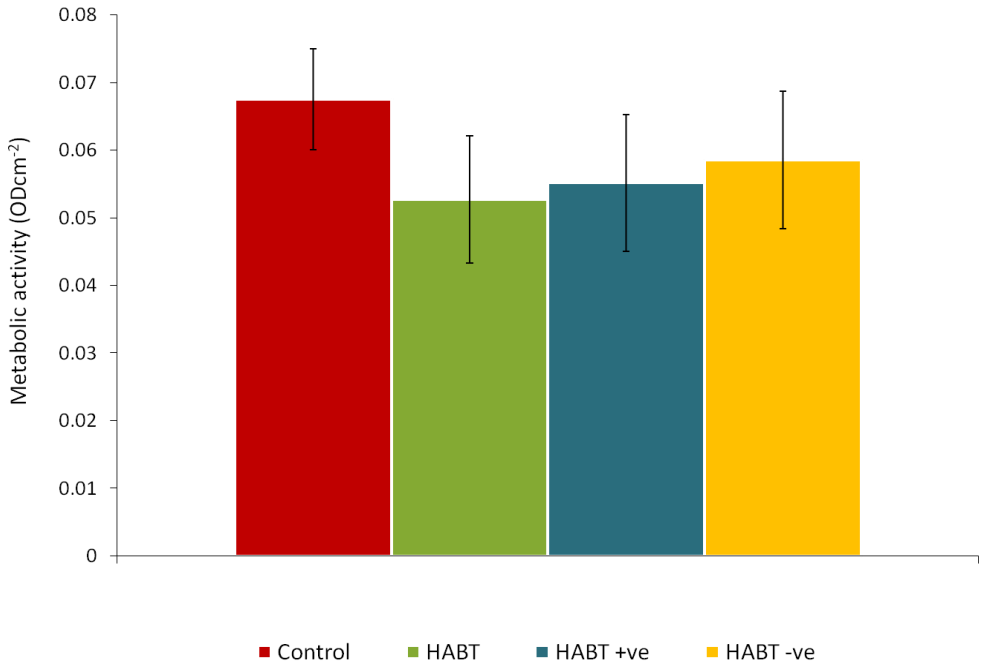

Figure 5.8 Cell activity 24h after seeding

5.1.1.7 Investigation of the surfaces of HA and HABT as prepared for cell culture

The surfaces of the ceramics were scanned using a profilometer (Section 3.4). The average roughness (R_a), maximum roughness (R_{max}) and ten-point height (R_z) were then calculated. As illustrated in Figure 5.9, the average roughnesses of the HA and HABT ceramics were both approximately 0.5µm. The maximum roughnesses were in the range of 3-4µm and the ten-point roughness between 2 and 2.5µm. No statistically significant differences ($p<0.05$) were found on the two materials. For reference, the average roughness of tissue culture plastic is under 0.1µm [205].

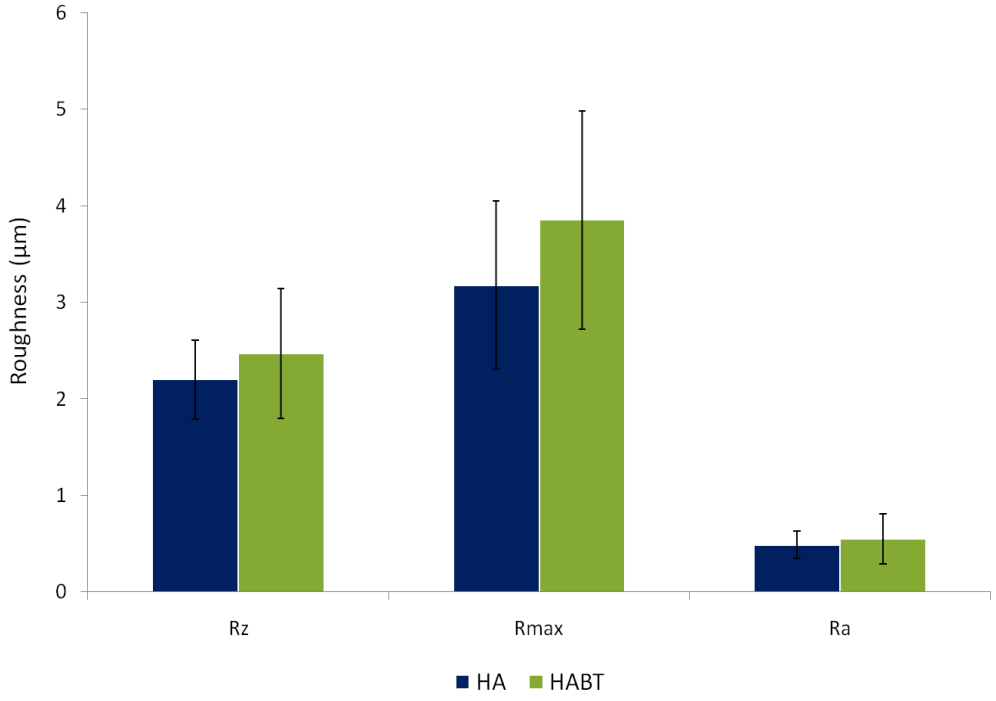

Figure 5.9 Surface roughness of HA and 90%BT ceramics as prepared for cell culture

The three-dimensional micro-topography plots (Figure 5.10) indicate the presence of similar surface features on the two types of ceramic.

The SEM images indicate the presence of parallel grooves created in the process of the surface finishing on both the HA and the HABT. These grooves are indicated by the black arrows in Figure 5.11. Also apparent are pores in the ceramic, indicated by the white arrow in Figure 5.11b. Contrary to indications from the microtopography plots, these appear to be more numerous on the surface of the HABT, with the grooves more prominent on the HA surface. Qualitative evaluation shows the pores to be 5-10μm in diameter and the grooves to be spaced at 2-10μm.

5.1.1.8 The piezoelectric coefficients of HABT ceramics as prepared for cell culture

The method of preparation of ceramics for the measurement of piezoelectric properties is not applicable to the preparation of materials for cell culture. Both *in vivo* and *in vitro*, it is not desirable to add silver electrodes to the surface of the material. It is therefore necessary to measure the piezoelectric coefficient of the ceramics as prepared for cell culture in order to assess whether their electrical properties remain significant in these conditions. Samples of poled HABT were prepared and their piezoelectric charge coefficients measured as described in Section 3.4, without the application of silver electrodes. The direct piezoelectric coefficient 24h after poling without electrodes was found to be $57.8 \pm 10.8 pCN^{-1}$.

In addition to this measurement, a pilot study on the ageing of piezoelectric properties in cell culture conditions was carried out and is included as Appendix D. Briefly, all changes in d_{33} in HABT ceramics containing 90% BT stored over a period of 10 days in culture medium at 37°C were within the range of error of the Berlincourt piezometer. No significant ageing effect was observed.

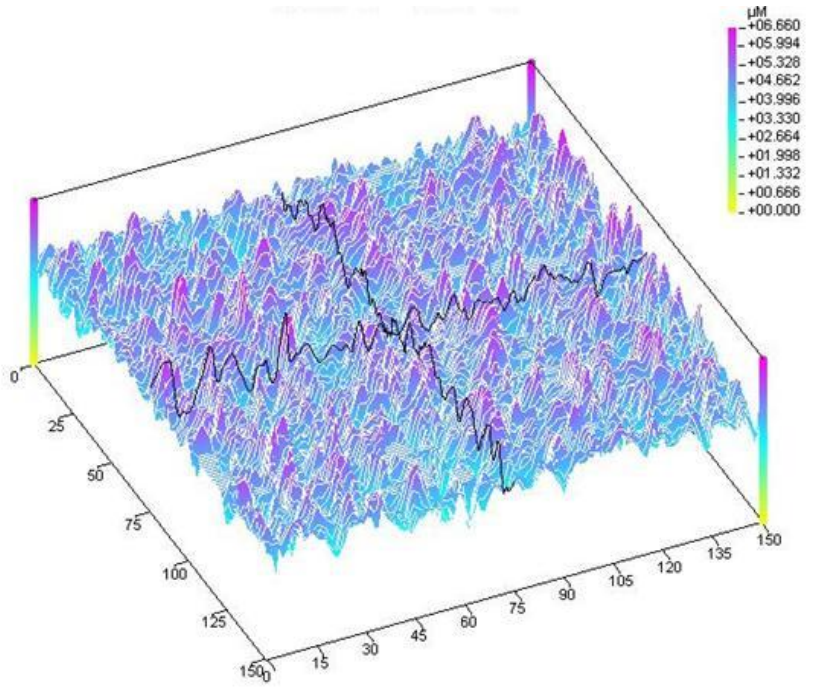

(a)

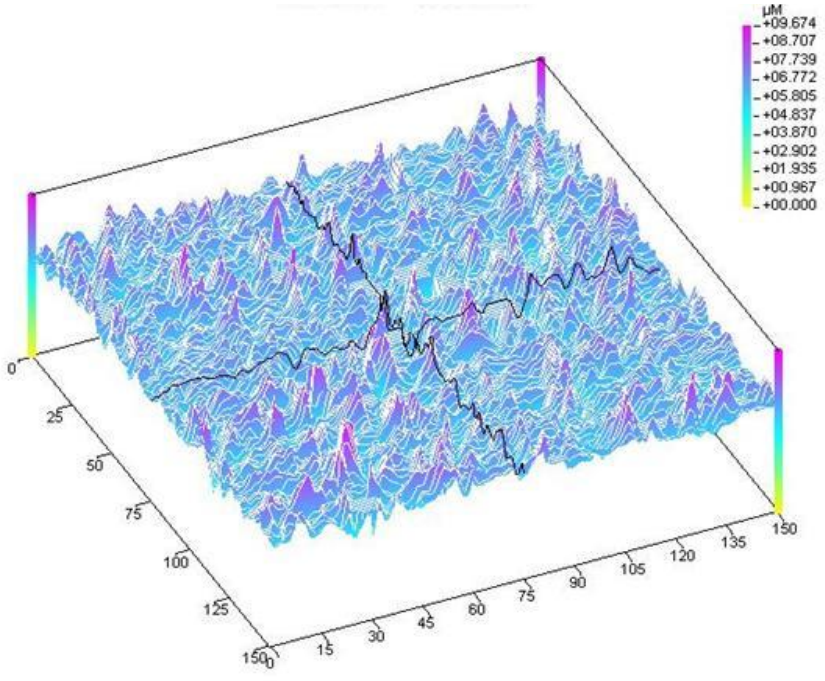

(b)

Figure 5.10 3D nanotopography plots showing the surfaces of (a) HA and (b) HABT ceramics as prepared for cell culture

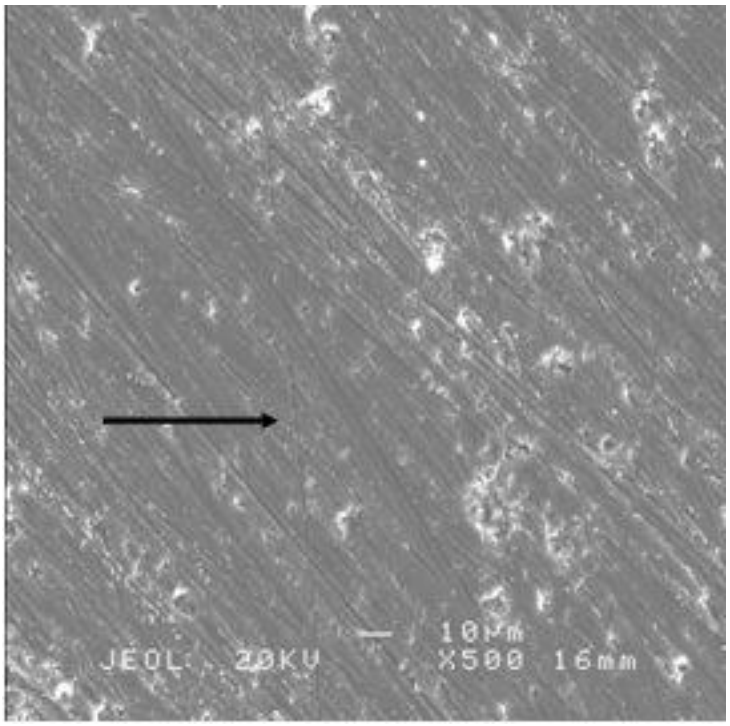

(a)

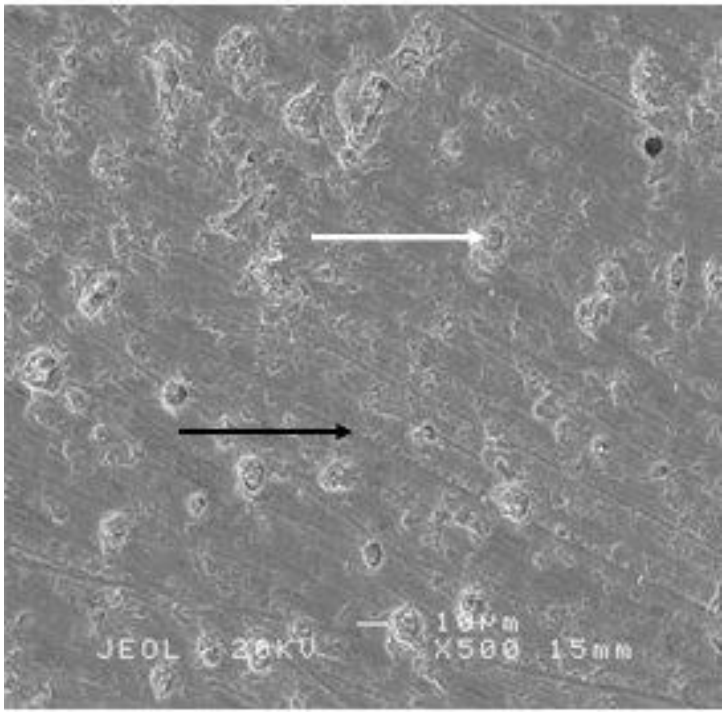

(b)

Figure 5.11 SEM micrographs showing the surfaces of (a) HA and (b) HABT ceramics as prepared for cell culture. The black and white arrows indicate grooves and pores in the surface respectively.

5.1.1.9 Investigation of the effect of seeding technique and variation of material surface

In order to investigate whether the chosen seeding density, the surface roughness of the ceramics and the presence of FCS in the soaking medium induced any effect masking any influence from the surface chemistry or electrical state of the ceramics, experiments were carried out varying each of these factors with respect to the standard seeding protocol.

Saos-2 cells were seeded on the ceramics using one of three variations to the standard protocol before being incubated for 24h, lysed and subjected to an LDH assay to give an indication of the total cell population [173]. This assay was used in preference to cell counts as it was considered that the numbers of cells in the altered seeding conditions would be too low for accurate manual counts to be taken. The experiment was carried out twice on triplicates of each sample type to give six data points for each seeding condition (n=6).

The changes to the seeding conditions were:

i. No serum – serum-free medium was used for the soaking of tablets before cell seeding.
ii. Low density – a seeding density of 10 000 cells/cm^2 was used (the standard seeding method used 20 000 cells/cm^2, see Section 3.5.2).
iii. 1μm polished – an additional finishing step was added to the tablet preparation in order to produce a smoother surface finish as described in Section 3.5.2. The surface roughness of these discs was also measured.

Irrespective of the seeding conditions tested, no statistically significant difference ($p<0.05$) in the quantity of LDH present in the lysed samples was found to result from the addition of BT to the HA (Figure 5.12). With the standard seeding conditions, the difference between the cells cultured on the tissue culture plastic control and those cultured on HA was found to be statistically significant ($p<0.05$). In addition, no significant difference was found between the different seeding conditions. The unusually large standard deviations in the data obtained from the low density seeding test indicated that the small amounts of LDH present were outside the accurate range of the assay. This part of the test was therefore not carried forward to examine the effect of poling HABT on cell attachment using the varied seeding conditions.

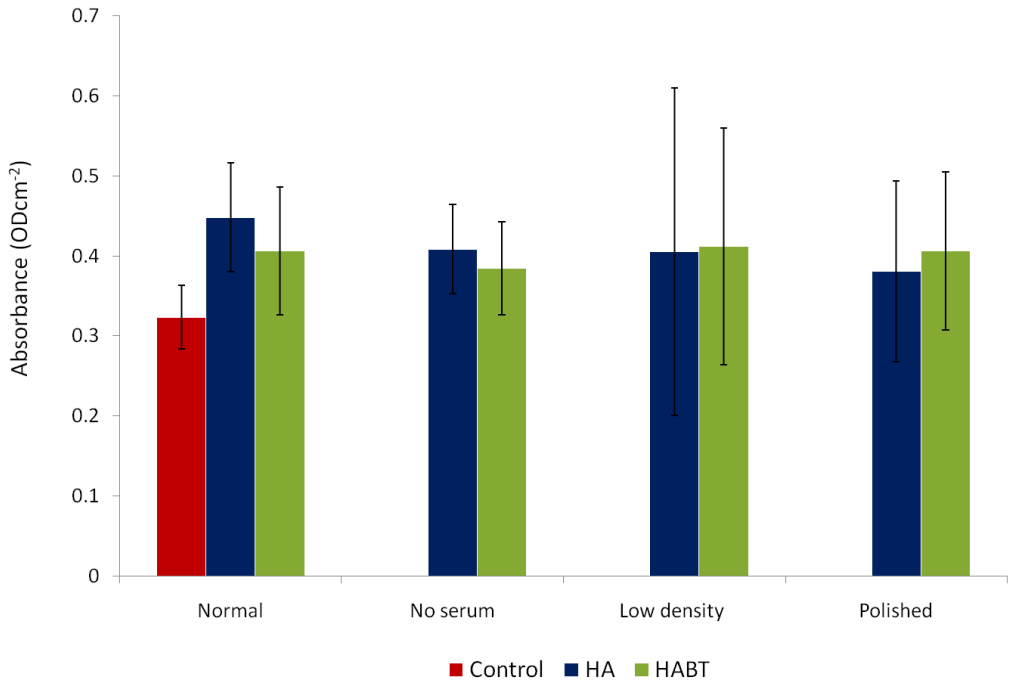

Figure 5.12 Total LDH found in lysed cultures with modifications to standard seeding pattern on HA and HABT

Figure 5.13 shows the influence of poling HABT on the size of the cell population as measured using the LDH assay in various seeding conditions (normal, no serum, polished). When the standard seeding conditions were used, a larger cell population was found on the poled materials than the unpoled, though only the difference between the control and the positively charged HABT was statistically significant ($p<0.05$). This trend was also found in tablets presoaked in serum-free medium, but with no statistically significant differences. On 1µm polished tablets no increase in the cell population was found on the poled discs. Higher standard deviations were observed for this group than for the standard seeding method.

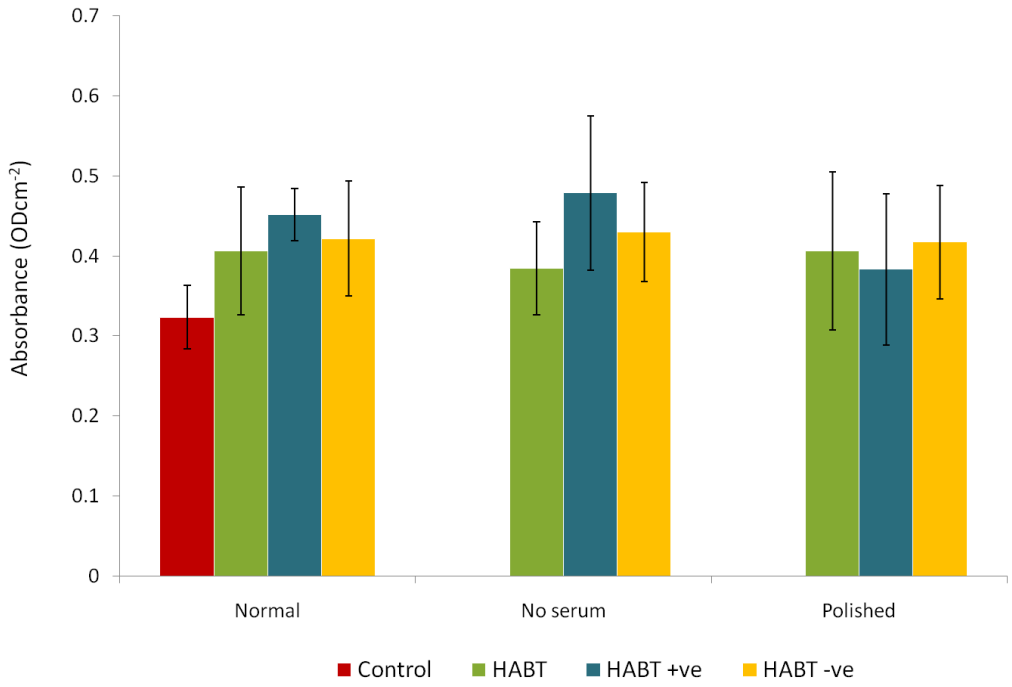

Figure 5.13 Total LDH found in lysed cultures with modifications to standard seeding pattern on unpoled HABT and on the positive and negative surfaces of poled HABT

In addition to cell culture testing, the polished discs were scanned using a profilometer and their R_a, R_{max}, and R_z values are shown in Figure 5.14. In contrast to surfaces prepared by the standard method, samples of HA and HABT have significantly different ($p<0.05$) roughnesses when 1µm polished. For comparison, the mean roughness parameters for discs prepared using the standard (as presented in Figure 5.9) and 1µm polishing techniques are given in Table 5.1.

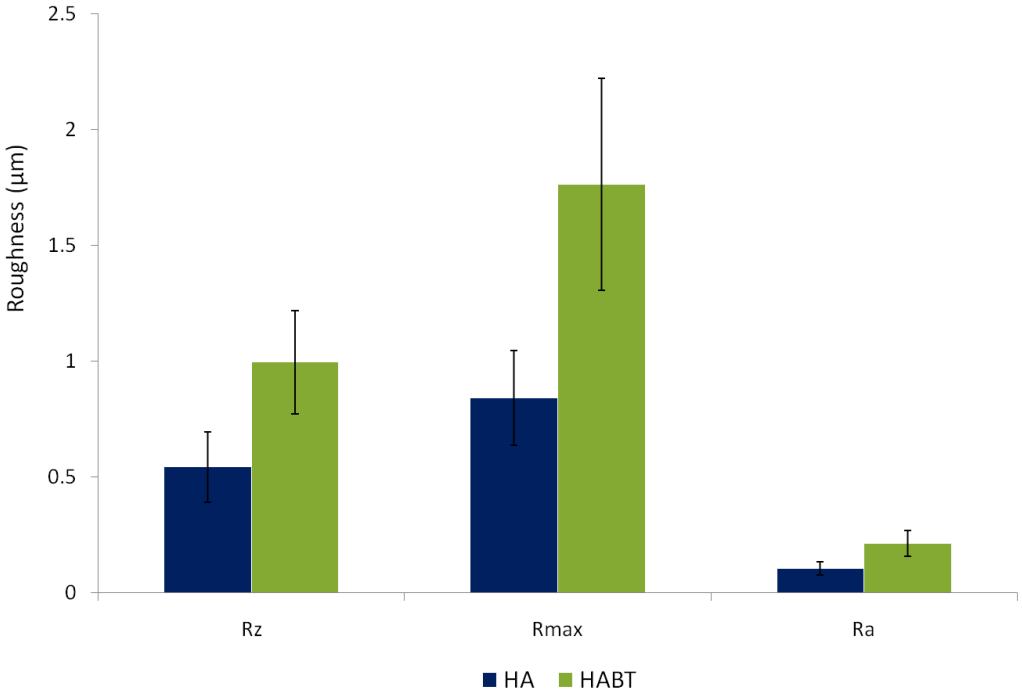

Figure 5.14 Roughness of 1µm polished discs of HA and HABT

Table 5.1 Mean roughness parameters for HA and HABT discs prepared by the standard and 1 μm polishing methods

Roughness parameter	Material	Standard preparation method (μm)	1μm polished discs (μm)
R_z	HA	2.20	0.54
	HABT	2.47	0.99
R_{max}	HA	3.17	0.84
	HABT	3.85	1.67
R_a	HA	0.49	0.1
	HABT	0.55	0.21

For the assessment of the morphology of cells cultured in the varied conditions, cells were seeded on HA and BT samples and examined by SEM. The micrographs obtained for cells seeded without serum, an example of which is given in Figure 5.15, showed cells to be well attached to the ceramic. Mean cell surface areas and mean cell lengths were comparable on all of the materials and were ~400μm^2 and ~37μm on HA.

Cells seeded at the lower seeding density (Figure 5.16) displayed similar distribution patterns to those seeded at higher density, with some areas of the surface densely populated and others vacant. The cells displayed large lamellipodia (indicated by black arrows on Figure 5.16), indicating that cell migration was occurring. Again, cell sizes were not influenced by composition or poling.

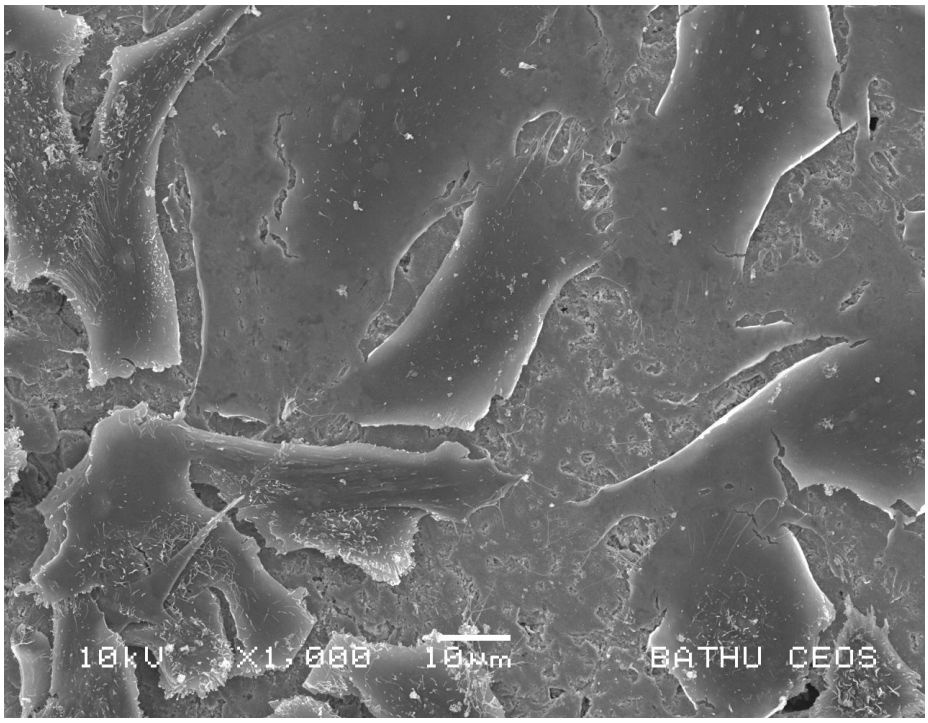

Figure 5.15 Cells seeded HABT without serum

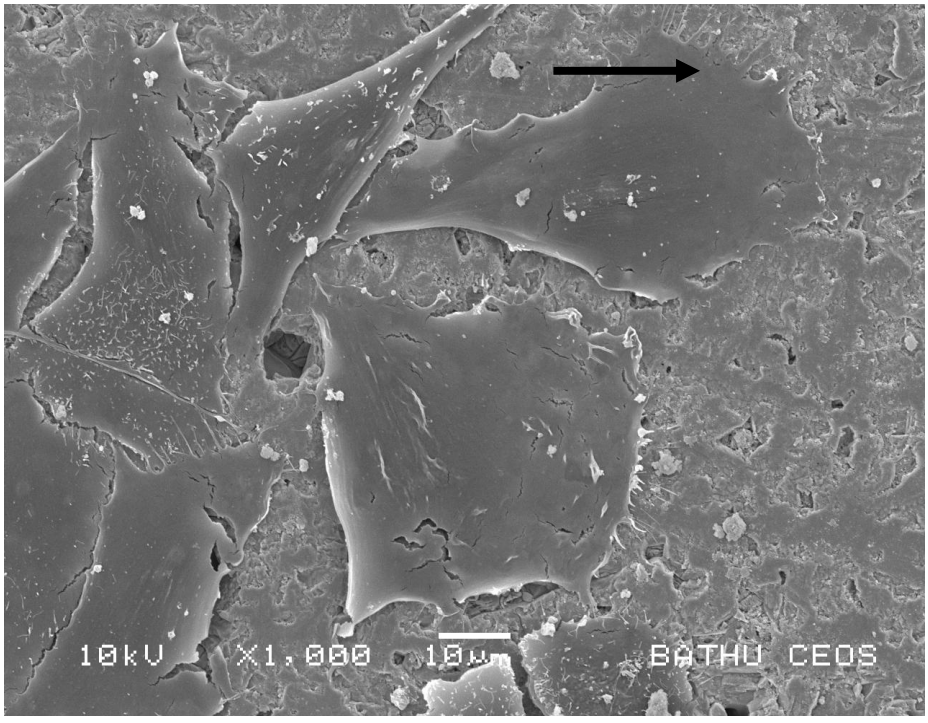

Figure 5.16 Cells seeded at low seeding density on HABT, with a black arrow indicating the large lamellipodia

5.1.2 Discussion

5.1.2.1 The effect of adding BT to HA

The results of the cell count and viability study carried out 24h after seeding show that though both the HA and HABT ceramics encourage fewer cell attachments than the tissue culture plastic (a material designed to promote cell attachment), the addition of the BT to the HA does not inhibit the attachment of Saos-2 cells. It can be concluded from these results that HABT ceramics do not limit the viability of osteoblast-like cells cultured on their surface in the short term. The metabolic activity of cells grown on the HABT ceramic was also found to match that of cells grown on the commercially available HA ceramic, supporting the assertion that the material is biocompatible. This trend was later confirmed by the measurement of the cell population using the LDH assay.

When assessing the cell viability data it should be noted that, as dead Saos-2 cells often detach from the substrate surface, some dead cells were lost to the count when the culture medium was removed before trypsinisation. The trypan blue staining, therefore, measured only the number of dead cells still attached to the substrate surface.

Examination by SEM showed the cell populations on the two ceramics to be comparable in their seeding patterns. Cells grew in clusters, leaving some areas of the material vacant. As similar behaviours were seen on all surfaces examined, this is unlikely to have been caused by variations in the surface chemistry. This behaviour may be typical of the phenotype of the Saos-2 cells, though it is not explicitly identified as such in the literature. It may also have been influenced by the seeding technique employed, particularly if cells were not sufficiently evenly distributed in the seeding suspension. The presence of lamellipodia may suggest the future migration of cells into the vacant areas on the surface.

Images produced by SEM do not reveal differences in cytoskeleton arrangement or cell volume. Future work using staining or confocal microscopy may reveal more about the nature of the cellular attachments to the different ceramics. Differences in cell morphology and attachment illustrated by Davies *et al* [123], in particular gaps between the material and cell body, may not be clear on SEM micrographs.

For the most part, cells were flat and in intimate contact with the surfaces of both ceramics. This further supports the conclusion that the HABT ceramic is equally suitable as a substrate for cell attachment as commercially available HA and is not cytotoxic to Saos-2 cells in the short term.

Some differences were found in the sizes of the cells on the two materials. In general, cells were smaller on the HABT ceramics than on HA at 24h after seeding. In studies carried out at longer incubation times (7 days), at which point cells were more confluent, all cells were found to be smaller in both surface area and cell length than those examined at early time points. This reduction in cell size linked to population confluence is a documented feature of the Saos-2 cell line [157]. As large variations in seeding density were observed at this early time point on all ceramics, it may be the case that the area of cells on the HABT of which the images were taken was simply more confluent than that selected on the HA. Only two images were assessed for each material (with four cells measured per image). This may not be representative of the entire cell population in terms of cell confluence and therefore cell size. Data obtained by this test at this incubation time may therefore be used to obtain an indication of cell sizes, but it is not appropriate to draw conclusions comparing the two populations. The longest dimensions of the cells here (approximately 57μm on HA and 48μm on HABT) are of the same order of magnitude as cell sizes previously reported for the Saos-2 cell line (59-73μm) [161].

No previously published work has examined the attachment of human cells to HABT ceramics. The results found in this study are, nevertheless, in general agreement with the work of Feng *et al* [6], a longer-term *in vivo* study using canine subjects, in suggesting the biocompatibility of HABT ceramics. This study, along with other work on biological responses to materials containing BT after long incubation or implantation periods, will be compared more fully to the current work in Chapter 6.

The *in vitro* biocompatibility of a different BT-containing composite, P(VDF-TrFE)/BT, was assessed by Beloti *et al*. In agreement with the current study, the composite was found to be biocompatible at 24h after seeding. Increased cell adhesion was seen in comparison with a commercially available control. The number of cells on the test material 24h after seeding was 70-80% of the original number of cells seeded [128]. This is in direct agreement with the results found on both the HA and the HABT in the current study.

The presence of compounds other than HA and BT in the sintered HABT ceramics was suggested by the XRD testing. No published data is available on the biocompatibility of these compounds for comparison with the results found here.

5.1.2.2 The effect of poling of HABT ceramics on cell attachment

As shown in Chapter 4, the poling of HABT ceramics results in a remnant polarisation. In the case of the HABT ceramic containing 90% BT, this was found to be $0.021 Cm^{-2}$, indicating that a residual surface charge is present on the poled materials.

The viability of Saos-2 cells cultured on HABT ceramics was unaffected by the poling of the material. Cell numbers were, however, shown by the manual cell counts to be significantly higher on both the negative and positive surfaces of the poled HABT than on the unpoled ceramic. This trend was confirmed by the LDH assay, though the differences were not statistically significant in the second study. Cell morphology was

comparable on all three ceramics. The differences in morphology suggested by Davies were not apparent [123]. Some features, such as cell-material spaces were, however, difficult to assess using SEM. Differences in cell sizes should be considered with reference to the discussion of the cell sizing technique in the previous section.

When compared to the higher cell numbers found on the poled ceramic, the similar level of cell activity found for the total population on each material implies a lower activity per cell on the poled ceramics. This may be caused by the higher cell population on the poled ceramics as cells in densely populated areas have less need to proliferate and are therefore likely to have lower metabolic activity.

As stated in the literature review, cellular behaviour on charged and piezoelectric substrates at 24h after seeding is not well defined. The results of the current study concur with the observations of Schneider *et al* in finding increased cell attachment on both positive and negative surfaces [127]. They differ, however, from trends identified on titanium [124] and poled HA [83], where either positive or negative surfaces, but not both, encouraged cell attachment. The trend observed in the current study also differs from cellular attachment trends on P(VDF-TrFE)/BT ceramics, in which no differences were found in cell attachment on poled and unpoled material [129]. These differences support the suggestion that the influence of surface charge cannot be considered independently from the surface chemistry of the material.

No published research on the metabolic activity of cells at 24h or less of incubation was found. It is clear, however, that though cell responses to the positive and negative materials appear to be similar 24h after seeding, the mechanisms by which the two surfaces influence the cells are likely to be different [125, 132].

Mechanisms by which surface charge may increase cell attachment on positive and negative surfaces have been proposed in the literature, as discussed in Chapter 2. In

the case of the model for cell behaviour on negative surfaces, it is notable that, in contrast with the results of the current study and despite finding higher cell numbers at later time points, the authors did not observe increased cell numbers at 24h after seeding [83].

5.1.2.3 Verification of cell culture parameters

The piezoelectric coefficient of HABT as prepared for cell culture

The piezoelectric coefficient of the non-electroded HABT ceramic prepared for cell culture (d_{33} = 57.8pCN^{-1}) was lower than that measured for materials with metallic electrodes applied to their surfaces (d_{33} = 72.7pCN^{-1}). The presence of electrodes allows for a build up of surface charge on the material, increasing charge collection and decreasing the resistance between the sample and the electrode of the piezometer, leading to a higher reading. The coefficient measured is higher than those of materials found by previous studies to influence biological responses [6, 130, 134].

Surface roughness and topography

The roughness of culture substrates has been shown to influence cell behaviour, as discussed in Section 2.6.3. The roughness of both HA and HABT (R_a=0.49 - 0.55μm) were in a range considered as "smooth" by previous investigators [43, 185]. They were comparable on the two materials studied. Surface roughness need not be considered as an influence on cell behaviour when interpreting the results of the current study.

Some differences in the presence of grooves and pores on the surfaces of the HA and HABT ceramics were revealed by the SEM microscopy. In the published studies reviewed (see Section 2.6.3), differences in cell function initiated by surface features were often associated with modifications in cell morphology or alignment. In the current study, cells bridged, rather than conformed to, pores in the HABT surface (as seen in Figure 5.5). This concurs with an existing study for defects of a comparable size

(10μm) [188]. Cells did not align with any grooves on the HA surface, contrary to the findings of some previously reported studies. The effect of the observed differences in surface morphology on the cells in the current study appears, therefore, to be limited at this time point.

Variations in cell seeding protocol

The results of the study into the effect of variations in the seeding method gave no indication that a change in protocol was necessary. The absence of serum in the seeding process induced changes in cell morphology and size, but not in the number of cells. This supports the assertion that cell attachment is mediated by adsorbed serum proteins *in vitro*. Discrepancies in cell size between cultures seeded with and without serum, though still subject to the limitations in measurement discussed previously, were large. This implies a reduction in the quality of cell attachments in serum-free conditions, resulting in increased deviation in data gathered from these cultures and a decrease in the statistical significance of the results.

If, as suggested in the literature (see Section 2.6), surface chemistry and charge influence protein adsorption and as a result alter cell attachment, the enhanced differences between responses to the HA and HABT in cultures exposed to serum are not surprising. As trends observed up to this point were subtle, it was desirable to maintain the use of serum in the seeding process in order to highlight any effect of changes in surface chemistry or charge.

At the reduced seeding density (10 000 cells/cm^2 as opposed to 20 000 cells/cm^2), results seem to be outside the range of the assay and are therefore not useful. Consequently, it was decided that any reduction in seeding density would limit the range of assays which could be used and was therefore not appropriate.

On the 1μm polished tablets, large variations were seen in cell populations, possibly indicating unfavourable attachment conditions. The large differences in roughness between the two materials as a result of the polishing process were not desirable for reasons discussed in section 2.6. The original tablet preparation process was therefore considered to be the most appropriate.

5.1.3 Conclusions

The attachment, viability, morphology and metabolic activity of the cells are not affected by the incorporation of BT into the ceramic. HABT composites are therefore biocompatible in the short term.

The piezoelectric coefficient of the HABT material as prepared for cell culture is within a range that may reasonably be expected to induce improved cell responses when subjected to mechanical loading.

The roughnesses of the discs of HA and HABT were comparable, though some variations in surface features were observed. The seeding method used was tested and found to be appropriate.

The poling of the piezoelectric ceramics does not reduce the potential biocompatibility of the material. In contrast with some published results, poling encouraged cell attachment irrespective of the nature of the surface charge. None of the other factors tested was influenced by the modification of the electrical state of the ceramic.

5.2 Proliferation of osteoblast-like cells on HABT ceramics

In Section 5.1, the *in vitro* biocompatibility of HABT ceramics containing 90% BT was established with respect to cell adhesion at 24h after seeding. However, cell adhesion alone is not an adequate indicator of biocompatibility when a specific function is required [204]. It is also necessary to observe cellular responses over longer time periods in order to understand their development on the material surface and to assess longer term cytotoxicity.

In this section, cellular proliferation and development on HA and HABT ceramics up to 14 days after seeding are examined. As in the previous chapter, the effects of poling the HABT ceramics are also considered, examining both positive and negative surfaces.

As previously described in Sections 3.3 and 3.5.1, discs were manufactured, poled by corona poling and prepared for cell culture. Saos-2 cells were cultured on the surface of the ceramics which were then incubated for up to 14 days according to methods detailed in Section 3.5.2. Cells were also seeded on tissue culture plastic as a control. Cell proliferation, viability, morphology, metabolic activity and differentiation were examined using the methods described in Section 3.5.3.

5.2.1 Results

5.2.1.1 Cell morphology at seven days after seeding

For the examination of cell morphology and spreading, cells were seeded onto discs of HA and of unpoled, positive and negative HABT. They were incubated for seven days before being prepared for SEM.

After seven days the cells substantially covered the surfaces of all of the materials examined. The micrographs in Figure 5.17 were taken at the same magnification (x500) as those shown in Figure 5.1. A reduction in cell size (i.e. cell length and surface area) was observed on all materials compared to earlier time points, with cells on all materials in the region of 400-500μm^2 in surface area and ~30μm in length. The distribution of cells on the surface became more uniform and closely packed in comparison with micrographs from the earlier time point (24h after seeding). A more detailed view of cells cultured on HABT is shown in Figure 5.18a. This image is representative of cells on all of the materials examined. Cells were found to be attached to both the materials and to other cells and displayed a similar morphology irrespective of the composition or electrical state of the substrate. Figure 5.18b shows the uniform spreading of cells across the material.

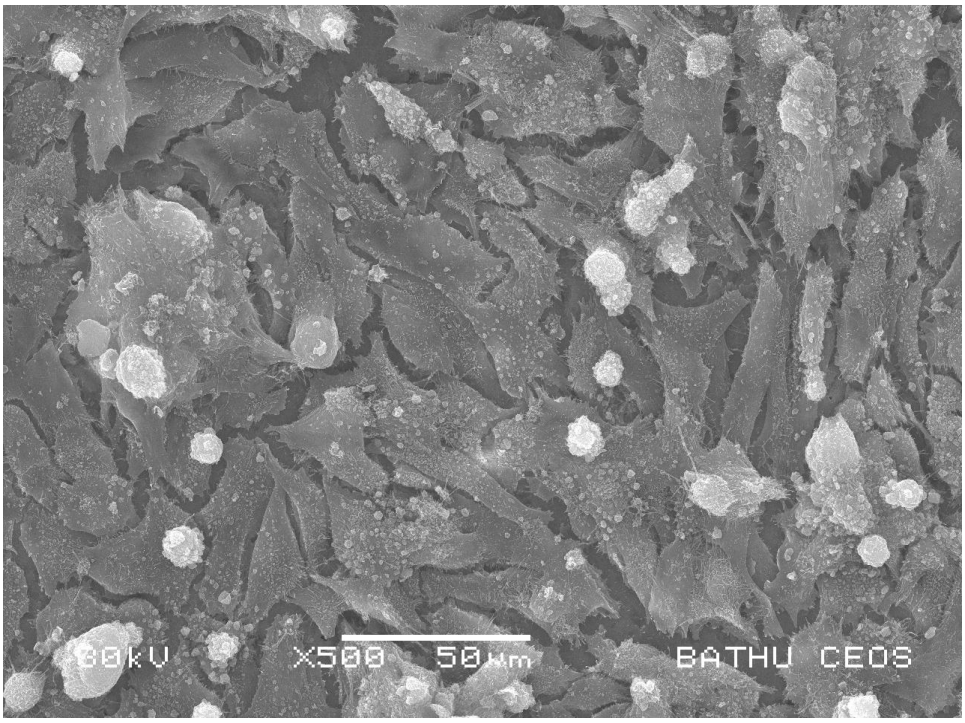

(a)

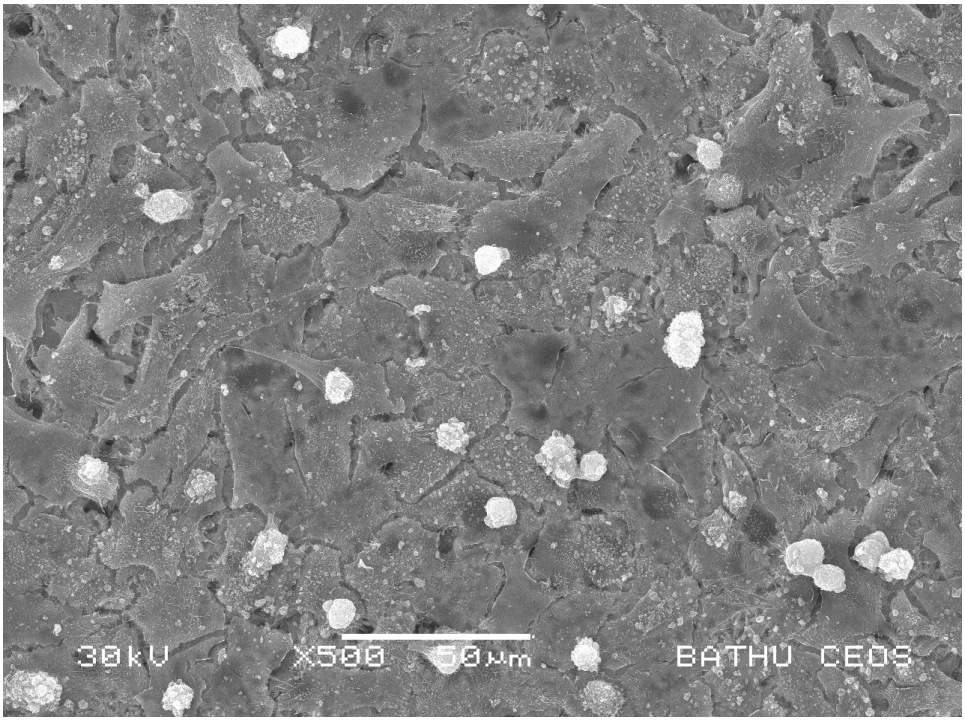

(b)

Figure 5.17 SEM micrograph showing cells on (a) HA and (b) HABT, seven days after seeding

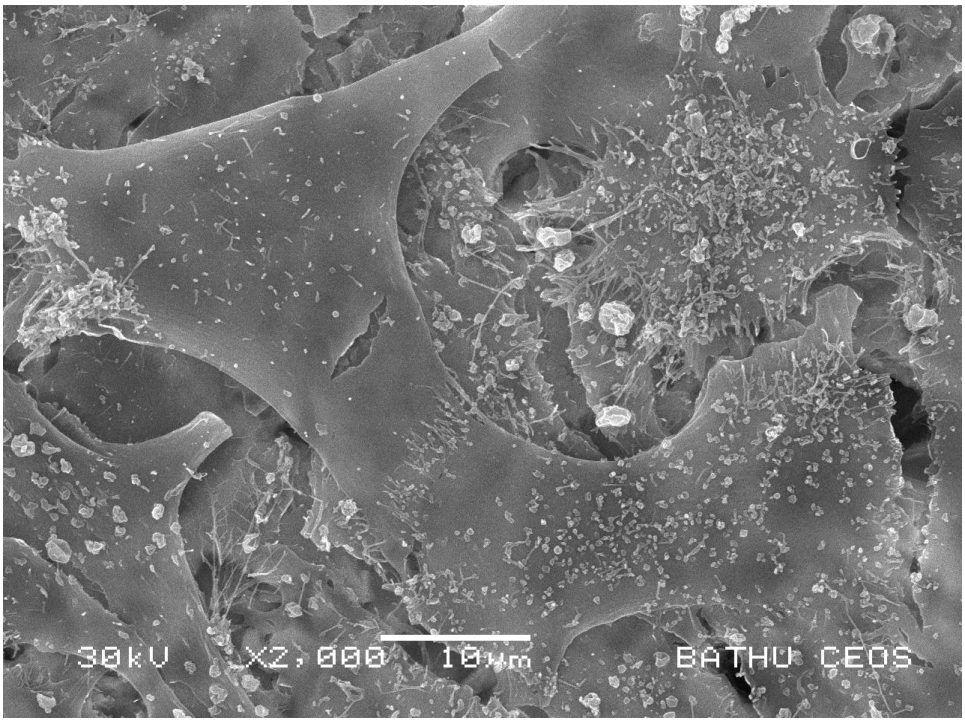

(a)

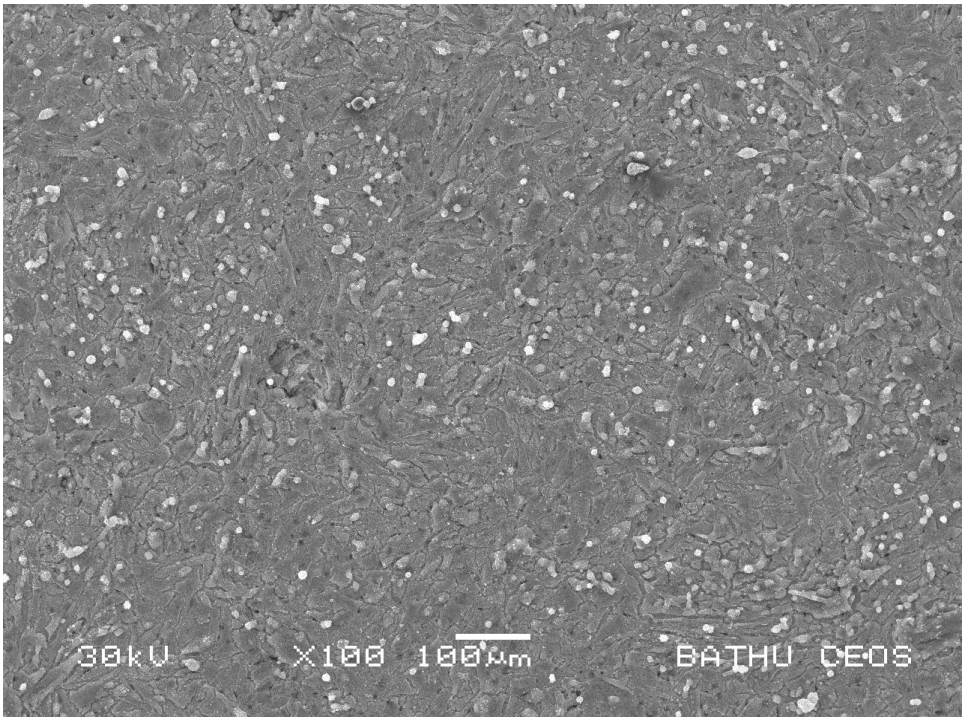

(b)

Figure 5.18 SEM micrographs showing (a) the morphology (x2000) and (b) the uniform distribution of Saos-2 cells (x100) seven days after seeding on HABT and the negative surface of poled HABT respectively

5.2.1.2 Cell proliferation

Variation of composition

To determine the cytocompatibility of HABT compared to that of HA up to 7 days after seeding, cells were cultured on both ceramics and incubated for 3 or 7 days. Cells were then removed from the materials using trypsin, dyed with trypan blue and counted. Each experiment included six samples (n=6) for each time point and was carried out twice to confirm the trends found. The data given in this section are from the first run of the experiment.

The number of cells found on each ceramic and the relative viabilities of these cell populations are shown in Figure 5.19. As found at 24h after seeding, the composition of the ceramic (HA or HABT) did not influence the viability of the cells at either time point. Cell viability was in the range of 91-96% at three days and 89-93% at seven days after seeding on all materials tested, as shown in Figure 5.20. The proliferation of the cells remained unaffected by the addition of 90% BT to the HA. Around 33 500 cells/cm^2 were found on the ceramics after three days of incubation. In addition, at seven days after seeding the cell population on both ceramics, around 200 000 cells/cm^2, matched that found on tissue culture plastic. From this data, cell population doubling times, calculated using Equation 2.10, were found to be 43 hours on the tissue culture plastic controls and 37 hours on the HA and HABT ceramic discs.

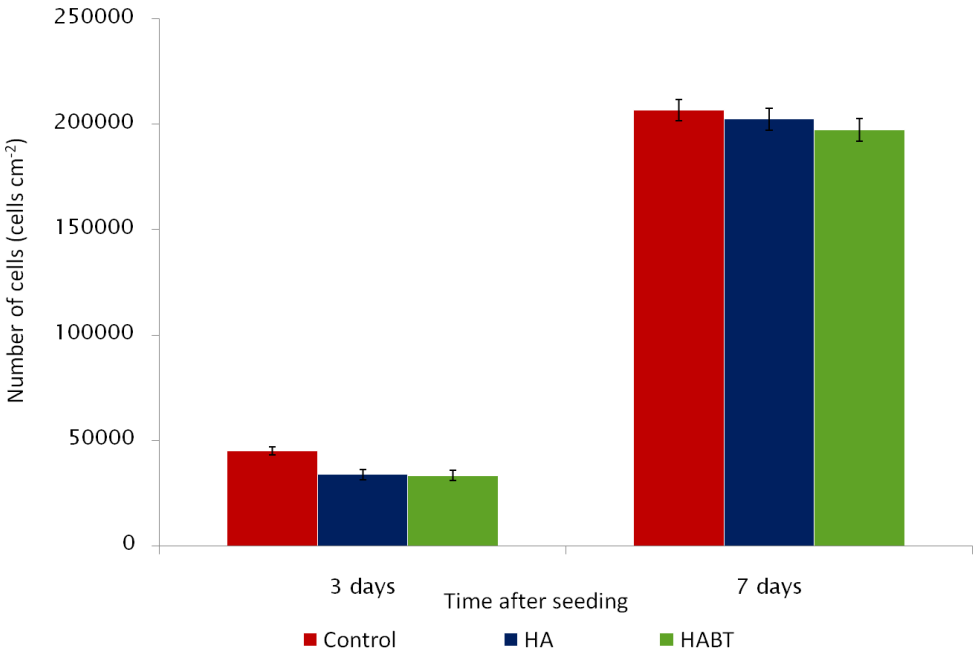

Figure 5.19 Cell population on HA and HABT ceramics

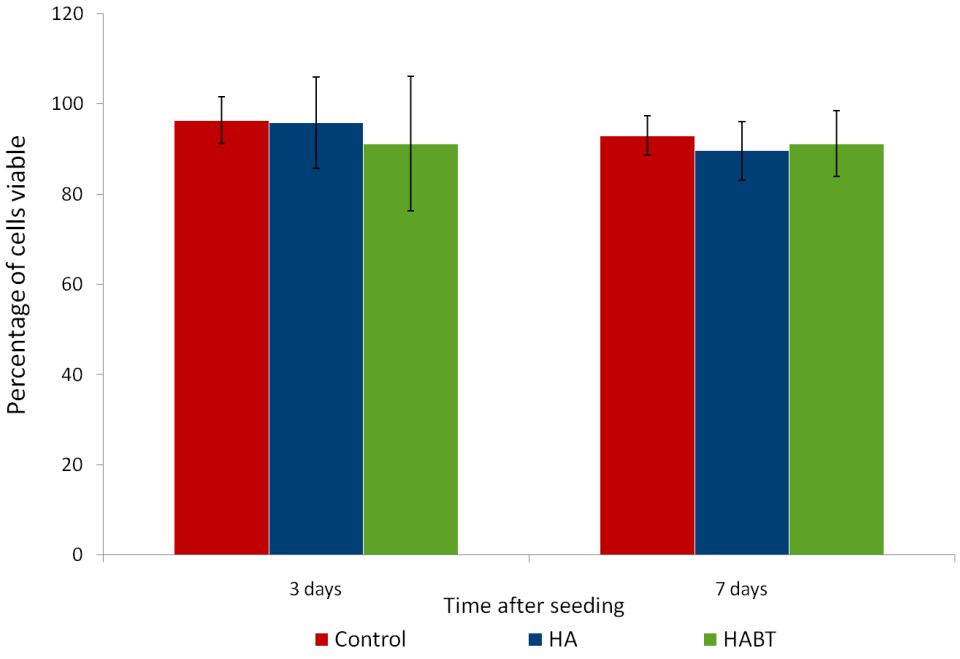

Figure 5.20 Viability of cells on HA and HABT ceramics

The effect of poling

The influence of the presence of a positive or negative surface charge induced by the polarisation of the HABT ceramic on cell proliferation and viability was assessed up to seven days after seeding. Cells were cultured on unpoled HABT ceramics and on the positive and negative faces of poled HABT. Cells were counted and their viability determined after three and seven days of incubation. The numbers of samples and repeats were the same as those described in the previous experiment. The numbers of cells found and the percentage of those cells found to be viable are given in Figures 5.21 and 5.22 respectively.

As discussed in Section 5.1, 24h after seeding a significant ($p<0.05$) increase was observed in the numbers of cells found on poled ceramics of both polarities in comparison with unpoled ceramics. Three days after seeding this trend remained apparent but was no longer statistically significant, with 19 200 ± 2000 cells/cm^2 on the unpoled material and 22 500 - 25 000 cells/cm^2 on the poled surfaces. After seven days the cell populations were again all found to match those on the tissue culture plastic controls, in the order of 200 000 cells/cm^2. Cell population doubling times calculated from this data using Equation 3.1 were 39 hours on the control and 28-32 hours on the three types of HABT. Cell viability was in the range of 91-96% at both time points.

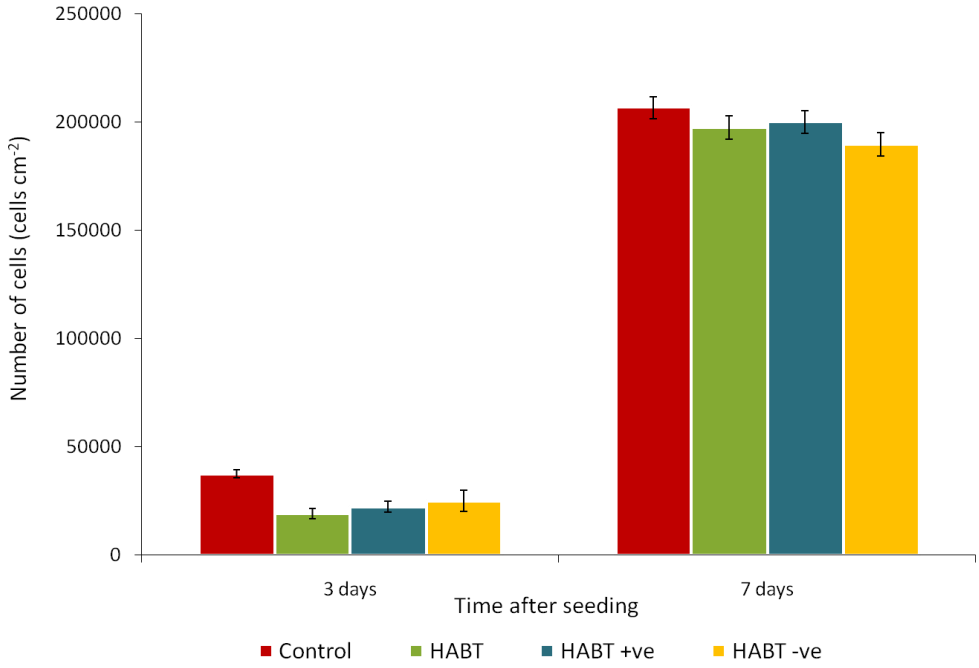

Figure 5.21 Cell numbers on HABT ceramics in various electrical states

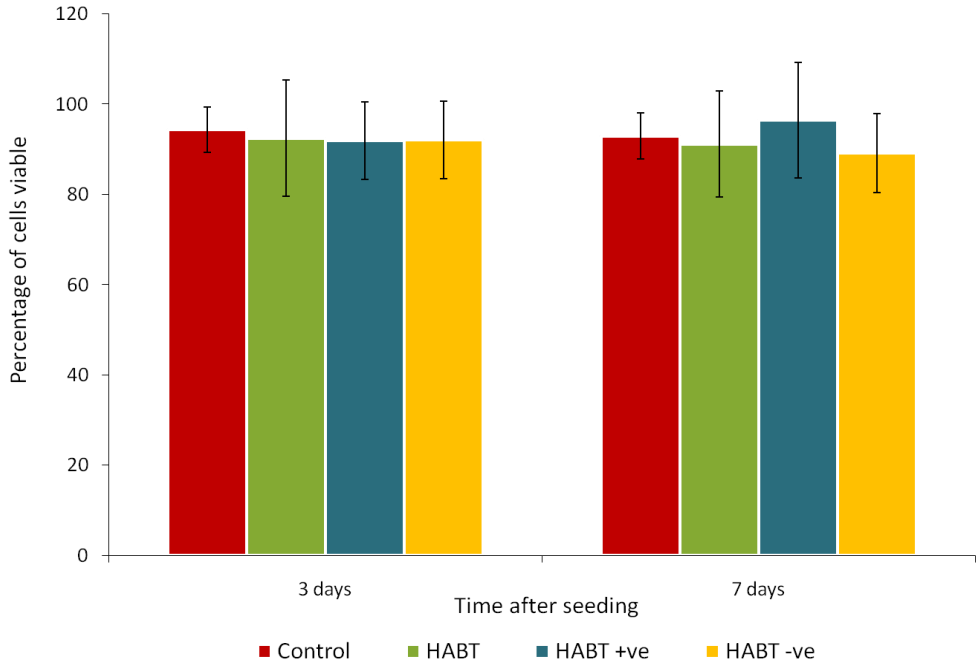

Figure 5.22 Viability of cells on HABT ceramics in various electrical states

5.2.1.3 Cell proliferation at 7 and 14 days after seeding

In addition to the direct counting of cells using a haemocytometer, at 7 and 14 days after seeding, cell proliferation was assessed by the measurement of the total DNA present in the cell population. A Quant-IT Picogreen assay kit was used to measure the DNA present in the lysate of cells cultured on discs of HA and unpoled, positively and negatively poled HABT. The experiment was run three times in triplicate and the data was combined to give nine data points for each material (n=9) at each time point. Results were normalised by the culture surface area and are given in Figures 5.23 and 5.24.

At 7 days after seeding, the quantities of DNA measured seven days after seeding did not follow the pattern predicted by the manual cell counts carried out at the same incubation time. The results from the HA and the negatively charged HABT were comparable to those found on the tissue culture plastic control (180-190ngcm^{-2}). However, significantly less DNA (120-140ngcm^{-2}) was found on the unpoled and positively charged HABT samples.

In contrast to this, 14 days after seeding a different pattern was evident. The electrical state of the HABT did not significantly influence the level of DNA measured. The results for these materials matched those for the tissue culture plastic controls, on which 205ngcm^{-2} of DNA was found. However, the amount of DNA found on the HA discs was significantly higher than that found on both the tissue culture plastic control and the unpoled HABT at 297ngcm^{-2}.

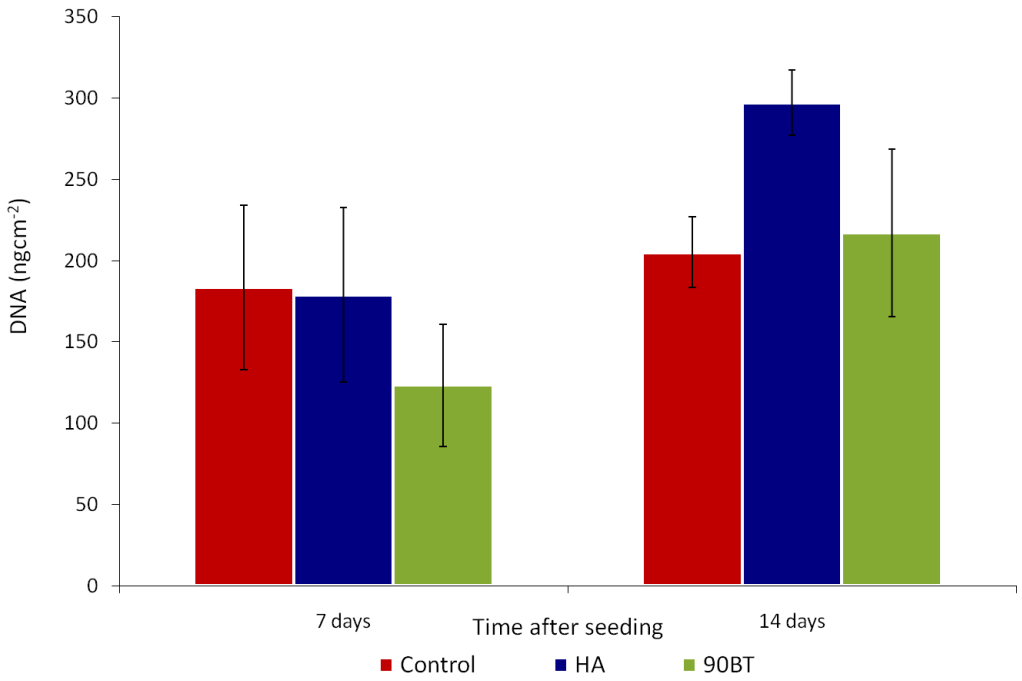

Figure 5.23 Cell proliferation on HA and unpoled HABT at 7 and 14 days after seeding

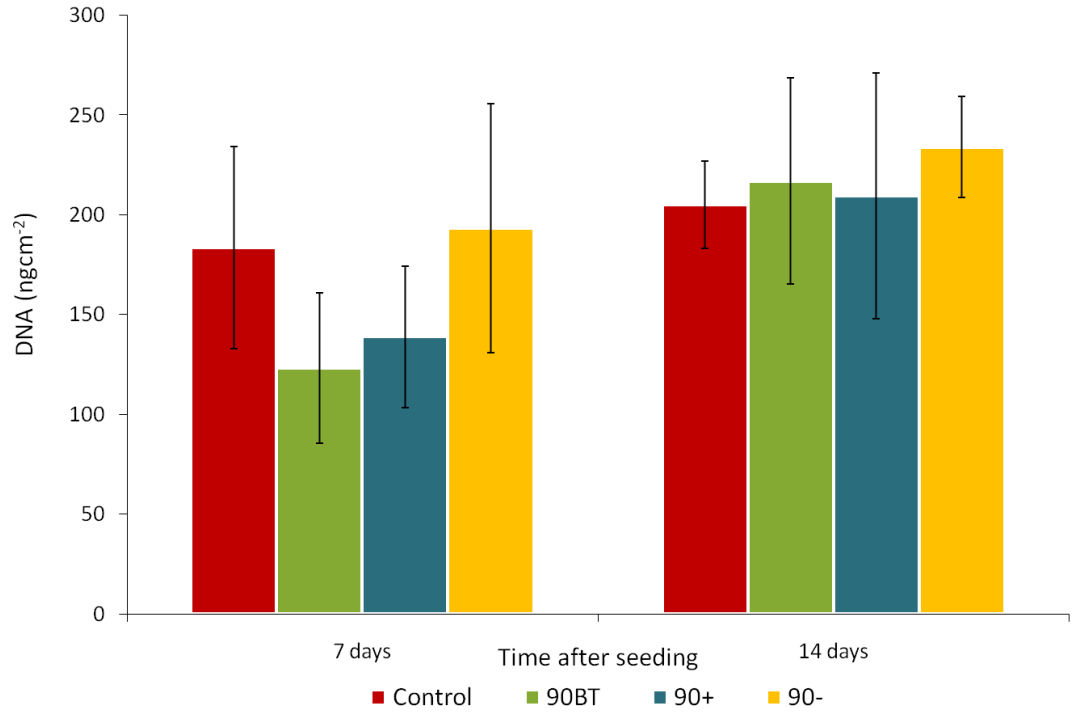

Figure 5.24 Cell proliferation on unpoled HABT and the positive and negative surfaces of poled HABT at 7 and 14 days after seeding

5.2.1.4 Cell activity at 7 and 14 days after seeding

In order to gain a better understanding of the functioning of cells cultured on the test materials at longer culture times, the metabolic activities of cells cultured on discs of HA and unpoled, positively and negatively charged HABT were measured at 7 and 14 days after seeding. The results are given in Figures 5.25 and 5.26, showing values of 0.27-0.30 $ODcm^{-2}$ for all materials.

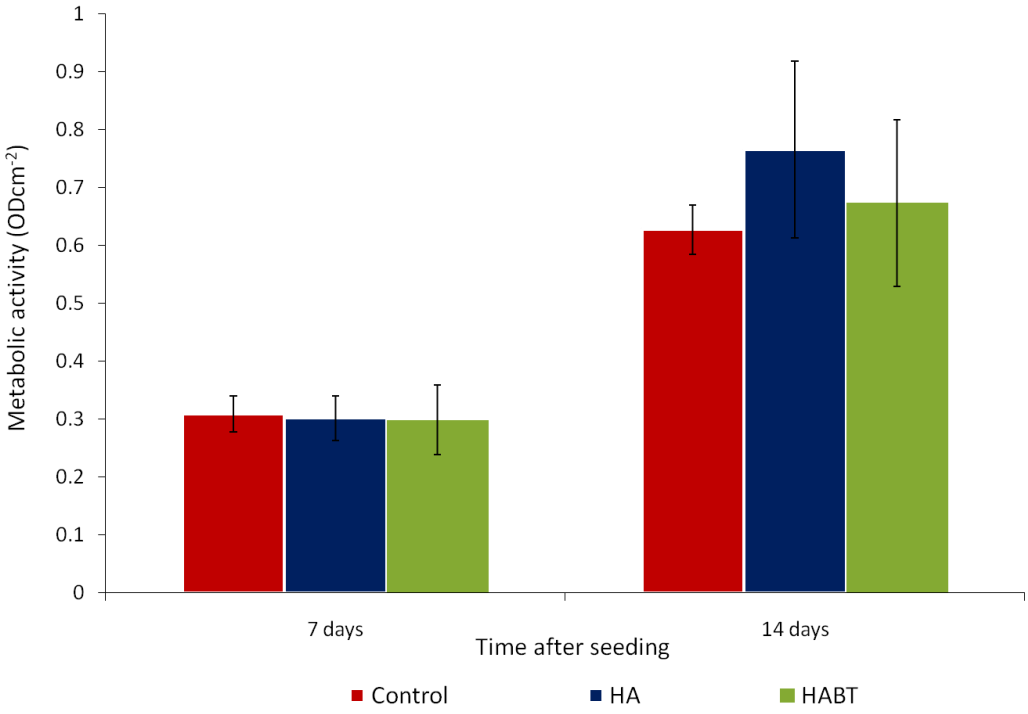

Figure 5.25 Cell activity on HA and HABT at 7 and 14 days after seeding

Neither the chemical composition nor the electrical state of the ceramics was found to influence cell activity after seven days of incubation. At the later time point, the apparent difference between the metabolic activity of the cells grown on HA and HABT discs, with those on the HA appearing more active than those on the HABT (0.73±0.1 $ODcm^{-2}$ compared to 0.68±0.05 $ODcm^{-2}$), was statistically significant ($p<0.05$) in only one of the two runs of the experiment. No other statistically significant differences were detected.

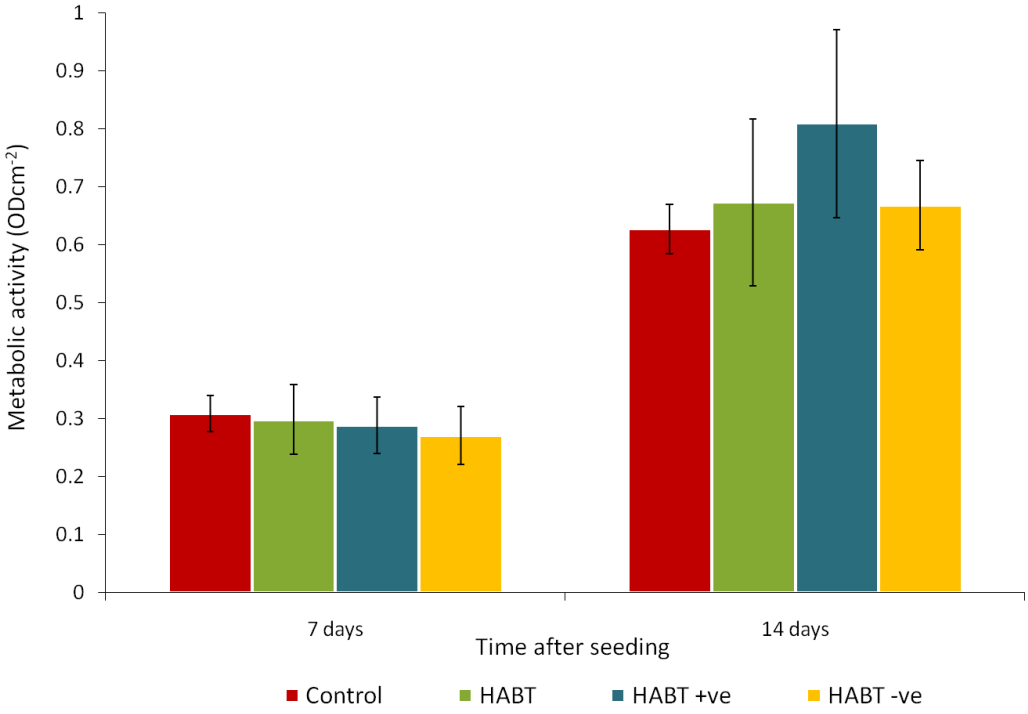

Figure 5.26 Cell activity on unpoled HABT and the positive and negative surfaces of poled HABT

5.2.1.5 Cell differentiation at 7 and 14 days after seeding

Alkaline phosphatase (ALP) is an early marker of osteoblastic differentiation, as described in Section 2.1.3. It is produced by Saos-2 cells in standard culture conditions. Increased production of ALP in a cell population indicates increased cellular differentiation. Production of ALP by cells cultured on discs of HA and unpoled, positively and negatively charged HABT was measured at 7 and 14 days after seeding.

The samples tested were taken from the same cell cultures for which the total DNA was determined. The total ALP measurement was normalised for each sample by the amount of DNA found in the same well. The results, shown in Figure 5.27 and 5.28, indicated no statistically significant differences ($p<0.05$) induced by altering the composition or electrical state of the ceramic. The difference between the cells grown on the control and on the unpoled HABT was, however, statistically significant. After 14 days of incubation the cells grown on the negatively charged surface of poled HABT were found to produce significantly lower amounts of ALP than those grown on the other ceramics. Amounts of ALP measured ranged from 1.55-1.8nmol/ngDNA.

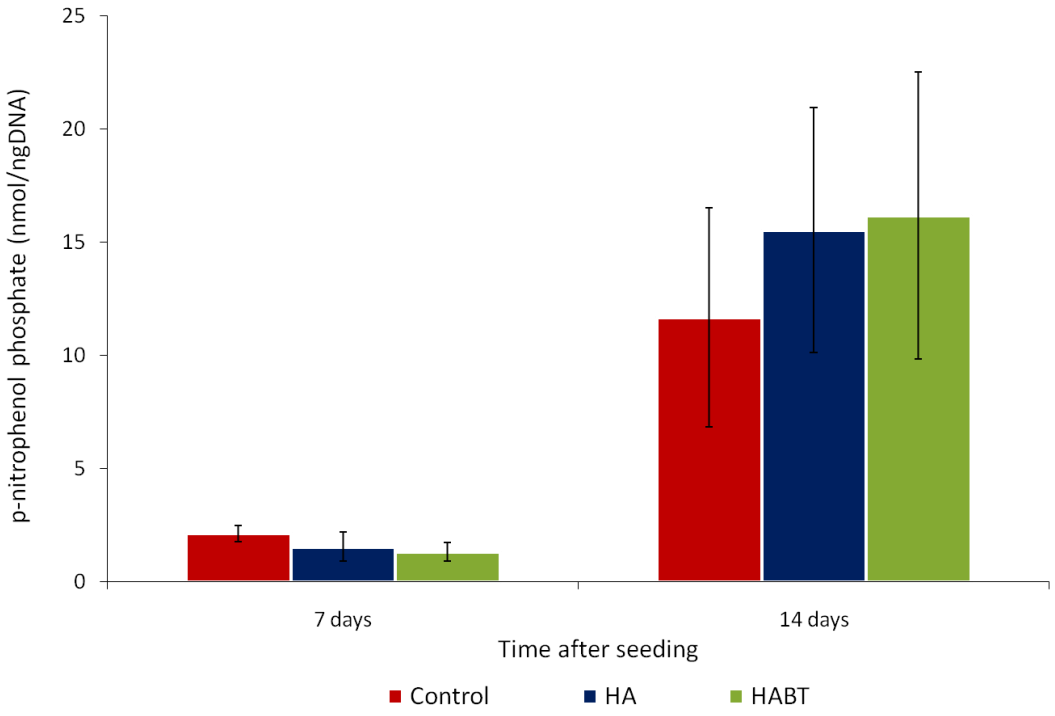

Figure 5.27 Differentiation of cells on HA and unpoled HABT at 7 and 14 days after seeding

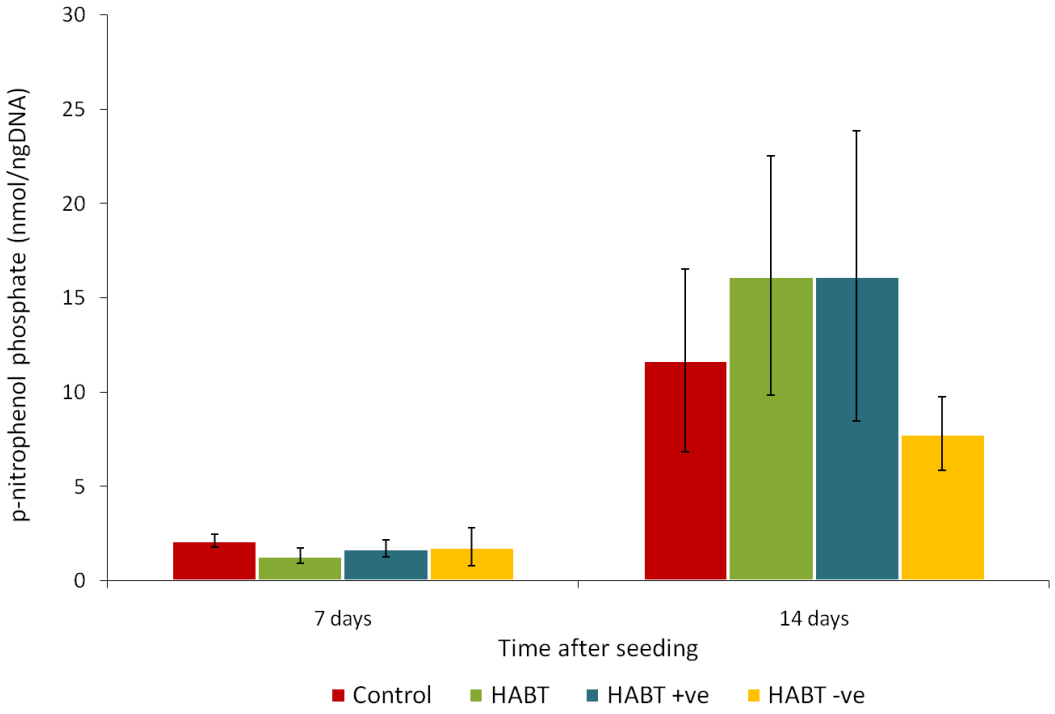

Figure 5.28 Differentiation of cells on unpoled HABT and the positive and negative surfaces of poled HABT at 7 and 14 days after seeding

5.2.2 Discussion

Three days after seeding no statistically significant differences were observed in cell proliferation or viability irrespective of composition or electrical state. In general, it appears that this remains the case at seven days after seeding, with no differences observed in cell proliferation, viability or morphology. In addition the level of differentiation of the cells was consistent on all materials examined. This finding does not concur with trends observed in some cell populations in the literature on charged materials [83]. This may be the result of differences in the magnitudes of the surface charges in question. The polarisation charge of HA (14.9μCcm^{-2}) has previously been shown to be higher than that of BT (6.84μCcm^{-2}) [116].

The cell count and total DNA measurements, however, appear to be contradictory after seven days of incubation. In general, the amount of DNA detected may be considered to be representative of the size of the cell population [171]. The amounts of DNA in the

samples were within the range of accuracy of the Picogreen assay [172] and were in its linear range according to the standards used. Cell counts at this time point may be less accurate than at shorter incubation times. The production of extracellular matrix and the increased density of the population may have made the detachment of all of the cells and their even distribution in the suspension more difficult. Variation in the DNA content of cells throughout their life cycle may also lead to some difference in outcome between the haemocytometer cell count and the Picogreen assay.

The results, when considered collectively, indicate, but do not prove, that variations exist in the size of cell populations at 7 days after seeding. As the metabolic activity, morphology and differentiation of the cells were all unaffected by changes in chemistry and electrical state of the ceramic, the populations generally appear to be comparable. Variations in the topography of the disc surfaces (see Section 5.3) did not affect cell proliferation, in agreement with published results [206]. No variations in morphology or spreading pattern were observed at 7 days after seeding. The limitations of the SEM investigation indentified previously (Section 5.1.2.1) are also applicable to these images. However, the uniformity of cell spreading and the good cell-cell and cell-material interactions visible here indicate that cells grow well on the HABT discs in all electrical states. The differences in surface features on the HA and HABT ceramics reported in Section 5.1 did not appear to induce alterations in cell morphology at any of the time points examined.

At 14 days after seeding there were increased indications of variation between the populations. A raised amount of DNA indicated a larger cell population on HA discs compared with both the control and the HABT and corresponded with an increase in metabolic activity. There was no increase in ALP production, suggesting that all populations were at the same stage of differentiation.

The poling of the HABT induced a change in differentiation but not in total DNA or cell activity at 14 days after seeding. Cells on the negative surface produced less ALP, indicating the population was less well differentiated than that on the neutral or positive surfaces. The large standard deviations in this data may indicate that the quantities of ALP measured were outside of the linear range of the assay. This did not appear to be the case in comparison with the standard curve, however the standards used in this instance did not measure the reaction directly, being based on diluted samples of the reaction product. In any future repeat of this experiment, samples should be diluted further (in excess of the x10 dilution used in this case) in order to ensure the accuracy of the readings.

It appears that despite the attachment of cells to the substrate being essential for their subsequent development, the differences observed in cell numbers and activity 24h after seeding were not directly carried through to later time points. This is particularly obvious for the positively charged HABT, for which there was no evidence of a raised cell population on the material later than 24h after seeding.

The HABT ceramics have been shown by this study to support cell proliferation and activity up to and beyond the point of population confluence and do not appear to affect cell viability when used as cell culture substrates for up to 14 days *in vitro*. This result is in agreement with existing studies in indicating the good potential biocompatibility of BT-containing materials [6, 92, 128].

The clear improvement in bone tissue growth observed *in vivo* by Feng *et al* [6] on HABT implants in comparison with unpoled HA has not been reproduced here, possibly due to the fact that the samples in the current study were not mechanically loaded during the *in vitro* testing. This corroborates their conclusion that stress generated potentials in the HABT ceramics were the origin of the improvement in biological response to the grafts.

In contrast with the current study, in which the poling of HABT induced variations in cell behaviour, earlier studies did not find any influence from poling [129]. This is particularly significant as the material previously tested had a greater remnant polarisation ($0.33 Cm^{-2}$) than that used in the current study ($0.016 Cm^{-2}$). Comparing the two outcomes, it appears that the influence of surface electrical characteristics on biological responses cannot be examined in isolation. Rather, electrical signals must be considered as acting in conjunction with the surrounding ions, proteins and surface characteristics for each biomaterial. It is unlikely that an "ideal" electrical state for cell attachment which is applicable to all materials can be defined.

5.2.3 Conclusions

Cell responses to HABT were comparable with those to HA at three days after seeding. The increase in attachment observed at 24h after seeding did not result in an increased cell population at this time point.

HABT was shown to be a suitable substrate for osteoblast-like cell proliferation up to 14 days after seeding. However, some inconsistencies were observed in cell responses. After 7 days, some variations were observed in cell population, but not in other factors tested. The morphologies of the cells on the HA and HABT ceramics were comparable and were unaffected by the poling of the HABT composite. In general, HABT may be considered to be biocompatible at this incubation time.

At 14 days after seeding indications were found of a reduction in cell differentiation caused by the electrical state of the HABT ceramic. Further work is therefore justified to continue the investigation of the possible inhibition of cell differentiation by the negative surface of poled HABT ceramics. A clearer picture of the impact of poling on differentiation could be obtained by measuring ALP production at later time points in

addition to measuring other differentiation markers such as osteopontin and osteocalcin. The mineralisation of ECM may also be assessed using this cell line. Differences in outcomes between this study and previous work on HABT suggest that mechanical loading of the poled composites, producing stress-generated potentials, are necessary if an improved biological response is to be induced.

5.3 Macrophage responses to HABT ceramics

5.3.1 Introduction

Macrophages are known to play a key role in determining the host response to any implanted material. They mediate immune and inflammatory responses and are implicated in the recruitment of osteoprogenitor cells (see Section 2.1.5). It is therefore pertinent to investigate the responses of macrophages to potential bone graft materials.

As discussed in Section 2.4, studies have been carried out into the *in vivo* and *in vitro* immune response to HA. No such work has been carried out on materials containing BT. This section discusses initial experiments investigating the cytotoxicity of HA and HABT in bulk and particulate forms. The influence of pre-soaking the test materials in complete culture medium on the outcome of testing is also considered. The methods used for seeding and analysing macrophage cell cultures are described in Sections 2.6.2 and 2.6.3.

5.3.2 Results

5.3.2.1 Presoaked materials

Cytotoxicity

The cytotoxicity of HA, HABT and the positive and negative surfaces of poled HABT to J774.2 macrophages was investigated. In accordance with the standard method for the

seeding of Saos-2 cells, the materials were presoaked in complete culture medium (containing 10% FCS) for 24h before the macrophages were seeded onto them. The experiment was run three times on triplicates of each material (n=9). Some data points were noted at the time of carrying out the experiment to be subject to experimental error and were excluded from the results. A minimum of six data points per material was included in the statistical analysis.

The results, shown in Figure 5.29, indicate that though HABT appeared to be more toxic to macrophage cells than the tissue culture plastic control, irrespective of its electrical state, the difference was not statistically significant. Cell viability on controls and HABT ceramics was 20-35%. However, the HA discs were found to be significantly more cytotoxic, with around 60% of the macrophages in the culture dead after 24h of exposure to the material.

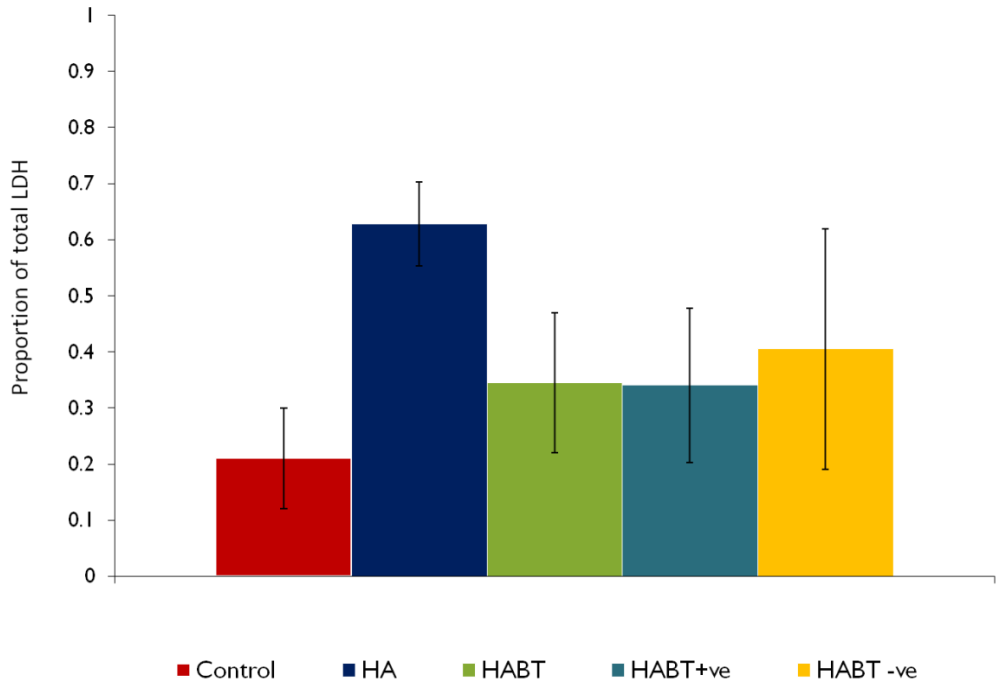

Figure 5.29 Cytotoxicity of HA, HABT and poled HABT (% total LDH) after 24h

Cytokine expression

The expression of pro-inflammatory cytokine IL1-β by J774.2 murine macrophages exposed to HA, HABT and the positive and negative faces of poled HABT for 24h was assessed. As in the Saos-2 attachment studies, the tablets were soaked for 24h in complete medium before the seeding of the cells. Tissue culture plastic was used as a control culture surface. Positive controls were obtained by stimulating cells with LPS and ATP. No IL1-β in either the pro- or active form was found in the cell culture supernatants, however, in cell lysate some evidence of pro-IL1-β was found. As shown in Figure 5.30, in the first run of the experiment all ceramics, but not the tissue culture plastic control, induced the production of pro-IL1β. In the second run of the experiment, some evidence of a pro-IL1β production was evident. In the third run, no response was found.

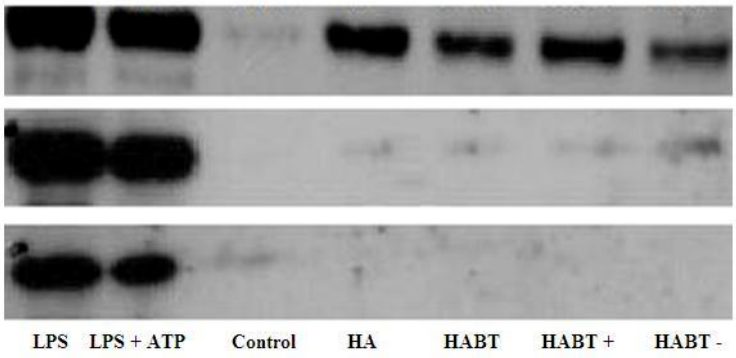

Figure 5.30 Pro-IL1-β (37kDa) detected in lysate of J774.2 macrophages on presoaked ceramics after 24h. Each row displays the results from one of the three runs of the same experiment.

5.3.2.2 Unsoaked materials

Cytotoxicity

The cytotoxicity of HA and HABT J774.2 macrophages seeded without pre-soaking in complete culture medium was mesured. As the previous experiments indicated no influence of poling on the macrophage response, only unpoled HABT was included in this experiment. An investigation of the possible influence of particulate matter on

macrophage responses was included. The experiment was run three times on triplicates of each material (n=9). Again, data points noted, at the time of carrying out the experiment, to be subject to experimental error were excluded from the results, which are shown in Figure 5.31. A minimum of six data points per material was included in the statistical analysis.

The pre-soaking of cells in serum-containing medium was found to modify the response of J774.2 macrophages to HA discs. Without pre-soaking, no difference was found between the cytotoxicity of the tissue culture plastic controls, HA and HABT, on all of which cell viability was around 20%. An increased cytotoxicity was found in both ceramics in particulate form, with a statistically significant difference between HABT particles and discs. The difference between the results found on the HA discs and the HA particles was not statistically significant.

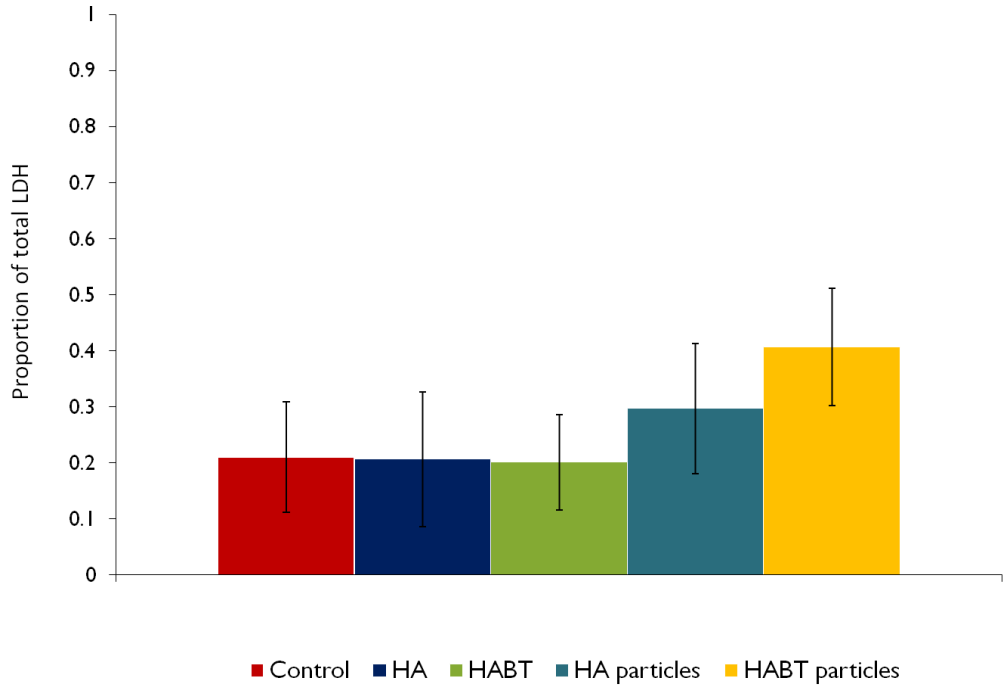

Figure 5.31 Cytotoxicity of HA and HABT in bulk and particulate forms (% total LDH) after 24h

Cytokine expression

The expression of pro-inflammatory cytokine IL1-β by J774.2 murine macrophages exposed to HA and HABT discs and to particles of HA and HABT (particle size < 100μm) for 24h was investigated using western blotting. The cells were applied to the sterilised materials without pre-soaking the samples in culture medium. Positive controls were obtained by stimulating cells with LPS and ATP. As in the test on presoaked tablets, no IL1-β was detected in the cell culture supernatant for any of the samples tested. The experiment was repeated four times. Each run is represented by one line of Figure 5.32, showing the protein bands observed at 37kDa, the molecular weight if pro-IL1- β.

In the first run, pro-IL1-β was detected in the lysate of cells exposed to the dense HA and HABT discs, with a less dense band appearing for the HA particles. In the second run, an indication of pro-IL1β production was found in cells exposed to HA in both bulk and particulate forms. No other proinflammatory responses were indentified. In both the third and fourth runs of the experiment no pro-IL1-β was detected on any material.

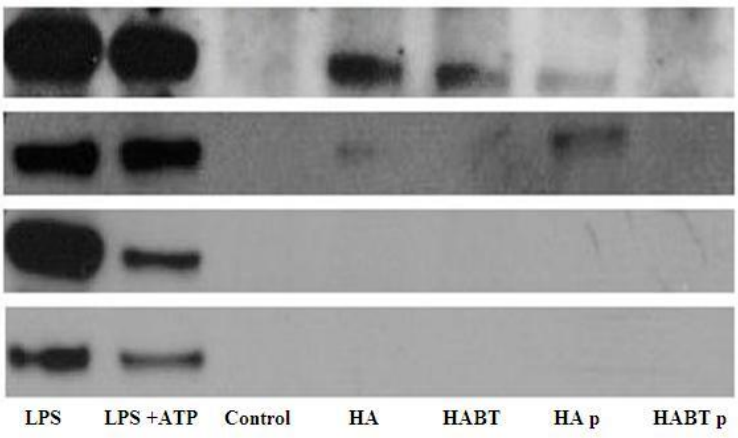

Figure 5.32 Pro-IL1-β (37kDa) detected in lysate of J774.2 macrophages on non-soaked ceramics. HA p and HABT p = particles. Each row displays the results from one of the four runs of the same experiment.

5.3.3 Discussion

The soaking of the ceramic discs in complete culture medium was initially included in the preparation protocol in order to maintain a common protocol for all cell culture experiments. It is clear from the results that the soaking distinctly modified the macrophage response. The HA discs were cytotoxic to the J774.2 macrophages after soaking. Observations from the second experiment, in which soaking was not carried out, concur with *in vivo* studies in the literature (as discussed in Section 2.4) in finding that HA is not cytotoxic. The differences in the results suggests that the adhered proteins on the HA differed from those on the HABT. Possible contamination of some discs with adherent endotoxins, resulting in production of pro-IL1-β not related to the material chemistry, should not be discounted [49].

In both experiments some indication of the production of pro-IL1-β was detected in cells cultured on the HA discs. Though some blots indicate a pro-inflammatory response to HA in agreement with other published work [142], others show no production of pro-IL1-β. This variation renders the results of this experiment inconclusive.

The HABT ceramic was not found to be cytotoxic to J774.2 macrophages irrespective of the use of serum-containing soaking medium. This, along with the comparable cytokine results found on the HA and HABT, is a further indication of the biocompatibility of HABT ceramics *in vitro*. A further observation is that the response of the cells did not depend on the electrical state of the ceramic.

The observed increase in cytotoxicity of particulate forms of both HA and HABT was as predicted by the literature [142] The differences observed in the cells cultured on the two types of ceramic may result from varying time scales in responses as opposed to an increase in cytotoxicity or cytokine release. Future work is therefore justified, testing

cell responses at a range of incubation times in order to properly detail the time course of cytokine expression.

Variations found in the cytokine production may result from differences in the concentrations or volumes of samples loaded into the gels. Repeat experiments in which the equal loading of the samples is tested would allow for comparison of the amount of cytokine produced by measurement of the level of relative intensity of the band on the western blot. This could be achieved by assessing the quantity of β-actin present, a protein which should not vary between equally loaded samples. Equally, a Bradford assay could be used to determine the protein content of samples before running the western blot.

Though the J774.2 has been shown to be a good model for human monocyte behaviour, differences exist in immune responses between species [207]. A clearer indication of possible immune responses to HABT in humans could be obtained by repeating these experiments using primary monocytes derived from human blood.

Inflammatory responses are greatly affected by the size of particles encountered by macrophages (see Section 2.1.5). Further refinement of particle size categories tested would provide a better understanding of immune responses to HABT debris or particulate matter.

5.3.4 Conclusions

This preliminary investigation into immune and inflammatory responses to HA and HABT substitutes showed that the pre-soaking of materials in serum-containing medium before cell seeding influences the responses of macrophages. When pre-soaked, HA was found to be cytotoxic to the J774.2 cell line. The cytotoxicity of HABT was comparable to that of the tissue culture plastic control. When not pre-soaked, neither HA nor HABT ceramics are more cytotoxic to these cells than a tissue culture plastic control. In particulate form, HABT ceramic is more cytotoxic than in bulk form. Some evidence of a pro-inflammatory response to HA and HABT was detected, but the results of this study were variable and therefore inconclusive. Further work may establish better the pattern of proinflammatory responses caused by HA and HABT ceramics.

This chapter described the examination of *in vitro* biological responses to HABT ceramics in terms of osteoblast-like cell attachment, longer-term osteoblast-like cell behaviour and macrophage responses. The key findings from the studies of each of these sections are given in the following section.

5.4 Key findings

Attachment of osteoblast-like cells to HABT ceramics:

i. The inclusion of 90% BT in HABT composites does not influence the viability of cells cultured on the ceramic.
ii. After 24h of incubation, the HABT ceramic has biocompatibility comparable to that of commercially available HA.
iii. The poling of HABT ceramics encourages increased cell attachment.
iv. After 24h of incubation, the poling of the HABT ceramic does not influence cell morphology or the total metabolic activity of the cell population.
v. The nature of the surface polarisation (positive or negative) did not influence biological responses.

Proliferation of osteoblast-like cells on HABT ceramics:

i. HABT ceramics support osteoblast-like cell growth up to 14 days after seeding *in vitro.*
ii. HABT ceramics do not appear to cause variations in the viability Saos-2 cells.
iii. HABT ceramics do not modify cell spreading or morphology.
iv. The ceramic chemistry and electrical state may modify cell behaviour at longer incubation times (14 days).
v. The nature of the surface charge (positive or negative) may have some influence on cell behaviour at longer incubation times (14 days).
vi. The influence of surface charge is likely to be material specific.

Macrophage responses to HABT ceramics:

i. Neither HA nor HABT are cytotoxic to J774 macrophages in bulk form.

ii. The size of the ceramic sample (particle or bulk form) affects macrophage responses.

iii. Protein adsorption modifies macrophage responses to HA.

iv. Neither the positive or negative surface of poled ceramics induces an increased proinflammatory response.

v. Further work on inflammatory responses to HA and HABT ceramics is needed.

6 Summary and conclusions

The aim of this project was to investigate HA-piezoelectric composites as novel bone graft materials. A review of the literature revealed that HABT composites may be suitable for this application. The current study has substantially added to the understanding of these composites as potential bone graft substitutes. Specifically, the objectives of the study were to manufacture a range of HABT composites and to characterise their piezoelectric properties, composition and structure. After selecting an appropriate material for biological testing, the effects of the changes in the material and variations of electrical state on *in vitro* biological responses were to be determined. These objectives have been successfully achieved and a summary of the main conclusions and suggestions for future work follow.

For the first time, the electrical properties of HABT ceramics have been examined extensively. Their piezoelectric coefficients (d_{33}, d_{31} and g_{33}), permittivity and microstructure were found to be dependent on the proportion of BT included in the material. This trend may result from domain pinning and matrix clamping as well as the presence of non-piezoelectric phases in the composite. HABT composites containing more than 70% BT displayed piezoelectric coefficients. The ferroelectric nature of 90 and 95% BT composites have been confirmed by the assessment of their piezoelectric hysteresis. These composites had piezoelectric charge coefficients (d_{33}) of 72.8±6.6pCN^{-1} and 86.3±7.9pCN^{-1} respectively. The highest piezoelectric voltage coefficient was 14x10^{-3}Vm^{-1}Pa^{-1}, found in the 90% BT ceramic. Its remnant polarisation was 0.008Cm^{-2}, with a coercive field of 0.66kVmm^{-1}. These properties, with reference to previously published work, may be expected to result in an improved biological response when compared to the response to existing HA graft materials. As a result of its strong and consistent piezoelectric properties, the HABT ceramic containing 90% BT was considered to be the most appropriate for use in biological testing.

In vitro testing of the HABT composite was carried out using human osteoblast-like cells. This work represents the first assessment of HABT ceramics using human cells. The viability of cells cultured on the HABT was found to be comparable to that on HA, a material widely accepted to be biocompatible. The composite supported the proliferation and function of osteoblast-like cells up to the longest time period tested (14 days). The morphology, activity and differentiation of the cell populations on HA and HABT were substantially similar up to 7 days after seeding, indicating the biocompatibility of HABT ceramics to human cells. HABT ceramics have been shown in this study to be suitable substrates for cell attachment.

The remnant polarisation of poled HABT resulted in an increase in cell attachment, as measured by a count of the cell population at 24h after seeding. This effect was observed irrespective of the nature (positive or negative) of the polarisation. Other factors measured at this incubation time, including the metabolic activity of the cell population, cell morphology and viability, were comparable on poled and unpoled HABT. The results obtained at 14 days after seeding were less consistent. Some variations in cell population and differentiation were identified. Future work is needed to clarify cell behaviour at this incubation time.

This study also includes the first examination of immune responses to HABT ceramics. The HABT composite was found to induce macrophage responses comparable to those of cells cultured on HA when materials were not presoaked in serum-containing medium. Immune responses were dependent on the physical nature of the sample, discs of ceramic being less cytotoxic to macrophages than sub-100μm ceramic particles. The response was not influenced by either the positive or negative surfaces of poled HABT.

This study identified *in vitro* responses to HABT ceramics. It has shown HABT composites to be promising materials for use as bone graft substitutes. They are

biocompatible in the short term *in vitro*. Their piezoelectric properties are of a suitable magnitude to offer a stimulus to induce improved biological responses in comparison to standard HA graft materials.

In the context of the published literature, the results of this study indicate that responses to charged surfaces and stress-generated potentials are likely to be material specific. They depend on factors such as dissolved ions around the material and surface characteristics as well as electrical stimulus. In the case of HABT ceramics, mechanical loading is likely to be necessary to induce improvements in biological responses when compared to HA.

This is the first study to report macrophage and human osteoblast-like cell responses to HABT ceramics. Tests were carried out under static conditions and will provide a useful benchmark for further studies which could include investigation of the effect of applying cyclic loadings.

Some of the experimental results and findings included in this thesis have been presented in a number of conference and journal papers; details of which are included in Appendix E.

Future work for the advancement of this research is proposed in the following section.

Future work

Previous work into HABT ceramics was very limited, but identified the possibility of producing piezoelectric ceramics with optimal properties for use as bone graft substitutes. The current study has provided a base for understanding the properties of HABT ceramics and the *in vitro* biological responses to them. The expansion of this understanding would be facilitated by additional work including the following:

i. Examination of *in vitro* cell responses to HABT at extended incubation times including further analysis of cell differentiation and function.
ii. Modification of the manufacturing of HABT ceramics, for example changes to the sintering cycle, with the aim of improving the piezoelectric properties of composites containing a higher proportion of HA.
iii. The use of a bioreactor capable of the mechanically loading the ceramics to allow the determination of the influence of cyclic loading on short- and long-term cell responses *in vitro.*
iv. Investigation of immune and inflammatory responses to both HA and HABT ceramics.
v. Investigation of the mechanism by which piezoelectric and charged material influence bone responses. This could include studies on single crystal piezoelectrics, HABT, piezoelectric polymers and poled hydroxyapatite.

7 References

1. Laurencin, CT. Ed. Bone Graft Substitutes 2003, ATSM International: West Conshohocken, USA.
2. Boyan, BD, McMillan, J, Lohmann, CH, Ranly, DM, and Schwartz, Z. Bone graft substitutes: Basic information for successful clinical use with special focus on synthetic graft substitutes, in Bone Graft Substitutes, Laurencin CT, Editor. 2003, ASTM International, West Conshohocken, USA.
3. Zhu, PX, Masuda, Y, and Koumoto, K. The effect of surface charge on hydroxyapatite nucleation. Biomaterials, 2004. 25(17): 3915-3921.
4. MacGinitie, LA, Stanley, GD, Bieber, WA, and Wu, DD. Bone streaming potentials and currents depend on anatomical structure and loading orientation. Journal of Biomechanics, 1997. 30(11-12): 1133-1139.
5. Cowin, SC and Moss, ML. Mechanosensory mechanisms in bone, in Bone Mechanics Handbook, Cowin SC, Editor. 2001, CRC Press, Boca Raton.
6. Feng, JQ, Yuan, HP, and Zhang, XD. Promotion of osteogenesis by a piezoelectric biological ceramic. Biomaterials, 1997. 18(23): 1531-1534.
7. Nordin, M and Frankel, VH. Biomechanics of bone, in Basic Biomechanics of the Musculoskeletal System, Frankel VH and Nordin M, Editors. 2001, Lippincot, Williams and Wilkins, Hagerstown, USA.
8. Blanton, PL and Biggs, NL. Density of fresh and embalmed human compact and cancellous bone. American Journal of Physical Anthropology, 1968. 29(1): 39-44.
9. Jee, WSS. Integrated bone tissue physiology: Anatomy and physiology, in Bone Mechanics Handbook, Cowin SC, Editor. 2001, CRC Press, Boca Raton.
10. Park, JB and Lakes, RS. Biomaterials: An introduction. 2nd ed. 1992, Plenum Press, New York.
11. Currey, J. Incompatible mechanical properties in compact bone. Journal of Theoretical Biology, 2004. 231(4): 569-580.

12. Suchanek, W and Yoshimura, M. Processing and properties of hydroxyapatite-based biomaterials for use as hard tissue replacement implants. Journal of Materials Research, 1998. 13(1): 94-117.
13. Seeman, E and Delmas, PD. Bone quality - the material and structural basis of bone strength and fragility. New England Journal of Medicine, 2006. 354(21): 2250-2261.
14. Pritchard, JJ. The Osteoblast. The Biochemistry and Physiology of Bone, ed. Bourne GH. Vol. 1. 1972, Academic Press, London.
15. Vaananen, K. Osteoclast function: Biology and mechanisms, in Principles of Bone Biology, Bilezikian JP, Raisz LG, and Rodan GA, Editors. 1996, Academic Press, London.
16. Majeska, RJ. Cell biology of bone, in Bone Mechanics Handbook, Cowin SC, Editor. 2001, CRC: Boca Raton.
17. Marks, SM and Hermey, DC. The structure and development of bone, in Principles of Bone Biology, Bilezikian JP, Raisz LG, and Rodan GA, Editors. 1996, Academic Press, London.
18. Amodio, SGP. Novel roles of bone lining cells in bone remodelling, in Inter-university Research School of Dentistry (IOT). 2005, Universiteit van Amsterdam: Amsterdam.
19. Kapanen, A. Biocompatibility of orthopaedic implants on bone forming cells, in Department of Anatomy and Cell Biology and Biocenter Oulu. 2002, University of Oulu: Oulu.
20. Holtrop, ME. Light and electron microscopic structure of bone-forming cells., in Bone volume 1: The osteoblast and osteocyte, B.K.Hall, Editor. 1989, The Telford Press: Caldwell, New Jersey.
21. Katagiri, T and Takahashi, N. Regulatory mechanisms of osteoblast and osteoclast differentiation. Oral Diseases, 2002. 8(3): 147-159.
22. Wan, M and Cao, X. Bmp signaling in skeletal development. Biochemical and Biophysical Research Communications, 2005. 328(3): 651-657.

23. Karsenty, G and Wagner, EF. Reaching a genetic and molecular understanding of skeletal development. Developmental Cell, 2002. 2(4): 389-406.
24. van Driel, M, Pols, HAP, and van Leeuwen, J. Osteoblast differentiation and control by vitamin d and vitamin d metabolites. Current Pharmaceutical Design, 2004. 10(21): 2535-2555.
25. Poole, KE and Reeve, J. Parathyroid hormone -- a bone anabolic and catabolic agent. Current Opinion in Pharmacology Gastrointestinal/Endocrine and Metabolic Diseases, 2005. 5(6): 612-617.
26. Hayden, JM, Mohan, S, and Baylink, DJ. The insulin-like growth-factor system and the coupling of formation to resorption. Bone, 1995. 17(2): S93-S98.
27. Parfitt, AM. The physiologic and clinical significance of bone histomorphometric data, in Bone histomorphometry: Techniques and interpretation, Recker RR, Editor. 1983, CRC Press, Boca Raton.
28. Manolagas, SC. Birth and death of bone cells: Basic regulatory mechanisms and implications for the pathogenesis and treatment of osteoporosis. Endocrine Reviews, 2000. 21(2): 115-137.
29. Knothe Tate, ML, Adamson, JR, Tami, AE, and Bauer, TW. The osteocyte. The International Journal of Biochemistry and Cell Biology, 2004. 36: 1-8.
30. Junquiera, LC, Carneiro, J, and O'Kelly, R. Basic histology 9th edition. 1998, Appleton and Lange, Stanford, USA.
31. Martin, RB. Toward a unifying theory of bone remodeling. Bone, 2000. 26(1): 1-6.
32. Tamarkin, DA. Bone development and growth. 2004 [cited 2006 17/02/2006]; Available from: http://distance.stcc.edu/AandP/AP/AP1pages/Units5to9/bone/bonedev.htm.
33. Turner, CH. Three rules for bone adaptation to mechanical stimuli. Bone, 1998. 23(5): 399-407.
34. Martin, T, T.W. Osteoclast-derived activity in the coupling of bone formation to resorption. Trends in Molecular Medicine, 2005. 11(2): 76-81.

35. Raisz, LG. Physiology and pathophysiology of bone remodeling. Clinical Chemistry, 1999. 45(8): 1353-1358.
36. Ralston, S. Bone anatomy and cell biology. 2002 [cited 2006 16/02/2006]; University of Aberdeen webpages]. Available from: http://www.abdn.ac.uk/medicine_therapeutics/bone/bone%20anatomy%20and%20cell%20biology.hti.
37. Wolff, JD. "Der gesetz der transformation der knochen". 1892, Berlin: A. Hirschwald.
38. Nijweide, PJ, Burger, EH, Nulend, JK, and Van der Plas, A. The osteocyte, in Principles of bone biology, Bilezikian JP, Raisz LG, and Rodan GA, Editors. 1996, Academic Press, London.
39. Frost, HM. A 2003 update of bone physiology and Wolff's law for clinicians. Angle Orthodontist, 2004. 74(1).
40. Bubanj, S and Obradovic, B. Mechanical force and bones density. Facta Universitatis, Physical Education and Sport, 2002. 1(9): 37-50.
41. Rodin, GA and Martin, TJ. Role of osteoblasts in hormonal control of bone resorption - a hypothesis. Calcified Tissue International, 1981. 33: 349-351.
42. Sikavitsas, VI, Temenoff, JS, and Mikos, AG. Biomaterials and bone mechanotransduction. Biomaterials, 2001. 22(19): 2581-2593.
43. Li, JL, Liu, DW, Ke, HZ, Duncan, RL, and Turner, CH. The P2X(7) nucleotide receptor mediates skeletal mechanotransduction. Journal of Biological Chemistry, 2005. 280(52): 42952-42959.
44. Xia, Z and Triffitt, JT. A review on macrophage responses to biomaterials. Biomedical Materials, 2006. 1(1): R1-R9.
45. Silva, SN, Pereira, MM, Goes, AM, and Leite, MF. Effect of biphasic calcium phosphate on human macrophage functions *in vitro*. Journal of Biomedical Materials Research, 2003. 65A(4): 475-481.
46. Ingham, E and Fisher, J. The role of macrophages in osteolysis of total joint replacement. Biomaterials, 2005. 26(11): 1271-1286.

47. Kim, DH, Novak, MT, Wilkins, J, Kim, M, Sawyer, A, and Reichert, WM. Response of monocytes exposed to phagocytosable particles and discs of comparable surface roughness. Biomaterials, 2007. 28(29): 4231-4239.
48. Champagne, CM, Takebe, J, Offenbacher, S, and Cooper, LF. Macrophage cell lines produce osteoinductive signals that include bone morphogenetic protein-2. Bone, 2002. 30(1): 26-31.
49. Gorbet, MB and Sefton, MV. Endotoxin: The uninvited guest. Biomaterials, 2005. 26(34): 6811-6817.
50. Laurencin, CT. Bone grafts and bone graft substitutes. Othopedic Network News, 1999. 10: 10-17.
51. Finkemeier, CG. Bone-grafting and bone-graft substitutes. Journal of Bone and Joint Surgery (A), 2002. 84A(3): 454-464.
52. Younger, EM and Chapman, MW. Morbidity at bone graft donor site. Journal Orthopedic Trauma, 1989. 3: 192-195.
53. National joint registry statsonline www.Njrcentre.Org.Uk. 2007 [cited 2007 16/12/2008]; Available from: www.njrcentre.org.uk.
54. Hofer, S, Leopold, S, and Jacobs, J. Clinical perspectives on the use of bone graft based on allografts, in Bone graft substitutes, Laurencin CT, Editor. 2003, ASTM International, West Conshohocken, USA.
55. www.exeterhip.co.uk. Medical professionals - exeter techniques - femoral revision. 2006 [cited 2006 17th January]; Available from: http://www.exeterhip.co.uk/ex_pag_femoral-revision.htm.
56. Mashoof, AA, Siddiqui, SA, Otero, M, and Tucci, JJ. Supplementation of autogenous bone graft with coralline hydroxyapatite in posterior spine fusion for idiopathic adolescent scoliosis. Orthopedics, 2002. 25(10): 1073-1076.
57. Kwon, B and Jenis, LG. Carrier materials for spinal fusion. Spine J, 2005. 5(6 Suppl): 224S-230S.

58. Chapman, MW and Finkemeier, CG. Treatment of supracondylar nonunions of the femur with plate fixation and bone graft. Journal of Bone and Joint Surgery (A), 1999. 81A(9): 1217-1228.
59. Hing, KA. Bone repair in the twenty-first century: Biology, chemistry or engineering? Phil Trans R Soc Lond A, 2004. 362: 2821-2850.
60. Dorozhkin, SV. Calcium orthophosphate cements for biomedical application. Journal of Materials Science 2008. 43(9): 3028-3057.
61. Moore, WR, Graves, SE, and Bain, GI. Synthetic bone graft substitutes. Australian and New Zealand Journal of Surgery, 2001. 71(6): 354-361.
62. LeGeros, RZ. Properties of osteoconductive biomaterials: Calcium phosphates. Clinical Orthopaedics and Related Research, 2002. 395: 81-98.
63. Liu, D-M. Influence of porous microarchitecture on the in-vitro dissolution and biological behaviour of porous calcium phosphate bioceramics. Materials Science Forum, 1997. 250: 183-208.
64. Gittings, JP. Fabrication and properties of novel open porous calcium phosphate bioceramics, Department of Mechanical Engineering. University of Bath, 2005.
65. Park, JB and Bronzino, JD. Eds. Biomaterials: Principles and applications. 2003, CRC Press, Boca Raton.
66. De Bruijn, JD, Klein, CPAT, de Groot, K, and van Blitterswijk, CA. The ultrastructure of the bone-hydroxyapatite interface *in vitro*. Journal of Biomedical Materials Research, 1992. 26(10): 1365-1382.
67. Ducheyne, P and Qiu, Q. Bioactive ceramics: The effect of surface reactivity on bone formation and bone cell function. Biomaterials, 1999. 20(23-24): 2287-2303.
68. Frank, RM, Klewansky, P, Hemmerle, J, and Tenenbaum, H. Ultrastructural demonstration of the importance of crystal size of bioceramic powders implanted into human periodontal lesions. Journal of Clinical Periodontology, 1991. 18(9): 669-680.

69. Thomson, RC, Yaszemski, MJ, Powers, JM, and Mikos, AG. Hydroxyapatite fiber reinforced poly(alpha-hydroxy ester) foams for bone regeneration. Biomaterials, 1998. 19(21): 1935-1943.
70. Chapman, MW, Bucholz, R, and Cornell, C. Treatment of acute fractures with a collagen-calcium phosphate graft material - a randomized clinical trial. Journal of Bone and Joint Surgery (A), 1997. 79A(4): 495-502.
71. White, E and Shors, EC. Biomaterial aspects of Interpore 200 porous hydroxyapatite. Dental Clinics of North America, 1986. 30(1): 49-67.
72. Hsu, YH. Fabrication of porous calcium phosphate bioceramics, Department of Mechanical Engineering. University of Bath, 2005.
73. Kuhne, JH, Bartl, R, Frisch, B, Hammer, C, Jansson, V, and Zimmer, M. Bone formation in coralline hydroxyapatite effects of pore size studied in rabbits. Acta Orthopaedica Scandinavica, 1994. 65: 246-252.
74. Kuboki, Y, Takita, H, Kobayashi, D, Tsuruga, E, Inoue, M, Murata, M, Nagai, N, Dohi, Y, and Ohgushi, H. Bmp-induced osteogenesis on the surface of hydroxyapatite with geometrically feasible and nonfeasible structures: Topology of osteogenesis. Journal of Biomedical Materials Research, 1998. 39(2): 190-199.
75. Eggli, PS, Muller, W, and Schenk, RK. Porous hydroxyapatite and tricalcium phosphate cylinders with 2 different pore-size ranges implanted in the cancellous bone of rabbits - a comparative histomorphometric and histologic-study of bony ingrowth and implant substitution. Clinical Orthopaedics and Related Research, 1988(232): 127-138.
76. Karageorgiou, V and Kaplan, D. Porosity of 3d biomaterial scaffolds and osteogenesis. Biomaterials, 2005. 26(27): 5474-5491.
77. Sampath, T and Reddi, A. Bone morphogenetic protein (bmp) implants as bone graft substitutes- promises and challenges, in Bone graft substitutes, Laurencin CT, Editor. 2003, ATSM International, West Conshohocken, USA
78. Ziegler, J, Anger, D, Krummenauer, F, Breitig, D, Fickert, S, and Guenther, KP. Biological activity of recombinant human growth factors released from

biocompatible bone implants. Journal of Biomedical Materials Research, 2008. 86A: 89–97.

79. Cazalbou, S, Eichert, D, Ranz, X, Drouet, C, Combes, C, Harmand, MF, and Rey, C. Ion exchanges in apatites for biomedical applications. Journal of Materials Science: Materials in Medicine, 2005. 16: 405– 409.
80. Patel, N, Brooks, RA, Clarke, MT, Lee, PMT, Rushton, N, Gibson, IR, Best, SM, and Bonfield, W. *In vivo* assessment of hydroxyapatite and silicate-substituted hydroxyapatite granules using an ovine defect model. Journal of Materials Science: Materials in Medicine, 2005. 16: 429– 440.
81. Thian, ES, Huang, J, Best, SM, Barber, ZH, Brooks, RA, Rushton, N, and Bonfield, W. The response of osteoblasts to nanocrystalline silicon-substituted hydroxyapatite thin films. Biomaterials, 2006. 27(13): 2692-2698.
82. Landi, E, Logroscino, G, Proietti, L, Tampieri, A, Sandri, M, and Sprio, S. Biomimetic mg-substituted hydroxyapatite: From synthesis to *in vivo* behaviour. Journal of Materials Science: Materials in Medicine, 2008. 19(1): 239-247.
83. Ohgaki, M, Kizuki, T, Katsura, M, and Yamashita, K. Manipulation of selective cell adhesion and growth by surface charges of electrically polarized hydroxyapatite. Journal of Biomedical Materials Research, 2001. 57(3): 366-373.
84. Fukada, E and Yasuda, I. On the piezoelectric effect of bone. Journal of the Physical Society of Japan, 1957. 12(10): 1158-1162.
85. Pienkowski, D and Pollack, SR. The origin of stress-generated potentials in fluid-saturated bone. Journal of Orthopedic Research, 1983. 1(1): 30-41.
86. McElhaney, JH. The charge distribution on the human femur due to load. Journal of Bone and Joint Surgery (A), 1967. 49A: 1561-1571.
87. Bassett, CAL. Biological significance of piezoelectricity. Calcified Tissue Research, 1968. 1(252-272).
88. Hastings, GW and Mahmud, FA. Electrical effects in bone. Journal of Biomedical Engineering, 1988. 10: 515-521.

89. Dent, ACE. Novel active fibre composites, Department of Mechanical Engineering. University of Bath, 2008
90. Park, JB, Recum, AFV, Kenner, GH, Kelly, BJ, Coffeen, WW, and Grether, MF. Piezoelectric ceramic implants - a feasibility study. Journal of Biomedical Materials Research, 1980. 14(3): 269-277.
91. Park, JB, Kenner, GH, Brown, SD, and Scott, JK. Mechanical property changes of barium-titanate (ceramic) after *in vivo* and *in vitro* aging. Biomaterials Medical Devices and Artificial Organs, 1977. 5(3): 267-276.
92. Park, JB, Kelly, BJ, Kenner, GH, Vonrecum, AF, Grether, MF, and Coffeen, WW. Piezoelectric ceramic implants - invivo results. Journal of Biomedical Materials Research, 1981. 15(1): 103-110.
93. Haertling, GH. Ferroelectric ceramics: History and technology. Journal of the American Ceramic Society, 1999. 82(4): 797-818.
94. Panteny, SR. Microstructural, mechanical and electrical characterisation of piezoelectric particulate composites with dielectric modelling. Department of Mechanical Engineering, University of Bath, 2003
95. www.matweb.com. Matweb material property data 2005, [cited 2005 25/11/05]; Available from: http://www.matweb.com/search/SpecificMaterial.asp?bassnum=CCHAN2.
96. Tresser, JF, Alkoy, S, and Newnham, RE. Piezoelectric sensors and sensor materials. Journal of Electroceramics, 1998. 2(4): 257-272.
97. Jaffe, B, Cooke, WR, and Jaffe, H. Piezoelectric ceramics. 1971, Academic Press, London
98. Bradt, RC and Ansell, GS. Aging in tetragonal ferroelectric barium titanate. Journal of the American Ceramic Society, 1969. 52(4): 192-198.
99. van Randeraat, J. Piezoelectric Ceramics. 2 ed. 1974, Mullard Ltd, London
100. Smith, RC and Ouanies, Z. A domain wall model for hysteresis in piezoelectric materials, in ICASE Report 99-52. 1999, Institute for Computer Applications in Science and Engineering: Hampton, USA

101. Nelson, LJ. Characterisation and modelling of active fibre composites in Department of Mechanical Engineering. 2005, University of Bath: Bath
102. Damjanovic, D. Hysteresis in piezoelectric and ferroelectric materials, in The Science of Hysteresis, Mayergoyz and Bertotti G, Editors. 2005, Elsevier: Amsterdam.
103. Maeder, M. Lead free piezoelectric materials. Journal of Electroceramics 2004. 13: 385-392.
104. 2002/95/EC, Directive 2002/95/EC of the European parliament and of the council of 27 January 2003 on the restriction of the use of certain hazardous substances in electrical and electronic equipment. 2002.
105. Goyer, RA. Lead toxicity: Current concerns. Environmental Health Perspectives, 1993. 100: 177-187.
106. Aba, A and Ergun, C. Phase stability in hydroxyapatite/barium titanate piezo bioceramics. Diffusion and Defect Data Part A, Defect and Diffusion Forum, 2008. 273/276: 1-7.
107. Hauke, T, Steinhausen, R, Seifert, W, Beige, H, and Kamlah, M. Modeling of poling behavior of ferroelectric 1-3 composites. Journal of Applied Physics, 2001. 89: 5040–5047.
108. Hackenberger, W, Pan, M-J, Vedula, V, Pertsch, P, Cao, W-W, Randall, C, and Shrouta, T. Effect of grain size on actuator properties of piezoelectric ceramics. SPIE Proceedings Series 1998. 3324: 28-36.
109. Cao, WW and Randall, CA. Grain size and domain size relations in bulk ceramic ferroelectric materials. Journal of Physics and Chemistry of Solids, 1995. 57(10): 1499-1505.
110. Arlt, G and Sasko, P. Domain configuration and equilibrium size of domains in $BaTiO_3$ ceramics. Journal of Applied Physics, 1980. 51: 4956–4960
111. Fukada, E and Yasuda, I. Piezoelectric effects in collagen. Japanese Journal of Applied Physics, 1964. 3(2): 117-121.

112. Maeda, H, Tsuda, K, and Fukada, E. The dependence on temperature and hydration of piezoelectric, dielectric and elastic constants of bone. Japanese Journal of Applied Physics, 1976. 15(12): 2333-2336.
113. Hastings, GW and Mahmud, FA. The electromechanical properties of fluid-filled bone: A new dimension. Journal of Materials Science: Materials in Medicine, 1991. 2: 118-124.
114. Cowin, SC, Weinbaum, S, and Zeng, Y. A case for bone canaliculi as the anatomical site of strain generated potentials. Journal of Biomechanics, 1995. 28(11): 1281-1297.
115. Tate, MLK. Interstitial fluid flow, in Bone mechanics handbook, Cowin SC, Editor. 2001, CRC Press, Boca Raton
116. Nakamura, S, Takeda, H, and Yamashita, K. Proton transport polarization and depolarization of hydroxyapatite ceramics. Journal of Applied Physics, 2001. 89(10): 5386-5392.
117. Royce, BSH. Field-induced transport mechanisms in hydroxyapatite. Annals of the New York Academy of Sciences, 1974. 238: 131-138.
118. Takeda, H, Nakamura, S, Yamada, K, Tsuchiya, T, and Yamashita, K. Dielectric properties of poled hydroxyapatite ceramics. Key Engineering Materials, 2000. 181-182: 35-38.
119. Hwang, KS, Song, JE, Jo, JW, Yang, HS, Park, YJ, Ong, JL, and Rawls, HR. Effect of poling conditions on growth of calcium phosphate crystal in ferroelectric BaTiO3 ceramics. Journal of Materials Science: Materials in Medicine, 2002. 13(1): 133-138.
120. Jeong, JH, Kwak, IJ, Kim, HI, Ong, JL, Rawls, HR, and Park, YJ. Biocompatibility of negatively charged barium titanate thin film formed on Ti, in The 81st General Session of the International Association for Dental Research. 2003: Gotenberg, Sweden.
121. Yamashita, K, Oikawa, N, and Umegaki, T. Acceleration and deceleration of bone-like crystal growth on ceramic hydroxyapatite by electric poling. Chemistry of Materials, 1996. 8(12): 2697-2700

122. Shelton, RM, Rasmussen, AC, and Davies, JE. Protein adsorption at the interface between charged polymer substrata and migrating osteoblasts. Biomaterials, 1988. 9(1): 24-29.
123. Davies, JE. The importance and measurement of surface charge species in cell behaviour at the biomaterial interface, in Surface Characterisation of Biomaterials, Ratner BD, Editor. 1988, Elsevier: Amsterdam
124. Qiu, K, Zhao, XJ, Wan, CX, Zhao, CS, and Chen, YW. Effect of strontium ions on the growth of ros17/2.8 cells on porous calcium polyphosphate scaffolds. Biomaterials, 2006. 27(8): 1277-1286.
125. Finke, B, Leuthen, F, Schroeder, K, Meuller, PD, Bergemann, C, Frant, M, Ohl, A, and Nebe, BJ. The effect of positively charged plasma polymerization on initial osteoblastic focal adhesion on titanium surfaces. Biomaterials, 2007. 28: 4251-4354.
126. Dekhtyar, N, Polyaka, N, and Sammons, R. Electrically charged hydroxyapatite enhances immobilisation and proliferation of osteoblasts. in 14th Baltic Conference on Biomedical Engineering and Medical Physics, 2008.
127. Schneider, GB, English, A, Abraham, M, Zaharias, R, Stanford, C, and Keller, J. The effect of hydrogel charge density on cell attachment. Biomaterials, 2004. 25(15): 3023-3028.
128. Beloti, MM, De Oliveira, PT, Gimenes, R, Zaghete, MA, Bertolini, MJ, and Rosa, AL. *In vitro* biocompatibility of a novel membrane of the composite poly(vinylidene-trifluoroethylene)/barium titanate. Journal of Biomedical Materials Research, 2006. 79A(2): 282 - 288.
129. Beloti, MM. Biocompatibility of BT, Personal Communication. 2008.
130. Gimenes, R, Zaghete, MA, Bertolini, M, Varela, JA, Coelho, LO, and Silva, NF. Composites P(VDF-TrFE)/BT used as bioactive membranes for enhancing bone regeneration. in Smart Structures and Materials 2004: Electroactive Polymer Actuators and Devices (EAPAD). 2004: SPIE, Bellingham, USA.

131. Kizuki, T, Ohgaki, M, Katsura, M, Nakamura, S, Hashimoto, K, Toda, Y, Udagawa, S, and Yamashita, K. Effect of bone-like layer growth from culture medium on adherence of osteoblast-like cells. Biomaterials, 2003. 24: 941-947.
132. Itoh, S, Nakamura, S, Nakamura, M, Shinomiyaa, K, and Yamashita, K. Enhanced bone ingrowth into hydroxyapatite with interconnected pores by electrical polarization. Biomaterials, 2006. 27: 5572–5579.
133. Schumacher, D, Strunz, V, and Gross, U. Does piezoceramic influence avian bone formation in the early postoperative phase? Biomaterials, 1983. 4: 215-217.
134. Marino, AA, Rosson, J, Gonzalez, E, Jones, L, Rogers, S, and Fukada, E. Quasi-static charge interactions in bone. Journal of Electrostatics, 1988. 21(2-3): 347-360.
135. Shimono, T, Matsunaga, S, Fukada, E, Hattori, T, and Shikinami, Y. The effects of piezoelectric poly-l-lactic acid films in promoting ossification *in vitro*. *In Vivo*, 1996. 10: 471-476.
136. Feng, J. An investigation on the ceramic composite of the biological piezoelectric implants, in Polymers and Biomaterials, Feng H, Han Y, and Huang L, Editors. 1991, Elsevier Science: Amsterdam. 367.
137. Silva, CC, Almeida, AFL, Oliveira, RSD, Pinheiro, AG, Es, JCG, and Sombra, ASB. Dielectric permittivity and loss of hydroxyapatite screen-printed thick films. Journal of Materials Science, 2003. 38: 3713 – 3720.
138. Parek, B, Joshi, M, and Vaidya, A. Characterisation and inhibitive study of gel-grown hydroxyapatite crystals at physiological temperature. Journal of Crystal Growth, 2008. 310(7-9): 1749-1753.
139. Callegeri, B and Belangero, WD. Analysis of the interface formed among the poly (vinylidene) fluoride (piezoelectric and non piezoelectric) and the bone tissue of rats. Acta Orthopedica Brasilica, 2004. 12(3): 160-166.
140. Sabokbar, A, Pandey, R, and Athanasou, NA. The effect of particle size and electrical charge on macrophage-osteoclast differentiation and bone resorption. Journal of Materials Science: Materials in Medicine, 2003. 14: 731-738.

141. Lee, MH, Han, DW, Baek, HS, Lim, HR, Lee, IS, Lee, KY, Kim, KT, Lee, SJ, and Park, JC. Differential cytokine responses of murine macrophage j774a.1 cells to stainless steel coated with and without hydroxyapatite. Surface & Coatings Technology, 2007. 201(9-11): 5729-5732.
142. Nadra, I, Boccaccini, AR, Philippidis, P, Whelan, LC, McCarthy, GM, Haskard, DO, and Landis, RC. Effect of particle size on hydroxyapatite crystal-induced tumor necrosis factor alpha secretion by macrophages. Atherosclerosis, 2008. 196(1): 98-105.
143. Fellah, BH, Josselin, N, Chappard, D, Weiss, P, and Layrolle, P. Inflammatory reaction in rats muscle after implantation of biphasic calcium phosphate micro particles. Journal of Materials Science-Materials in Medicine, 2007. 18(2): 287-294.
144. Horowitz, SM and Gonzales, JB. Inflammatory response to implant particulates in a macrophage/osteoblast co-culture model. Calcified Tissue International, 1996. 59(5): 392-396.
145. Rice, JM, Hunt, JA, and Gallagher, JA. Quantitative evaluation of the biocompatible and osteogenic properties of a range of biphasic calcium phosphate (BCP) granules using primary cultures of human osteoblasts and monocytes. Calcified Tissue International, 2003. 72(6): 726-736.
146. Williams, DF. The Williams dictionary of biomaterials. 1999, Liverpool: Liverpool University Press.
147. Biological evaluation of medical devices, in BS EN ISO 10993. 2003: UK.
148. Shelton, RM, Liu, Y, Cooper, PR, Gbureck, U, German, MJ, and Barralet, JE. Bone marrow cell gene expression and tissue construct assembly using octacalcium phosphate microscaffolds. Biomaterials, 2006. 27(14): 2874-2881.
149. Kim, SS, Park, MS, Jeon, O, Choi, CY, and Kim, BS. Poly(lactide-co-glycolide)/hydroxyapatite composite scaffolds for bone tissue engineering. Biomaterials, 2006. 27(8): 1399-1409.

150. Ignatius, AA, Schmidt, C, Kaspar, D, and Claes, LE. *In vitro* biocompatibility of resorbable experimental glass ceramics for bone substitutes. Journal of Biomedical Materials Research, 2001. 55(3): 285-294.
151. Chang, K, Chang, WHS, Huang, S, Huang, S, and Shih, C. Pulsed electromagnetic fields stimulation affects osteoclast formation by modulation of osteoprotegerin, rank ligand and macrophage colony-stimulating factor. Journal of Orthopaedic Research, 2005. 23(6): 1308-1314.
152. Dalby, MJ, Di Silvio, L, Harper, EJ, and Bonfield, W. *In vitro* evaluation of a new polymethylmethacrylate cement reinforced with hydroxyapatite. Journal of Materials Science: Materials in Medicine, 1999. 10(12): 793-796.
153. Fassina, L, Visai, L, Asti, L, Benazzo, F, Speziale, P, Tanzi, MC, and Magenes, G. Calcified matrix production by saos-2 cells inside a polyurethane porous scaffold, using a perfusion bioreactor. Tissue Engineering, 2005. 11(5-6): 685-700.
154. Meyer, U, Joos, U, and Wiesmann, HP. Biological and biophysical principles in extracorporal bone tissue engineering. Part I. International Journal Oral Maxillofacial Surgery, 2004. 33(4): 325-332.
155. Wilke, A, Orth, J, Lomb, M, Fuhrmann, R, Kienapfel, H, Griss, P, and Franke, RP. Biocompatibility analysis of different biomaterials in human bone marrow cell cultures. Journal of Biomedical Materials Research, 1998. 40A(2): 301-306.
156. Palsson, B and Bhatia, SN. Tissue engineering. 2004, Pearson Education, Inc, Upper Saddle River, USA.
157. Pautke, C, Schieker, M, Tischer, T, Kolk, A, Neth, P, Mutschler, W, and Milz, S. Characterization of osteocarcoma cell lines MG-63, Saos-2 and U2-OS in comparison to human osteoblasts. Anticancer Research, 2004. 24(6): 3743-3748.
158. McQuillan, DJ, Richardson, MD, and Bateman, JF. Matrix deposition by a calcifying human osteogenic sarcoma cell line (saos02). Bone, 1995. 16(4): 415-426.
159. Rouahi, M, Gallet, O, Champion, E, Dentzer, J, Hardouin, P, and Anselme, K. Influence of hydroxyapatite microstructure on human bone cell response. Journal of Biomedical Materials Research, 2006. 78A(2): 222-235.

160. Chen, Y, Mak, AFT, Wang, M, Li, J, and Wong, MS. PLLA scaffolds with biomimetic apatite coating and biomimetic apatite/collagen composite coating to enhance osteoblast-like cells attachment and activity. Surface and Coatings Technology, 2006. 201(3-4): 575-580.
161. Li, CY, Gao, SY, Terashita, T, Shimokawa, T, Kawahara, H, Matsuda, S, and Kobayashi, N. *In vitro* assays for adhesion and migration of osteoblastic cells (Saos-2) on titanium surfaces. Cell Tissue Research, 2006. 324: 369-375.
162. Olivier, V, Duval, JL, Hindie, M, Pouletaut, P, and Nagel, MD. Comparative particle-induced cytotoxicity toward macrophages and fibroblasts. Cell Biology and Toxicology, 2003. 19(3): 145-159.
163. Cortizo, MS, Molinuevo, MS, and Cortizo, AM. Biocompatibility and biodegradation of polyester and polyfumarate based-scaffolds for bone tissue engineering. Journal of Tissue Engineering and Regenerative Medicine, 2008. 33-42.
164. Anselme, K and Bigerelle, M. Modelling approach in cell/material interactions studies. Biomaterials, 2006. 27(8): 1187-1199.l
165. Degasne, I, Basle, MF, Demais, V, Hure, G, Lesourd, M, Grolleau, B, Mercier, L, and Chappard, D. Effects of roughness, fibronectin and vitronectin on attachment, spreading and proliferation of human osteoblast-like cells (saos-2) on titanium surfaces. Calcified Tissue International, 1999. 64: 499-507.
166. Wang, C, Duan, Y, Markovic, B, Barbara, J, Rolfe Howlett, C, Zhang, X, and Zreiqat, H. Proliferation and bone-related gene expression of osteoblasts grown on hydroxyapatite ceramics sintered at different temperature. Biomaterials, 2004. 25(15): 2949-2956.
167. Rea, SM, Brooks, RA, Best, SM, Kokubo, T, and Bonfield, W. Proliferation and differentiation of osteoblast-like cells on apatite-wollastonite/polyethylene composites. Biomaterials, 2004. 25(18): 4503-4512.

168. Postiglione, L, Domenico, GD, Ramaglia, L, Montagnani, S, Salzano, S, Meglio, FD, Sordone, L, Vitale, M, and Rossi, G. Behavior of saos-2 cells cultured on different titanium surfaces. Journal of Dental Research, 2003. 82(90): 692-696.
169. Price, N, Bendall, SP, Frondoza, C, Jinnah, RH, and Hungerford, D. Human osteoblast-like cells (MG63) proliferate on a bioactive glass surface. Journal of Biomedical Materials Research 1997. 37(3): 394-400.
170. Rachandran, R, Goodman, SB, and Smith, RL. The effects of titanium and polymethylmethacrylate particles on osteoblast phynoptic stability. Journal of Biomedical Materials Research, 2006. (77A): 512-517.
171. Kee, W, Leong, DTW, and Hutmacher, DW. The challenge to measure cell proliferation in two and three dimensions. Tissue Engineering, 2005. 11(1/2): 182-191.
172. Pabbruwe, MB, Stewart, K, and Chaudhuri, JB. A comparison of calorimetric and DNA quantification assays for the assessment of meniscal fibrochondrocyte proliferation in microcarrier culture. Biotechnology Letters, 2005. 27: 1451-1455.
173. Haslam, G, Wyatt, D, and Kitos, PA. Estimating the number of viable animal cells in multi-well cultures based on their lactate dehydrogenase activities. Cytotechnology, 2000. 32: 63-75.
174. Simon, M, Lagneau, C, Moreno, J, Lissac, M, Dalard, F, and Grosgogeat, B. Corrosion resistance and biocompatibility of a new porous surface for titanium implants. European Journal of Oral Sciences, 2005. 113(6): 537-545.
175. Ling, L-J, Ho, F-C, Y-T., C, Holborow, DW, Liu, T-Y, and Hung, S-L. Areca nut extracts modulated expression of alkaline phosphatase and receptor activator of nuclear factor b ligand in osteoblasts. Journal of Clinical Peridontology, 2005. 32(4): 353-359.
176. Matziolis, G, Tuischer, J, Kasper, G, Thompson, M, Bartmeyer, B, Krocker, D, Perka, C, and Duda, G. Simulation of cell differentiation in fracture healing: Mechanically loaded composite scaffolds in a novel bioreactor system. Tissue Engineering, 2006. 12(1): 201-208.

177. Kasten, P, Vogel, J, Luginbuhl, R, Niemeyer, P, Tonak, M, Lorenz, H, Helbig, L, Weiss, S, Fellenberg, J, and Leo, A. Ectopic bone formation associated with mesenchymal stem cells in a resorbable calcium deficient hydroxyapatite carrier. Biomaterials, 2005. 26(29): 5879-5889.
178. Boanini, E, Torriceli, P, Gazzano, M, Giardino, R, and Bigi, A. Nanocomposites of hydroxyapatite with aspartic acid and glutamic acid and their interaction with osteoblast-like cells. Biomaterials, 2006. 27: 4428-4433.
179. Yu, XJ, Botchwey, EA, Levine, EM, Pollack, SR, and Laurencin, CT. Bioreactor-based bone tissue engineering: The influence of dynamic flow on osteoblast phenotypic expression and matrix mineralization. Proceedings of the National Academy of Sciences of the United States of America, 2004. 101(31): 11203-11208.
180. Doran, PM. Bioprocess engineering principles. 1995, Academic Press, San Diego.
181. Dalby, MJ, Silvio, LD, Davies, GW, and Bonfield, W. Surface topography and HA filler volume effect on primary human osteoblasts *in vitro*. Journal of Materials Science: Materials in Medicine, 2000. 11(12): 805-810.
182. Wojciak-Stothard, B, Curtis, A, Monaghan, W, Macdonald, K, and Wilkinson, C. Guidance and activation of murine macrophages by nanometric scale topography. Experimental Cell Research, 1996. 223(2): 426-435.
183. Kieswetter, K, Schwartz, Z, Hummert, TW, Cochran, DL, Simpson, J, Dean, DD, and Boyan, BD. Surface roughness modulates the local production of growth factors and cytokines by osteoblast-like MG-63 cells. Journal of Biomedical Materials Research, 1996. 32A(1) 55-63.
184. Orsini, G, Assenza, B, Scarano, A, Piattelli, M, and Piattelli, A. Surface analysis of machined versus sandblasted and acid-etched titanium implants. International Journal of Oral Maxillofacial Implants, 2000. 15(6): 779-784.
185. Montanaro, L, Arciola, CR, Campoccia, D, and Cervellati, M. *In vitro* effects on MG63 osteoblast-like cells following contact with two roughness-differing fluorohydroxyapatite-coated titanium alloys. Biomaterials, 2002. 23(17): 3651-3659.

186. Stevens, MM and George, JH. Exploring and engineering the cell surface response. Science, 2005. 310(5751): 1135 - 1138.
187. Den Barber, ET, de Ruijter, JE, Smits, HTJ, Ginsel, LA, von Recum, AF, and Jansen, JA. Efect of parallel surface microgrooves and surface energy on cell growth. Journal of Biomedical Materials Research 1998. 29(4): 511-518.
188. Zinger, O, Zhao, G, Schwartz, Z, Simpson, J, Weiland, M, Landolt, D, and Boyan, B. Differential regulation of osteoblasts by substrate microstructural features. Biomaterials, 2005. 26(14): 1837-1847.
189. Powder diffraction file, pdf-2, database sets 1-45. International Centre for Diffraction Data.
190. Wang, L, Nemoto, R, and Senna, M. Microstructure and chemical states of hydroxyapatite/silk fibroin nanocomposites synthesized via a wet-mechanochemical route. Journal of Nanoparticle Research, 2002. 4: 535-540.
191. Kareiva, A, Tautkus, S, Rapalaviciute, R, Jorgensen, JE, and Lundtoft, B. Sol-gel synthesis and characterisation of barium titanate powders. Journal of Materials Science, 1999. 34: 4853-4857.
192. Fukada, E and Yasuda, I. Piezoelectric effects in collagen. Japanese Journal of Applied Physics, 1967. 3(2): 117-121.
193. Gilmore, RS and Katz, JL. Elastic properties of apatites. Journal of Materials Science, 1982. 17: 1131-1141.
194. Park, JG, Oh, TS, and Kim, YH. Dielectric properties and microstructural behaviour of b-site calcium-doped barium titanate ceramics. Journal of Materials Science, 1992. 27(21): 5713-5719.
195. Yu, L, Yu, S-W, and Feng, X-Q. Effects of electric fatigue on the butterfly curves of ferroelectric ceramics. Materials Science and Engineering: A, 2007. 459(1-2): 273-277.
196. Nowotny, J. Defect structure and electrical properties of barium titanate. Key Engineering Materials, 1992. 66-67: 1-44.

197. Scott, JF. Ferroelectrics go bananas. Journal of Physics: Condensed Matter, 2008. 20(2).
198. Dinnebier, RE and Billinge, SJL. Eds. Powder Diffraction: Theory and Practice. 2008, RSC Publishing: London.
199. Postiglione, L. Different titanium surfaces modulate the bone phenotype of saos-2 osteoblast-like cells. European Journal of Histochemistry, 2004. 48(3): 213-222.
200. Bitar, M, Brown, RA, Salih, V, Kidane, AG, Knowles, JC, and Nazhat, SN. Effect of cell density on osteoblastic differentiation and matrix degradation of biomimetic dense collagen scaffolds. Biomacromolecules, 2008. 9(1):129-135.
201. Verriera, S, Blakera, JJ, Maquetb, V, Hench, LL, and Boccaccinia, AR. PLLA/bioglasss composites for soft-tissue andhard -tissue engineering: An *in vitro* cell biology assessment. Biomaterials 2004. 25: 3013-3021.
202. Okuda, T, Ioku, K, Yonezawa, I, Minagi, H, Kawachi, G, Gonda, Y, Murayama, H, Shibata, Y, Minami, S, Kamihira, S, Kurosawa, H, and Ikeda, T. The effect of the microstructure of b-tricalcium phosphate on the metabolism of subsequently formed bone tissue. Biomaterials 2007. 28: 2612-2621.
203. Shu, R, McMullen, R, Baumann, MJ, and McCabe, LR. Hydroxyapatite accelerates differentiation and suppresses growth of MC3T3-E1 osteoblasts. Journal of Biomedical Materials Research, 2003. 67A(4): 1196–1204.
204. Wilson, CJ, Clegg, RE, Leavesley, DI, and Pearcy, MJ. Mediation of biomaterial-cell interactions by adsorbed proteins: A review. Tissue Engineering, 2005. 11.
205. Revell, CM, Dietrich, JA, Scott, CC, Luttge, A, Baggett, LS, and Athanasiou, KA. Characterization of fibroblast morphology on bioactive surfaces using vertical scanning interferometry. Matrix Biology, 2006. 25: 523-533.
206. Rea, SM, Best, SM, and Bonfield, W. Bioactivity of ceramic-polymer composites with varied compostion and surface topography. Journal of Materials Science: Materials in Medicine, 2004. 15: 997-1005.
207. Mestas, J and Hughes, CCW. Of mice and not men: Differences between mouse and human immunology. The Journal of Immunology, 2004. 172: 2731–2738.

Appendix A – Materials, consumables and equipment

Table A.1 Materials

Materials	Supplier	Catalogue number	Preparation notes (if any)
4-nitrophenol solution	Sigma	N7660	
4-nitrophenyl phosphate	Sigma	N2675	
Adenosine 5-triphosphate sodium salt	Sigma	A3377	
Alkaline buffer solution	Sigma	A9226	
Amersham advance western blot kit	GE Healthcare	RPN2135	
Antibiotic-antimycotic solution	Sigma	A5955	
Barium titanate powder	Morgan Electroceramics	Tycon P	
Caspase 3 antibody	New England Biolabs	9662	
Cell growth determination ki	Sigma	CGD-1	
Cytotoxicity determination kit (LDH)	Roche Diagnostics	11644793001	
Dimethyl sulfoxide	Sigma	D2650	
DMEM-F12	Fisher Scientific	HYC-001-074A	
Ethanol	Fisher Scientific	E/0600/17	
Fetal calf serum	Sigma	B9433	
Gluteraldehyde	Sigma	49633	
Glycine	Sigma	G8898	
Hexamethyl disilazane	Sigma	H4875	
Hydrofluoric acid	Sigma	47610	
Hydroxyapatite powder	Stryker	TCP130	
Igepal	Sigma		
IL1β antibody (Mouse)	Perbio Scientific	RMIL1B1	
Industrial methylated spirit	Sigma	458600	
J774.2 cell line	ECACC	85011428	
L-Glutamine	Sigma	G6392	Dissolve 1 vial of powder in 10ml sterile PBS
Lipopolysaccharide	Sigma	L4319	
McCoy's 5A medium	Sigma	M8403	
Methanol	Sigma	M3641	
NuPage 4-12% Bis-Tris Gel 1.0mmx10 well	Invitrogen	NP0321	
Osmium tetroxide	Sigma	75632	
Phosphate buffered saline	Sigma	P4417	Dissolve 1 tablet in 200ml distilled water. Sterilise in autoclave at 121°C for 1 hour.
Polyclonal rabbit anti-mouse immunogloins/HRP	Invitrogen	P0260	
Polyclonal swine anti-rabbit immunogloins/HRP	Invitrogen	P0217	
Potassium Ferrocyanide	Sigma	12643	
Precision Plus Protein Kaleidoscope Standards	Bio-Rad	161-0375	
Quant-IT PicoGreen kit	Invitrogen	P11495	
Running buffer, NuPage MES SDS	Invitrogen	NP0002	Dilute to 1x with H_20
Sample buffer, Llaemmli	Sigma	S3401	
Saos-2 cell line	ECACC	89050205	
Skim milk powder	Sigma	70166	
Sodium dodecyl sulfate	Sigma	L3771	
Sodium Hydroxide	Sigma	S0899	
Tri-hydrogen chloride	Sigma	646547	
Triton X-100	Sigma	T8532	
Trypan blue	Sigma	T8154	
Trypsin-EDTA solution 10X	Sigma	59418C	Dilute to 1X with sterile PBS.
Tween	Sigma	P2287	

Table A.2 Transfer buffer

Solution Components	Concentration
Glycine	192 mM
SDS	0.1% (w/v)
Tri-HCl	25 mM
Methanol	20 % (v/v)

Table A.3 Wash buffer

Solution Components	Concentration
Glycine	192 mM
SDS	0.1% (w/v)
Tri-HCl	25 mM
Methanol	20 % (v/v)

Table A.4 Consumables

Consumable	Sizes/types	Supplier	Catalogue number
Cut-off filters Nanosep 3K Omega		Pall Filtron Corporation	OD003C33
Gel loading tips		Alpha Laboratories	LW1100
Microcentrifuge tubes	1.5ml	Fisher Scientific	TKT-190-070N
Cryotubes	1ml	Nalgene	5000-1020
X-Ray film		Fuji	ST02-BOO2
Filter paper (Chromatography paper)	3mm	Whatman	3030-917
Nitrocellulose membrane (transblot transfer medium)		Bio-Rad	162-0112
Parafilm		Fisher Scientific	SEL-400-030P
Cling film		Fisher Scientific	SEL-360-010K
Flasks	T25, T75, T150	Triple Red	
Pipettes	10ml, 25ml	Fisher Scientific	FB51868/FB58227
Centrifuge tubes	50ml	Fisher Scientific	FB555956
Disposable haemocytometer	Fast Read	Immune Systems Ltd	
Culture plates	24 and 96 well	Triple Red	
SiC grinding paper	P600, P1200	Buehler	30-5223-600/1200
Pipette tips	1ml and 250µl	Fisher Scientific	FB34611/FB34593

Table A.5 Equipment

Equipment	Model	Supplier
Ultrasound bath		Deacon Ultrasonics Ltd
Mesh sieve	FB68878	Fisher Scientific
Sintering oven	BRF14/10	Elite Thermal Systems Ltd
Water bath	JB2	Grant
Freezer (-80°C)	Ultra low temperature	New Brunswick Scientific
Fridge		Scandinova
Freezer (-18°C)		Scandinova
Sputter coater	S310B	Edwards
Electrophoresis kit	Mini Protean II System	Bio-Rad
Centrifuge	BR4i	Jouan
Microscope	Eclipse TS100	Nikon
Category II laminar flow cabinet	HS12	Heraeus
Pipettor	Pipetteboy	Integra Biosciences
Pipettors		Fisherbrand
Isopropyl freezing vessel	Mr Frosty	Fisher Scientific
Impedence analyser	Solartron 1260	
X-Ray diffractometer		Phillips
Profilometer	Proscan 2000	
Scanning electron microscope	JSM6310	JEOL
Scanning electron microscope	JSM6480V	JEOL
X-ray film processor	RGII	Fuji

Appendix B – Volume fraction calculations

The mass of hydroxyapatite and barium titanate required for a disc of any given composition was calculated using the formula below.

$$m = \rho \times v \times X \tag{B.1}$$

Where m is the mass of powder required (g), ρ is density of the powder (g/cm^3), v is the volume of disc (cm^3) and X = proportion of disc to be made of that material.

Example:
Calculation of the quantities of powder required to make one disc with composition 20% HA, 80%BT by volume.

Estimated volume of disc

$$v = t\pi d^2 / 4 \tag{B.2}$$

Given d = 15mm, and disc thickness t = 2mm, v = 0.353 cm^3

For barium titanate, X = 0.8, ρ = 5.85 g/cm^3 (as stated by the manufacturer). Therefore,

$$m_{BT} = 5.85 \times 0.353 \times 0.8 = 1.65g$$

For hydroxyapatite, X = 0.2, ρ = 3.1 g/cm^3(as stated by the manufacturer). Therefore,

$$m_{HA} = 3.1 \times 0.353 \times 0.2 = 0.22g$$

Table B1 Quantities of HA and BT powders per disc by composition

% HA	Mass of HA per disc (g)	% BT	Mass of BT per disc (g)	Total mass of unsintered disc (g)
0	0	100	2.07	2.07
5	0.06	95	1.96	2.02
10	0.11	90	1.86	1.97
15	0.17	85	1.75	1.92
20	0.22	80	1.65	1.87
40	0.45	60	1.24	1.69
60	0.67	40	0.83	1.50
80	0.89	20	0.41	1.30
100	1.11	0	0	1.11

Appendix C – Proof of method studies

Disc resurfacing

Six discs of HA were ground according to the protocol for resurfacing detailed in Section 3.2. Six measurements of the depth of each disc were taken before and after the grinding process using digital callipers. The average amount of material removed was 48μm (from a thickness of 2-3mm), with a standard deviation of 9μm. The minimum depth of material removed was 38μm. As this depth is significantly larger than defects observed on the surface of the ceramic, it was judged that the material had been suitably resurfaced.

Trypsin study

Cells were seeded onto eight HA discs and six tissue culture plastic control wells as described in Section 3.3. After 24h of incubation, the cells were removed from six of the discs using trypsin and counted. The trypsin treatment and count were then repeated on the same discs to establish whether any cells had been left in place by the first treatment. The results of these counts are shown in Figure C1.

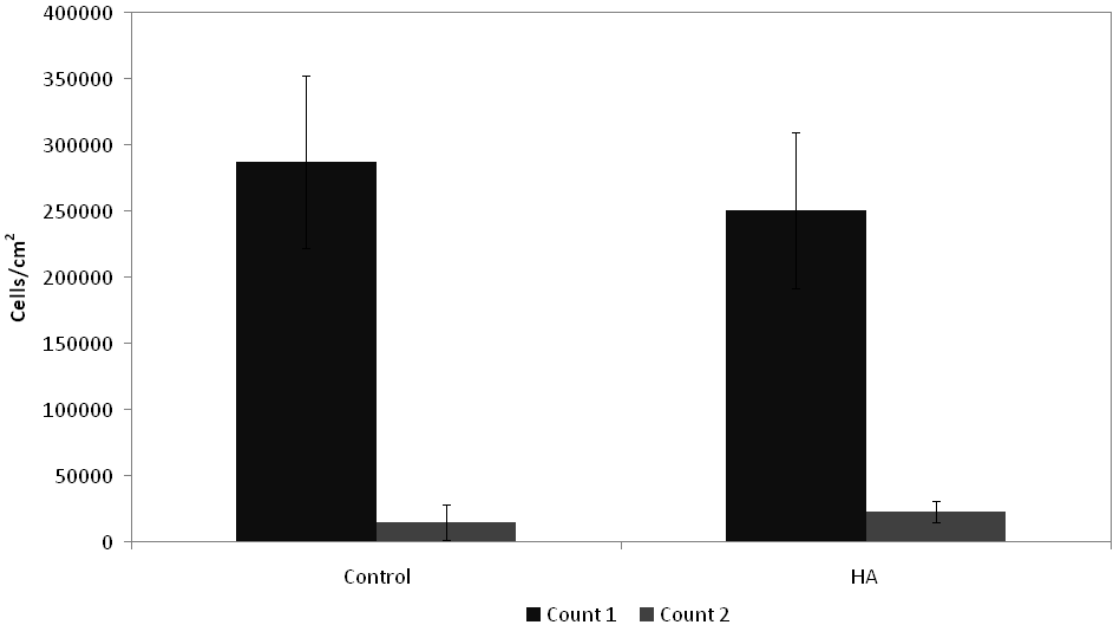

Figure C1 Cell numbers found by repeated trypsin treatments of the tissue culture plastic control and of HA discs

These results clearly show that the majority of cells are removed by one trypsin treatment. To confirm this, the remaining two HA discs were prepared for SEM; one with cells still in place on its surface, the other after one trypsin treatment. The images obtained are shown in Figure C2.

From these images it is clear that the cells were no longer present after the trypsin treatment. It was therefore concluded that the protocol for carrying out cell counts produced results that were representative of the cell population on the ceramic.

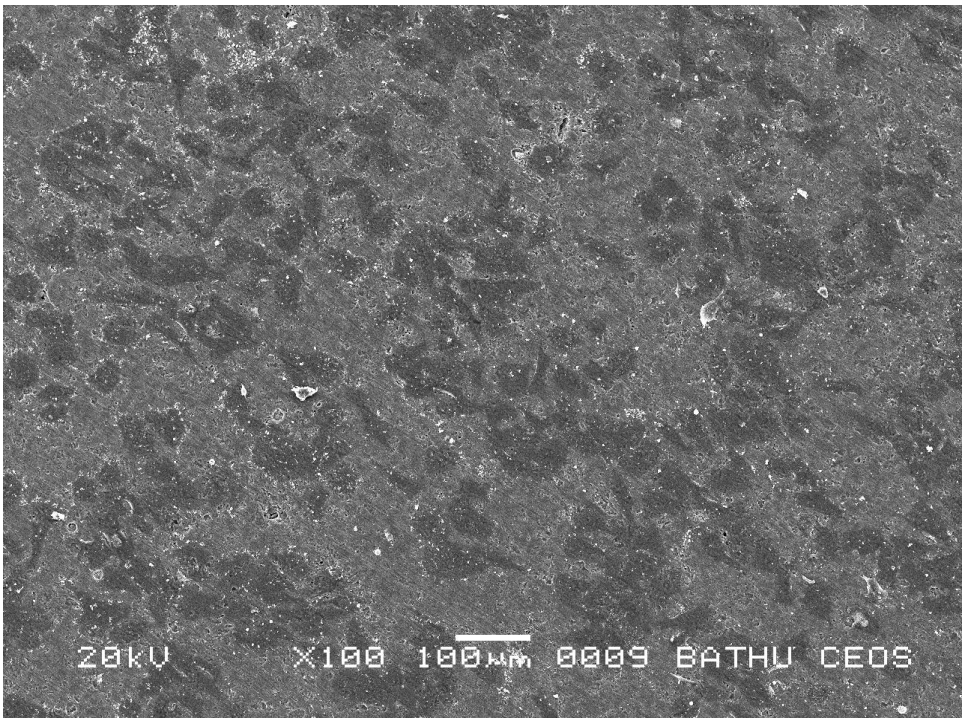

(a)

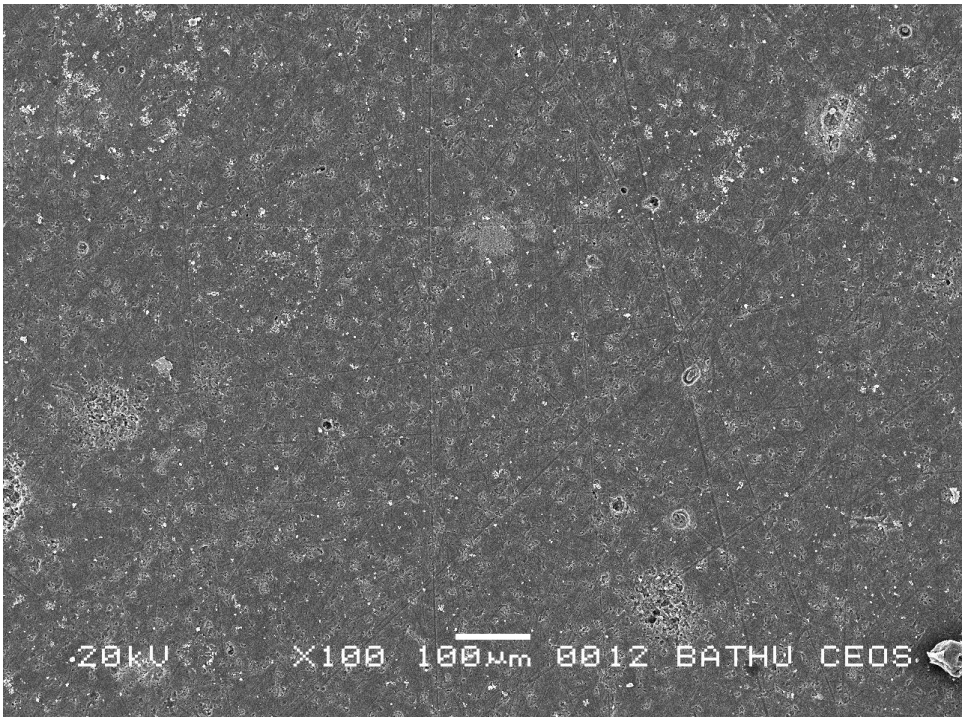

(b)

Figure C2 SEM micrographs of the surface of an HA disc a) before and b) after trypsin treatment to remove cells

Appendix D – The ageing of piezoelectric coefficients in cell culture conditions

The following experiment was designed to determine the effects, if any, of cell culture conditions on the rate of decay of the piezoelectric coefficient of the ceramic. Possible influences on the piezoelectric properties include soaking in liquid and the presence of proteins resulting from soaking in FCS on the ceramic surface

Eighteen samples of HABT were prepared as described in Section 3.2. They were poled using corona poling and 24h later their piezoelectric coefficients were measured. They were stored overnight in 70% IMS and rinsed twice in sterile PBS. They were then placed in 24-well plates, one tablet per well. Six of the wells were left dry. The other 12 wells were topped up with 1ml culture medium, six of them with medium containing FCS and six with serum-free medium. The plates were then incubated at 37°C and 5% CO_2. After 24h, half of the samples (three from each group) were removed and allowed to dry in air before their piezoelectric coefficient was re-measured. This process was repeated for the remaining samples after 10 days of incubation. The culture medium in this plate was changed every 2-3 days as for cell culture. The percentage of d_{33} lost by each sample over the incubation period was then calculated. The resulting data, shown in Figure D1, show the average loss in piezoelectric charge coefficient from the three samples tested in each case. The data are highly variable, with some negative values recorded, indicating that the d_{33} for a given sample appeared to rise during the 10 day incubation. This indicates that the changes in d_{33} in these materials are within the range of error of the piezometer and therefore cannot be considered to be significant.

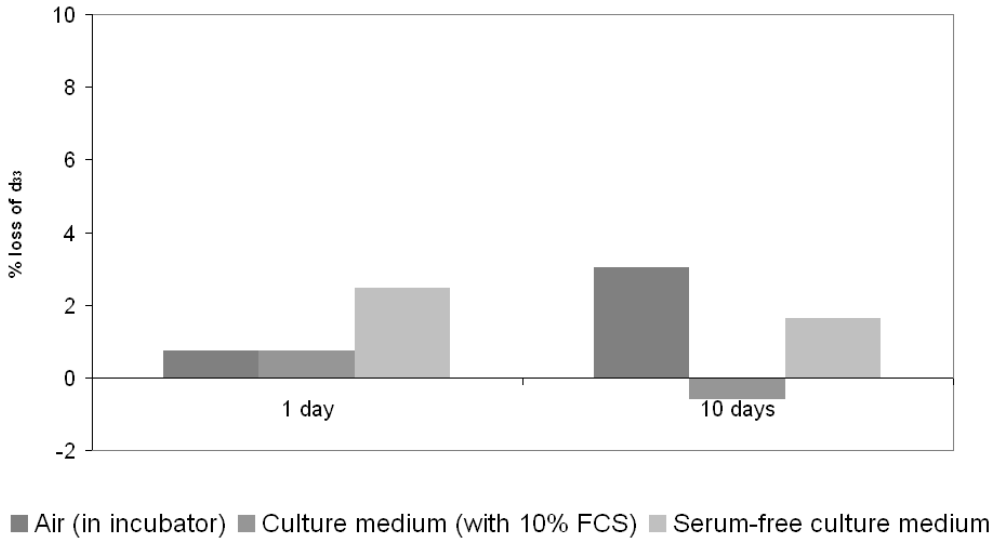

Figure D1 Ageing of piezoelectric coefficient stored in air, in complete culture medium and in serum-free culture medium

Appendix E – Publications and conference presentations

Conferee Presentations (Oral)

F.R. Baxter, I.G. Turner, C.R. Bowen, J. Gittings, and J.B. Chaudhuri, A study of the microstructure of HABT composites for use as bone substitutes, UKSB Annual Conference 2008, 26-27th June 2008, Liverpool, UK

F.R. Baxter, I.G. Turner, C.R. Bowen, J. Gittings, and J.B. Chaudhuri, The attachment of osteoblast-like cells to hydroxyapatite-barium titanate ceramics, World Biomaterials Congress, 28th May – 1st June 2008, Amsterdam, The Netherlands

F.R. Baxter, I.G. Turner, C.R. Bowen, J. P. Gittings, J.B. Chaudhuri and R.W.C. Lewis, The structure and properties of electroceramics for bone graft substitution, Bioceramics 20, 24th-26th October 2007, Nantes, France

F.R. Baxter, I.G. Turner, C.R. Bowen, J. P. Gittings, J.B. Chaudhuri and R.W.C. Lewis, The Structure and Properties of Electroceramics for Bone Graft Substitution, UKSB Annual Conference, 5th-6th July 2007, London, UK

J.P. Gittings, C.R. Bowen, I.G. Turner, F. Baxter and J. Chaudhuri, Characterisation and poling of ferroelectric-calcium phosphate biocomposites, Electroceramics X, 18-22 June 2006, Toledo, Spain

Conference presentations (Poster)

F.R. Baxter, C.R. Bowen, I.G. Turner, J.P. Gittings and J.B. Chaudhuri, Properties of ferroelectric-hydroxyapatite composites, 21st European Conference on Biomaterials, 9th-13th September 2007, Brighton, UK

C.R. Bowen, J.P. Gittings, I.G. Turner, F.R. Baxter and J.B. Chaudhuri, A study of the microstructure of HABT composites for use as bone substitutes, 21st European Conference on Biomaterials, 9th-13th September 2007, Brighton, UK

Journal publications

F.R. Baxter, I.G. Turner, C.R. Bowen, J.P. Gittings, J.B. Chaudhuri, An *in vitro* study of electrically active hydroxyapatite-barium titanate ceramics using Saos-2 cells, Journal of Materials Science: Materials in Medicine, Accepted, DOI 10.1007/s10856-009-3734-0 (2009)

J.P. Gittings, C.R. Bowen, A.C.E. Dent, I.G. Turner, F.R. Baxter and J.B. Chaudhuri, Electrical characterization of hydroxyapatite-based bioceramics, Acta Biomaterialia, In Press, DOI: 10.1016/j.actbio.2008.08.012 (2008)

F.R. Baxter, I.G. Turner, C.R. Bowen, J. P. Gittings, J.B. Chaudhuri and R.W.C. Lewis, The structure and properties of electroceramics for bone graft substitution, *Key Eng. Mat*. 361-363, 99-102 (2008)

J.P. Gittings, C.R. Bowen, I.G. Turner, F. Baxter, J. Chaudhuri, Characterisation of ferroelectric-calcium phosphate composites and ceramics, *Journal of the European Ceramic Society*, 27 (13-15) 4187-4190 (2007)

C. R. Bowen, J. Gittings, I. G. Turner, F. Baxter, and J. B. Chaudhuri, Dielectric and piezoelectric properties of hydroxyapatite-$BaTiO_3$ composites, *Applied Physics Letters* 89, 132906 (2006)